



HAL
open science

Etude probabiliste de la stabilité d'un barrage en remblais. Prise en compte des données in-situ

Xiangfeng Guo

► **To cite this version:**

Xiangfeng Guo. Etude probabiliste de la stabilité d'un barrage en remblais. Prise en compte des données in-situ. Mechanics of materials [physics.class-ph]. Université Grenoble Alpes [2020-..], 2020. English. NNT: 2020GRALI017 . tel-02891918

HAL Id: tel-02891918

<https://theses.hal.science/tel-02891918>

Submitted on 7 Jul 2020

HAL is a multi-disciplinary open access archive for the deposit and dissemination of scientific research documents, whether they are published or not. The documents may come from teaching and research institutions in France or abroad, or from public or private research centers.

L'archive ouverte pluridisciplinaire **HAL**, est destinée au dépôt et à la diffusion de documents scientifiques de niveau recherche, publiés ou non, émanant des établissements d'enseignement et de recherche français ou étrangers, des laboratoires publics ou privés.

THÈSE

Pour obtenir le grade de

DOCTEUR DE L'UNIVERSITE GRENOBLE ALPES

Spécialité : **Matériaux, Mécanique, Génie Civil, Electrochimie**

Arrêté ministériel : 25 mai 2016

Présentée par

Xiangfeng GUO

Thèse dirigée par **Daniel DIAS**
et codirigée par **Laurent PEYRAS** et **Pierre BREUL**

préparée au sein du **Laboratoire « Sols, Solides, Structures - Risques » (3SR)**
dans l'**École Doctorale « Ingénierie - Matériaux Mécanique Énergétique Environnement Procédés Production » (I-MEP2)**

Probabilistic stability analysis of an earth dam using field data

Thèse soutenue publiquement le **10/03/2020**,
devant le jury composé de :

M. Vaughan GRIFFITHS

Professeur à Colorado School of Mines (Rapporteur)

M. Daniel STRAUB

Professeur à Technical University of Munich (Rapporteur)

M. Sidi Mohammed ELACHACHI

Professeur à l'Université de Bordeaux (Examineur; Président de jury)

M. Julien BAROTH

Maître de Conférences à l'Université Grenoble Alpes (Examineur)

M. Eric ANTOINET

Ingénieur de recherche à Antea Group (Examineur)

M. Daniel DIAS

Professeur à l'Université Grenoble Alpes (Directeur de thèse)

M. Laurent PEYRAS

Ingénieur des Ponts (HDR) à INRAE (Co-directeur)

M. Pierre BREUL

Professeur à l'Université Clermont Auvergne (Co-directeur)

M. Claudio CARVAJAL

Ingénieur de recherche à INRAE (Co-encadrant)



Abstract

Uncertainties of soil properties are widely encountered in the field of geotechnical engineering especially for earth dams which are constructed with earthen materials. In recent years, there is an increasing need, motivated by the deficiencies of the traditional deterministic approach or guided by the national regulations such as in France, of accounting for these uncertainties for a safe assessment of large dams particularly in the framework of risk analysis studies. However, probabilistic analyses are still complex and not so easy to implement in practice due to the limited number of in-situ measurements, expensive computation efforts and lack of implementation of reliability methods in commercial simulation tools. Moreover, most of the previous studies are based on academic cases and hypothetical data.

This work attempts to deal with the aforementioned issues by providing a probabilistic analysis study for the stability of a real earth dam using available field data. This study includes the following main elements: (1) definition of the soil variability by using the available measurements; (2) development of the deterministic models; (3-4) dam probabilistic analyses using the random-variables and random-fields approaches; (5) three-dimensional reliability analysis of the considered dam. Advanced reliability methods, such as the adaptive surrogate modelling, are introduced for the studied earth dam problem. This allows accurately estimating the dam failure probability and the safety factor statistics with a significantly reduced calculation time. In addition, some issues, that remain unknown or unclear in the field of the dam probabilistic analysis, are discussed (e.g. global sensitivity analysis of the soil hydraulic and shear strength parameters; performance survey of five reliability methods; modelling/comparison of three different kinds of random fields: generic (unconditional-stationary), conditional and nonstationary). The presented work, based on real measurements, could be a good supplement to the existing probabilistic studies of geo-structures. Readers will find useful information from the obtained results in order to better solve the practical geotechnical problems in a probabilistic framework.

Key words: Earth dam; Slope stability; Reliability analysis; Sensitivity analysis; Random field; Polynomial Chaos Expansions

Résumé

Compte tenu de la nature des sols, des incertitudes sur leurs propriétés sont largement rencontrées en géotechnique, en particulier dans le domaine des barrages en terre. Actuellement, il est de plus en plus nécessaire de tenir compte de ces incertitudes pour l'évaluation de la sécurité des grands barrages, notamment dans le cadre des études d'analyse de risques. Cependant, les analyses probabilistes sont complexes et difficiles à mettre en œuvre en raison du nombre limité de mesures, des temps de calcul importants et des limites des méthodes fiabilistes implémentées dans les outils de simulation commerciaux. De plus, la plupart des études précédentes sont basées sur des cas académiques et des données hypothétiques.

Ce travail tente de résoudre les problèmes mentionnés ci-dessus en fournissant une étude d'analyse probabiliste pour la stabilité d'un barrage réel en terre en considérant les données in-situ disponibles. Cette étude inclut les éléments principaux suivants: (1) définition de la variabilité des sols en utilisant les mesures disponibles; (2) développement des modèles déterministes; (3-4) analyses probabilistes du barrage en utilisant des approches en variables aléatoires et en champs aléatoires; (5) analyse 3D de la fiabilité du barrage considéré. Des méthodes fiabilistes avancées (par exemple le métamodèle adaptatif) sont introduites. Cela permet d'estimer précisément la probabilité de rupture du barrage et les valeurs statistiques des facteurs de sécurité avec un temps de calcul significativement réduit. En outre, certaines questions, qui restaient floues dans le domaine de l'analyse probabiliste des barrages, sont discutées (e.g. l'analyse de sensibilité globale des paramètres hydrauliques et géo-mécaniques des sols ; l'étude des performances de cinq méthodes de fiabilité ; la simulation/comparaison de trois types de champs aléatoires : générique, conditionnel et non-stationnaire). Le travail présenté, basé sur des données réelles, pourrait être un bon complément aux études probabilistes existantes des ouvrages géotechniques. Les lecteurs pourront également trouver des informations utiles à partir des résultats obtenus afin de mieux résoudre les problèmes pratiques de géo-ingénierie dans un cadre probabiliste.

Mots clés : Barrage en terre ; Stabilité des pentes ; Analyse fiabilité ; Analyse sensibilité ; Champ aléatoire ; Chaos Polynomiaux

Acknowledgements

I would like first to express my deep appreciation to Prof. Daniel Dias, supervisor of this thesis, who has taught and guided me for over 6 years since 2013 (3 for master and 3 for PhD). Many thanks to him for giving me the chance to work in such an exciting field (probabilistic analysis) to which I have great passions and motivations to make contributions. During the past 3 years, his professional guidance, constructive suggestions and kind encouragements are invaluable and very helpful for my research activities. All I have learned from him (research and personality) will surely be a treasure for me in future life.

I would also thank my co-supervisors Dr. Claudio Carvajal, Dr. Laurent Peyras and Prof. Pierre Breul for their insightful guidance, their supports in accessing the original data, their comments in analysing the considered structure and their careful reviews of my manuscripts for journal papers and this thesis. The discussions with them helped mature many ideas presented in this work.

Besides my supervisor team, I offer my acknowledgements to all the members of my dissertation committee: Prof. Vaughan Griffiths, Prof. Daniel Straub, Prof. Sidi Mohammed Elachachi, Assoc. Prof. Julien Baroth and Dr. Eric Antoinet for their precious time to assess my thesis and participate in the defence, also for the questions which permitted me to have more points of view to evaluate my work and enrich it in a next stage. My special thanks and gratitude go to Prof. Vaughan Griffiths and Prof. Daniel Straub (reviewers) who provided me with a plenty of useful/insightful comments and suggestions for this thesis.

My research works and the improved knowledge about the geotechnical probabilistic analysis would have not been possible without the help and collaboration of several other researchers. I wish to acknowledge Mr. Alexandre Simon, Asst. Prof. Navid Jafari, Prof. Qiuqing Pan, Dr. Dianchun Du, Mr. Qiangqiang Sun, Ms. Siyang Zhou and Dr. Chana Phutthananon. I felt a great pleasure to work with them and these experiences permitted me to better understand the uncertainty quantification for different geotechnical problems (e.g. seismic and tunnel).

The present work is financially supported by China Scholarship Council. This funding (No. 201608070075) is greatly appreciated.

Lastly and on a more personal note, I wish to sincerely thank my family for the unconditional support. Special gratitude goes to my parents and my wife. Their endless love and patience have helped me overcome all the difficulties during my PhD study.

Table of contents

ABSTRACT	3
RESUME.....	4
ACKNOWLEDGEMENTS	5
TABLE OF CONTENTS.....	7
NOMENCLATURE.....	11
1 CHAPTER I: GENERAL INTRODUCTION.....	15
1.1 BACKGROUND AND MOTIVATION.....	16
1.2 OBJECTIVES	20
1.3 LAYOUT OF THE THESIS	22
2 CHAPTER II: LITERATURE REVIEW ABOUT RELIABILITY ANALYSIS METHODS AND PROBABILISTIC ANALYSIS OF EARTH DAMS	25
2.1 A BRIEF REVIEW OF RELIABILITY ANALYSIS METHODS	26
2.1.1 <i>Some basic reliability concepts.....</i>	<i>26</i>
2.1.2 <i>Approximation methods</i>	<i>28</i>
2.1.3 <i>Sampling methods.....</i>	<i>31</i>
2.1.4 <i>Surrogate modelling techniques.....</i>	<i>36</i>
2.2 DETAILED PRESENTATION OF THE METHODS EMPLOYED IN THIS WORK	41
2.2.1 <i>PCE, SPCE and adaptive SPCE.....</i>	<i>41</i>
2.2.2 <i>Sobol-based global sensitivity analysis</i>	<i>48</i>
2.2.3 <i>Random-fields generation.....</i>	<i>52</i>
2.2.4 <i>Other techniques related to the performed probabilistic analysis</i>	<i>58</i>
2.3 PREVIOUS STUDIES ABOUT PROBABILISTIC ANALYSIS OF EARTH DAMS.....	62
2.3.1 <i>Stochastic flows</i>	<i>62</i>
2.3.2 <i>Slope stability of dams.....</i>	<i>65</i>

2.3.3	<i>Internal erosion</i>	67
2.3.4	<i>Other existing studies</i>	68
2.4	CONCLUSION	70
3	CHAPTER III: SOIL VARIABILITY MODELLING AND COMPUTATIONAL MODEL DEVELOPMENT	73
3.1	PRESENTATION OF THE STUDIED DAM.....	74
3.2	SOIL VARIABILITY MODELLING.....	76
3.2.1	<i>Variability modelling of the γ_d</i>	77
3.2.2	<i>Variability modelling of the c' and ϕ'</i>	81
3.2.3	<i>Summary of the soil parameters</i>	85
3.3	DEVELOPMENT OF THE DETERMINISTIC MODELS.....	87
3.3.1	<i>The model SRM_FEM</i>	89
3.3.2	<i>The model SRM_FDM</i>	90
3.3.3	<i>The model LEM_GA</i>	91
3.4	CONCLUSION	98
4	CHAPTER IV: PROBABILISTIC STABILITY ANALYSIS WITH THE RANDOM-VARIABLES APPROACH	101
4.1	SENSITIVITY ANALYSIS.....	102
4.1.1	<i>Introduction</i>	102
4.1.2	<i>An adaptive PCE for GSA</i>	104
4.1.3	<i>Numerical results</i>	107
4.2	RELIABILITY ANALYSIS RESULTS	108
4.2.1	<i>Normal exploitation condition</i>	110
4.2.2	<i>Exploitation under seismic loading condition</i>	112
4.3	DISCUSSIONS	116
4.3.1	<i>Comparison between the two deterministic models</i>	116
4.3.2	<i>Effect of the distribution type for input variables</i>	118

4.4	CONCLUSION	120
5	CHAPTER V: PROBABILISTIC ANALYSIS USING THE RANDOM-FIELDS	
	APPROACH	123
5.1	PERFORMANCE SURVEY OF THE MODEL <i>LEM_GA</i> WITHIN SPATIALLY VARIED SOILS	124
5.2	COMPARISON OF FIVE RELIABILITY METHODS FOR HIGH DIMENSIONAL PROBLEMS	127
5.2.1	<i>The considered reliability methods for the comparative study</i>	<i>128</i>
5.2.2	<i>Reliability analysis using the reference method MCS.....</i>	<i>131</i>
5.2.3	<i>Comparison results from five reliability methods</i>	<i>138</i>
5.2.4	<i>Discussions on the results</i>	<i>140</i>
5.3	MODELLING AND COMPARISON OF DIFFERENT RANDOM FIELDS	144
5.3.1	<i>Introduction</i>	<i>144</i>
5.3.2	<i>Modelling of different RFs for γd with the available data.....</i>	<i>147</i>
5.3.3	<i>The obtained reliability analysis results</i>	<i>152</i>
5.3.4	<i>Effects of using the two complex RFs</i>	<i>154</i>
5.3.5	<i>Discussions of the obtained results.....</i>	<i>158</i>
5.4	CONCLUSION	161
6	CHAPTER VI: THREE-DIMENSIONAL PROBABILISTIC ANALYSIS	165
6.1	CONSTRUCTION OF THE 3D COMPUTATIONAL MODEL	166
6.2	3D PROBABILISTIC ANALYSIS RESULTS.....	170
6.2.1	<i>Results for the reference case</i>	<i>171</i>
6.2.2	<i>Influence of the correlation between c' and ϕ'.....</i>	<i>173</i>
6.3	COMPARISON WITH 2D RESULTS	176
6.4	EFFECTS OF USING A COARSE DETERMINISTIC MESH.....	181
6.5	ACCURACY INVESTIGATION OF THE CONSTRUCTED SURROGATE MODELS	186
6.6	CONCLUSIONS.....	188
7	CHAPTER VII: GENERAL CONCLUSIONS, RECOMMENDATIONS AND	
	PERSPECTIVES.....	191

7.1	CONCLUDING REMARKS FROM THE STUDIED DAM	193
7.2	RECOMMENDATIONS FOR RELATIVE STUDIES	195
7.3	LIMITATIONS AND FUTURE WORKS	197
8	REFERENCE.....	201

Nomenclature

Abbreviations

AbSPCE	Adaptive Bootstrap SPCE
CDF	Cumulative Density Function
CONsta	Conditional Stationary RFs
CoV	Coefficient of Variation
<i>ED</i>	Experimental design
FDM	Finite Difference Method
FEM	Finite Element Method
FORM	First Order Reliability Method
FOSM	First Order Second Moment
FoS	Factor of Safety
GA	Genetic Algorithm
GSA	Global Sensitivity Analysis
IS	Importance Sampling
K-L method	Karhunen-Loève expansion
LEM	Limit Equilibrium Method
LSF	Limit State Function
LHS	Latin Hypercube Sampling
LSS	Limit State Surface
MCS	Monte Carlo Simulation
MM	Moment Method
MPFP	Most Probable Failure Point (in FORM)
PDF	Probability Density Function
RF	Random Field
RSM	Response Surface Methodology
RV	Random Variable
SIR	Sliced Inverse Regression
SORM	Second Order Reliability Method
(S)PCE	(Sparse) Polynomial Chaos Expansions
SRM	Strength Reduction Method
SS	Subset Simulation
Std	Standard deviation

SVM	Support Vector Machine
UNnon	Unconditional Non-Stationary RFs
UNsta	Unconditional Stationary RFs

Symbols

● **Latin symbols**

$A^{M,p,q}$	Truncation set determined by M , p and q
B (B_{PCE})	Number of generated new EDs in bootstrap-PCE
c'	Cohesion
$f_j(\mathbf{x})$	Joint probability density function
g	Gravity acceleration
$g(\mathbf{x})$	Performance function
K_s	Hydraulic conductivity
l_x (l_z)	Horizontal (vertical) autocorrelation distance
M	Number of input variables
N_{call}	Number of calls to the deterministic model
N_{ED}	Size of ED
N_{MC}	Number of model evaluations in MCS
N_{RV}	Number of RVs
N_{SS}	Number of model evaluations in each simulation level of SS
p	Max degree in PCE
\mathbf{P}^*	Design point in FORM
Pf	Failure probability
Pf_{direct}	Failure probability of the dam under the considered seismic loading
Pf_{final}	Failure probability of the dam over the return period
P_{SS}	Intermediate failure probability in SS
q	q-norm in PCE
Q^2	Accuracy indicator in PCE
R^2	Coefficient of determination in PCE
R_f (R_s)	Failure (safe) domain
rK	Anisotropy coefficient of K_s

S_{KL}	Size of truncated K-L expansion
$\mathbf{x}^{(i)}$	i -th sample (size of M) in \mathbf{x}
x_i	i -th variable
$Var[\cdot]$	Variance
● Greek symbols	
$\beta_{C',\phi'}$	Correlation coefficient between C' and ϕ'
β_{HL}	Hasofer-Lind reliability index
γ_d	Dry density
ε_{Pf}	Acceptance threshold in AbSPCE
μ	Mean
$\rho(\mathbf{x}, \mathbf{x}')$	Autocorrelation function
σ	Standard deviation
$\Psi_\alpha(\xi)$	Multivariate polynomials in PCE
● Other symbols	
$\mathbb{E}[\cdot]$	Expectation
ϕ'	Friction angle

1 CHAPTER I: General introduction

1.1 Background and motivation

Dams, which can be defined as structures allowing a permanent or temporary storage of a volume of water, are widely used over the world as a response to the increasing need of development and management of water resources. They are constructed for single or multiple -purpose(s) including irrigation, hydropower, water supply, flood control, recreation, navigation, and tailing. According to the database of the International Commission Of Large Dams (ICOLD), around 58 000 large dams exist around the world (ICOLD, 2019). 65% of them can be classified into the category of earth dams which were built up by using earthen materials, while this proportion can raise up to 75% for embankment dams in which rock-filled dams are also considered.

Safety assessment is crucial for dams since their failures would induce considerable damages for human beings and economics. Regarding earth dams, there are mainly three failure modes: two related to structural failures (piping and slope instability) and one due to the flood overtopping. Foster et al. (2000a) presented a statistical summary of the embankment-dam failures occurred before 1986. The authors pointed out that the piping is the major reason of structural failures for these dams. They also found that the zoning conditions have significant impacts on the frequency of piping failures. For example, there was no failure report of piping in the embankment dams which are equipped with a central core up to 1986 whereas 16 large homogeneous earth-filled dams have been damaged by this type of failure. Therefore, the piping is not necessary the primary concern for central core earth dams and the slope stability issue should also be carefully treated in designing or assessing this kind of dams.

Earth dams usually involve a high degree of uncertainties, especially in their material properties since they are constituted by natural materials (compacted soils or rockfill), which makes their safety evaluation a difficult task. Properly considering soil variabilities and quantifying their effects on the dam behaviour are of great importance

for these structures. Traditionally, soil variabilities are taken into account by penalising the soil strength parameters with partial factors which are recommended by expert judgment or imposed by design codes, so that the designs or calculations are conservative. However, this approach may lead to unsafe designs if the variability is large as showed for the case of two slopes in Figure 1.1. Also, the designs, determined by partial factors, could be too conservative thus uneconomic in some cases. The probabilistic analysis is an effective solution which permits to better address the above-mentioned issues by providing complementary results. It allows accounting for soil variabilities in a more rational way (statistical approach) and quantifying their effects on the dam safety condition by using a reliability method such as the Monte Carlo Simulation (MCS) and the First-Order-Reliability-Method (FORM). In addition to providing a single safety factor estimate (as in the traditional deterministic approach), the available results in a probabilistic analysis include also the failure probability (P_f), design points and statistical moments (mean and variance) of safety factors. A sensitivity analysis can also be carried out in a probabilistic framework, so the sensitivity index of each input variable is available as well. Having more results, especially the ones (e.g. P_f and variance) which can reflect the effects of input uncertainties, are beneficial for designers to better understand the functioning mode of the problems and make more rational decisions. Therefore, it is worthy to implement probabilistic analyses for the safety assessment of earth dams, in order to account for soil variabilities and provide complementary information. Figure 1.2 shows the complementary results that a probabilistic analysis can bring to a traditional deterministic analysis.

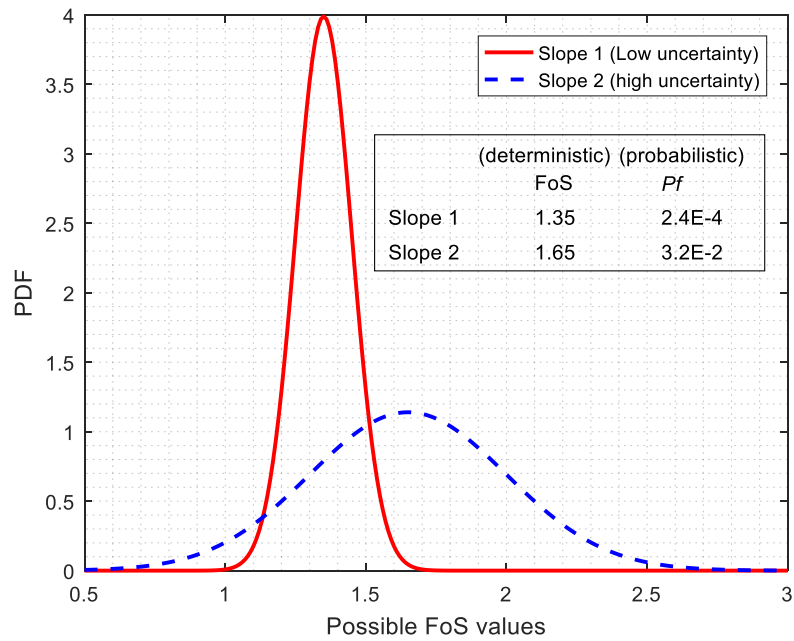


Figure 1.1 Limitation of using only the deterministic analysis evidenced by an example of two slopes (notes: FoS – factor of safety; PDF - probability density function)

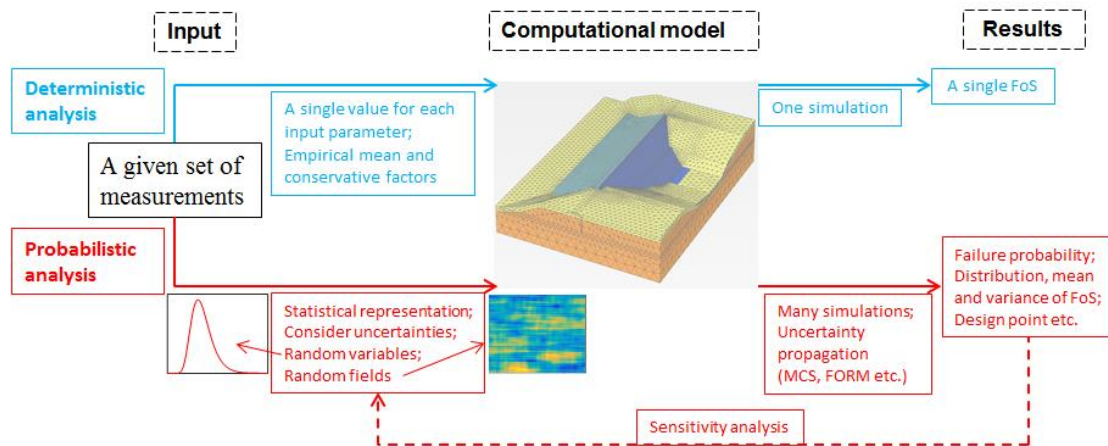


Figure 1.2 Contributions of a probabilistic approach to a deterministic analysis

Additionally, probabilistic analyses are being introduced into national design regulations in recent years such as in France. The French national codes on the safety of hydraulic works were modified in 2015 and request the owners of large dams to produce safety analysis reports in which the risk assessment is performed with probabilistic approaches. This represents an increasing demand of probabilistic-based guidelines for the safety evaluation of dams. In literature, there are some studies about

the probabilistic analysis of earth dams for three issues: stochastic flows inside dams (Ahmed, 2009; Calamak et al., 2013, 2012; Cho, 2012; Fenton and Griffiths, 1997, 1996), dam reliability regarding its slope stability (Babu and Srivastava, 2010; Calamak and Yanmaz, 2014; Chen and Chang, 2011; Ghanem et al., 2007; Gui et al., 2000; Preziosi, 2008) and dam failure probability due to internal erosion (Andreini et al., 2016; Foster et al., 2000b). Although previous studies permitted a better understanding of the soil uncertainties role on the dam reliability with respect to different failure modes, some common limitations can still be found (a review of these studies is presented in section 2.3): (1) most of the studies were based on simple homogeneous dams while the zoned dam with a clayed core was seldom considered; (2) almost all the studies worked on academic cases with hypothetical data, so the measurements collected during the site investigation, construction and monitoring phases were not explored; (3) the commonly used reliability methods in previous studies are MCS and FORM. There was no application of advanced methods (e.g. subset simulation and surrogate modelling) to earth dam problems; (4) for the spatial modelling of soil properties, only lognormal stationary random fields (RFs) were used. Other RF types, such as conditional and nonstationary ones, were not implemented in the dam probabilistic analysis; (5) almost all the studies were within a two-dimensional (2D) analysis. The three-dimensional (3D) geometry effects on the probabilistic estimates were investigated for slopes but not for dams; (6) there was no Global Sensitivity Analysis (GSA) in the previous studies. The contribution of the considered uncertainty input parameters to the dam reliability remains unknown. These limitations represent some improvement possibilities for this work and for future studies.

In a probabilistic analysis, uncertainties of soil properties can be represented by random variables (RVs) or random fields (RFs). The former is simple and easy to couple with any deterministic model in practice. In this approach, the soil is assumed to be homogeneous but different values are generated in different simulations for one soil

property according to a given distribution. Therefore, the RV method cannot explicitly account for the soil spatial variabilities. On the contrary, the RF approach is able to model the spatial variation of soils. For a soil property in one simulation, one RF, meaning a collection of different values in a discretized grid, is generated according to the soil parameter statistics and a given autocorrelation structure. However, this approach is more complex and needs extra computational efforts (e.g. quantification of the autocorrelation distances and generation of RFs) compared to the RV one. Figure 1.3 illustrates the principle idea of the two approaches.

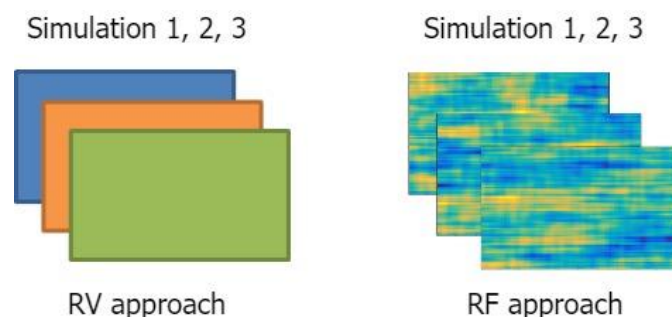


Figure 1.3 Comparison between the RV and RF approach used in a probabilistic analysis

1.2 Objectives

The previous section explains the importance of the safety assessment for earth dams, the necessity of using probabilistic analysis for these structures and the common limitations of the existing studies. Motivated by all these points, the present research work is established and is dedicated to probabilistically evaluating the stability condition of a real earth dam by using the available measurements and by implementing advanced probabilistic methods for soil spatial modelling (e.g. with conditional RFs) and for reliability analysis (e.g. metamodeling and GSA). The studied dam, located in the west of France, is a central core earth-filled dam. An advantage of this dam is that there are a large number of geo-localized measurements (density ones), which are beneficial for the statistical representation of soil variabilities. The present work can be regarded as an extension of the thesis of Mouyeaux (2017) which was based on the

same dam for the probabilistic analysis of pore water pressures and slope stability (using stationary RFs and classical reliability methods).

The main objectives of this work can be summarized as follows:

- Present a comprehensive probabilistic (including reliability and sensitivity) analysis, based on the exploitation of the available field data, of a central core earth dam by using both the RV and RF approaches and applying advanced reliability methods such as surrogate-enhanced MCS to dam problems.
- Provide insights into some issues that remain unknown or unclear in the field of dam probabilistic analysis, and give recommendations for future related studies. The issues treated in this work include: (1) the comparison between different slope stability analysis methods in a probabilistic framework (using limit-equilibrium method LEM and numerical methods such as finite element method FEM and finite difference method FDM); (2) the performance survey of different reliability methods for high dimensional stochastic problems; (3) the modelling of different RFs with a given set of data by using generic RFs (stationary and unconditional) as well as more complex RFs (conditional and non-stationary); (4) the investigation about the effect of the dam 3D geometry on the dam reliability.

In operational terms, this work aims to evaluate the slope stability of the considered dam in a probabilistic manner under normal operation conditions and seismic loadings. The obtained results can be used as a part of the risk analysis report required by the national regulations. More generally, this work aims to provide recommendations for future studies on the probabilistic analysis of dams.

1.3 Layout of the thesis

The thesis is organized as follows:

- CHAPTER I : this chapter gives a general introduction, in which the motivations, the objectives and the structure of the present work are presented.
- CHAPTER II : this chapter aims to provide two brief reviews on respectively two topics: the probabilistic analysis of earth dams and the reliability methods commonly used in the field of geo-structures. Additionally, the probabilistic analysis tools that are employed in this work or adapted to the dam problem are presented.
- CHAPTER III : in this chapter, the relevant measurements are statistically analyzed to model the soil variabilities by means of RVs and RFs. The development of three deterministic models is also presented. Particularly, a two-stage optimization procedure based on the genetic algorithm is proposed to enhance the performance of one deterministic model which is based on the limit equilibrium method (Morgenstern-Price in this work).
- CHAPTER IV : this chapter presents the probabilistic analysis results of the dam with the RV approach by considering two operation conditions (normal and seismic) for the dam and by using two slope stability analysis methods (LEM combined with the genetic algorithm and FDM-based strength reduction). The reliability analysis is performed by using the sparse Polynomial Chaos Expansion (PCE) -based MCS while the sensitivity indices are obtained with the PCE-based Sobol solution. Particularly, an active learning algorithm is proposed for the PCE-based sensitivity analysis and is applied to a 10-dimension problem involving hydraulic and geo-mechanical parameters of the dam compacted fill.
- CHAPTER V : this chapter presents the dam probabilistic analysis results obtained in the context of the RF approach. The effect of the horizontal autocorrelation distance on the dam Pf is investigated. Two complementary

studies are conducted: one compares the performance of five reliability methods for high dimensional problems related to the dam, another involves the modelling of different RFs with the available geo-localized data.

- CHAPTER VI: the objective of this chapter is to incorporate the dam 3D geometry in the probabilistic analysis and to investigate its possible impacts on the dam reliability. Therefore, a 3D computational model is constructed and coupled with the probabilistic analysis. The obtained results are compared with those of 2D. Particularly, the effects of input correlation and of using coarse mesh for deterministic models are examined.
- CHAPTER VII: this chapter presents the concluding remarks for the studied dam from a probabilistic analysis point of view, the recommendations for other related studies and the perspectives for possible future works.

The partial contents presented in CHAPTERs III - V were published in two papers ((Guo et al. 2018; Guo et al. 2019)), and there are also two papers under preparation: one about the modelling and comparison of different RFs while another relates to CHAPTER VI.

2 CHAPTER II: Literature review about reliability analysis methods and probabilistic analysis of earth dams

There are two main objectives in this chapter: (1) provide a general review of reliability analysis methods commonly used in geotechnical engineering, including a detailed presentation of the probabilistic approaches employed in this work; (2) provide an overview of previous studies on the probabilistic analysis of earth dams.

Firstly, nine reliability methods, including the classical First/Second - Order Reliability Method, the crude Monte Carlo Simulation and three surrogate modelling techniques, are briefly reviewed. Basic concepts and relevant references are given for each method. Then, some probabilistic approaches that are employed in this work are described in detail. This part covers the methods used for reliability analysis (PCE), global sensitivity analysis (Sobol index) and spatial modelling (different kinds of RFs). The Latin Hypercube Sampling, iso-probabilistic transformation and variogram analysis are also introduced in this part. In the end of this chapter, the previous probabilistic studies on earth dams are reviewed by dividing them into three groups which investigated the following issues: seepage, slope stability and internal erosion.

2.1 A brief review of reliability analysis methods

This section attempts to give a brief overview on the commonly used reliability methods. For the sake of clarity, the methods are classified into three categories: approximation methods, sampling methods and surrogate modelling methods. At the beginning, some basic concepts of reliability analysis are defined and explained.

2.1.1 Some basic reliability concepts

For a structure system in civil engineering, a failure occurs if one of the system responses (e.g. displacement or crack length) exceeds an allowable limit value. The failure can be induced by exceptional loadings such as seism and strong wind, or degradation of material strength.

Considering a system response that can be defined by a random vector (\mathbf{x}) composed of M random variables (x_1, x_2, \dots, x_M), there exists then two regions in the input space defined by the \mathbf{x} : safe R_s and failure R_f . The curve ($M=2$), surface ($M=3$) or hyperplane ($M>3$) which describes the boundary between the two domains (R_s and R_f) is the Limit State Surface (LSS). It is then possible to construct a function ($g(\mathbf{x})$) which can give positive/negative estimates for the safe/failure domain (see Eq. (2-1)). Accordingly, the $g(\mathbf{x})$ equals to 0 if the \mathbf{x} falls on the LSS. This function $g(\mathbf{x})$ is called as Performance Function or Limit State Function (LSF).

$$R_s: g(\mathbf{x}) > 0 \quad (2-1)$$

$$R_f: g(\mathbf{x}) \leq 0$$

The system failure probability (P_f) is defined as the probability of having a response falling into the failure domain. If the input random vector can be described by a joint probability density function ($f_j(\mathbf{x})$), the P_f can be expressed as follows:

$$P_f = \int_{R_f} f_j(\mathbf{x}) d\mathbf{x} \quad (2-2)$$

In general, the LSF is implicit for real-world engineering problems, so it is impossible to directly determine the failure domain R_f . As a result, various techniques were proposed to estimate the P_f through an approximation way (e.g. FORM) or by largely sampling in the input space (e.g. MCS). Some commonly used techniques in the field of geotechnical reliability analysis will be presented later.

Figure 2.1 visualizes the concepts given above within a 2D example. The bold black line in the $x_1 - x_2$ plane is the LSS which leads to $g(\mathbf{x}) = 0$. The ellipses represent the contours of the joint PDF $f_j(\mathbf{x})$ which are obtained by projecting the $f_j(\mathbf{x})$ on the plane. Under such a representation, the P_f is indeed the volume underneath the joint PDF in the R_f region.

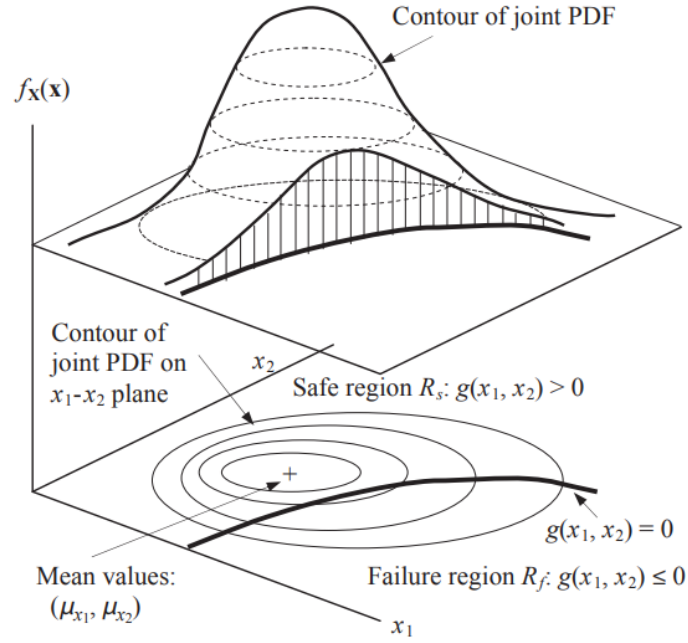


Figure 2.1 Demonstration of the safe/failure region, LSS, joint PDF and P_f (Chang, 2015)

2.1.2 Approximation methods

This class of reliability methods estimates the P_f by approximating the LSS locally at a reference point with a linear or quadratic expansion. The reference point is also called as design point \mathbf{P}^* and is considered as the Most Probable Failure Point (MPFP).

2.1.2.1 First-Order Reliability Method (FORM)

In the FORM, the input random vector \mathbf{x} is firstly transformed to a standard normal vector \mathbf{u} using the iso-probabilistic transformation method (Bourinet, 2018). The design point \mathbf{P}^* is then defined as the point that is on the LSS and closest to the origin of the standard normal space. The norm of \mathbf{P}^* is known as the Hasofer-Lind reliability index β_{HL} (Hasofer and Lind, 1974) and is directly related to the failure probability P_f :

$$P_f \approx \Phi_{SN}(-\beta_{HL}) = \Phi_{SN}(-\|\mathbf{P}^*\|) \quad (2-3)$$

where Φ_{SN} is the standard normal cumulative density function. The Eq. (2-3) is based on approximating the LSF by a hyperplane tangent to the LSS at \mathbf{P}^* and is under the assumption that the LSF is continuous, smooth and differentiable in the MPFP

neighborhood. Figure 2.2 illustrates the above-discussed terms related to the FORM in a standard normal space defined by two variables u_1 and u_2 . The length OP^* is the Hasofer-Lind reliability index (termed as β in Figure 2.2) while the vector \mathbf{a} shows the direction from the origin to the design point. Concerning the LSS, the $G(\mathbf{u})$ is the real one. The $G_1(\mathbf{u})$ and $G_2(\mathbf{u})$ is respectively the approximation made by FORM and SORM which will be presented later.

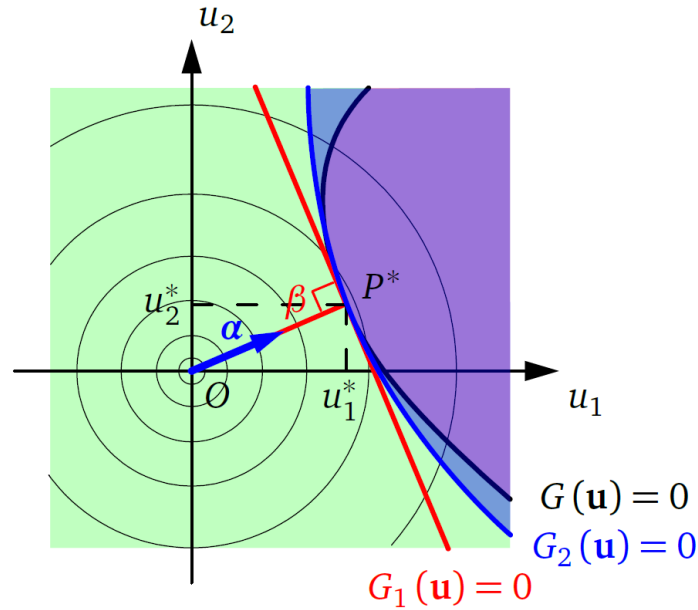


Figure 2.2 Approximation of the LSS by FORM and SORM (Bourinet, 2018)

It can be seen that the main effort of FORM lies in searching the design point \mathbf{P}^* using a suitable optimization algorithm based on the following equation:

$$\mathbf{P}^* = \operatorname{argmin}\{\|\mathbf{u}\|, G(\mathbf{u}) \leq 0\} \quad (2-4)$$

There are several methods available in literature to solve the above optimization problem (Lemaire et al. 2010). Most of them are based on an iterative search procedure, and a search direction along with a step length should be determined for each iteration. The search direction is highly related to the gradient of the LSF and can be assessed by finite differences with choosing a suitable perturbation step which has a significant impact on the convergence rate of the optimization algorithms for solving Eq. (2-4).

It is worth mentioning that the above-mentioned FORM is based on two assumptions: the MPFP is unique and the LSS is linear or weakly nonlinear. If one of the assumptions cannot be fulfilled, the result provided by the introduced FORM could be biased with noticeable errors. The first issue, which concerns the unique MPFP, can be improved by using the FORM developed by Kiureghian and Dakessianb (1998) in which several MPFPs could be considered.

Besides, the squared values of the components in the α vector are indicative for the relative importance of the corresponding random inputs in the standard normal space in the MPFP neighborhood. These α_i^2 values are known as Importance Factor of FORM and effective for independent RVs. For the cases with correlated RVs, further efforts are required to deduce the Important Factors that take into account the correlation structure (Bourinet, 2018).

2.1.2.2 Second-Order Reliability Method (SORM)

The SORM is a second-order refinement of the FORM solution. It approximates the LSS by a tangent hyper-paraboloid at the design point \mathbf{P}^* identified by FORM. The failure probability of the SORM can be regarded as a correction of the FORM result by considering the curvatures of the hyper-paraboloid.

For small curvatures $k_i < 1$, the failure probability Pf can be estimated by the Breitung formula (Breitung, 1989):

$$Pf_B = \Phi_{SN}(-\beta_{HL}) \prod_{i=1}^{M-1} (1 + \beta_{HL} k_i)^{-0.5} \quad (2-5)$$

where M represents the number of input variables. A more accurate computation of Pf is given by the Hohenbichler formula (Hohenbichler et al., 1987):

$$Pf_H = \Phi_{SN}(-\beta_{HL}) \prod_{i=1}^{M-1} \left(1 + \frac{\varphi_{SN}(\beta_{HL})}{\Phi_{SN}(-\beta_{HL})} k_i\right)^{-0.5} \quad (2-6)$$

where φ_{SN} is the standard Gaussian PDF. It is noted that the curvatures of the hyperparaboloid can be estimated by rotating the coordinates system such that one of its axes is the $\boldsymbol{\alpha}$ vector. For more details, readers can refer to Marelli et al. (2019).

2.1.3 Sampling methods

The common idea for this class of methods is to draw samples, randomly or intelligently, from the joint PDF, and then to find a Pf estimate according to the corresponding system responses in the outcome space. Four sampling-based methods, which are commonly used in the field of geotechnical reliability analysis, are presented in the subsequent sections.

2.1.3.1 Monte Carlo Simulation (MCS)

The MCS is an universal method to evaluate the complex integrals such as in Eq. (2-2) (Sudret, 2007). It offers a robust and simple way to estimate the distribution of a system response and then assess the associated Pf . By introducing an indicator function $I_{MC}(\boldsymbol{x})$ of the failure domain (i.e. $I_{MC}(\boldsymbol{x})=1$ if \boldsymbol{x} is located in R_f and $I_{MC}(\boldsymbol{x})=0$ otherwise), the Pf defined in Eq. (2-2) can be rewritten as:

$$Pf = \int_{R_f} f_j(\boldsymbol{x})d\boldsymbol{x} = \int I_{MC}(\boldsymbol{x}) \cdot f_j(\boldsymbol{x})d\boldsymbol{x} = \mathbb{E}[I_{MC}(\boldsymbol{x})] \quad (2-7)$$

where $\mathbb{E}[\cdot]$ represents the mathematical expectation. Practically, Eq. (2-7) can be approximated by the empirical mean of a large number $I_{MC}(\boldsymbol{x})$ values. For a crude MCS with sampling N_{MC} vectors on \boldsymbol{x} , the Pf is given by:

$$Pf \approx \frac{1}{N_{MC}} \cdot \sum_{i=1}^{N_{MC}} I_{MC}(\boldsymbol{x}^{(i)}) \quad (2-8)$$

The number of N_{MC} should be large enough in order to obtain an accurate estimate for the Pf . The coefficient of variation (CoV) of the MCS Pf estimate is given as (Phoon, 2008):

$$CoV_{Pf} = \sqrt{(1 - Pf)/(N_{MC} \cdot Pf)} \cdot 100\% \quad (2-9)$$

It is important to mention that the CoV_{Pf} is independent of the problem dimension (Bourinet, 2018). This independence is a key advantage of the MCS over other reliability methods such as the surrogate modelling. Additionally, the MCS works regardless of the LSF complexity, which is also an advantage over the FORM/SORM. However, a crude MCS suffers from a low computational efficiency. According to Eq. (2-9), around $100/Pf$ model evaluations are required if the target CoV_{Pf} is 10%.

The MCS can also be combined with the finite element method and random fields to assess the statistics of a model response or the Pf of a structure in consideration of the spatially varying properties. In such a specific situation, the method is called ‘random finite element method’ (Fenton and Griffiths, 1993; Griffiths and Fenton, 1993; Li et al., 2016).

2.1.3.2 Importance Sampling (IS)

IS is a powerful tool to reduce the variance of the MCS estimator in problems involving small failure probabilities. The main idea is to replace the original joint PDF by a new one in order to populate the failure domain more frequently.

In the context of IS, Eq. (2-7) can be written in a different manner by introducing a conveniently chosen distribution $H_{IS}(\mathbf{x})$ (called as IS PDF):

$$Pf = \int I_{MC}(\mathbf{x}) \cdot f_j(\mathbf{x}) d\mathbf{x} = \int I_{MC}(\mathbf{x}) \cdot \frac{f_j(\mathbf{x})}{H_{IS}(\mathbf{x})} \cdot H_{IS}(\mathbf{x}) d\mathbf{x} \quad (2-10)$$

The accuracy of the IS-based Pf estimate (Pf_{IS}) is dependent on the choice of the $H_{IS}(\mathbf{x})$. It exists an optimal choice for the IS PDF, which can lead to the minimum of the Pf_{IS} variance. A first solution of finding the optimal $H_{IS}(\mathbf{x})$ is to minimize the Pf_{IS} variance, which involves an optimization procedure. It can also be achieved by adaptively adjusting the IS PDF with wisely-selected samples, such as in the algorithm of Morio (2012). Alternatively, a near-optimal $H_{IS}(\mathbf{x})$ can be found through application of the cross-entropy method (Geyer et al. 2019). For more details about the selection of the $H_{IS}(\mathbf{x})$, readers are invited to refer to Kroese et al. (2011).

In the field of structural reliability, the most common and simple solution to perform the IS is to define a $H_{IS}(\mathbf{x})$ with the help of the design point \mathbf{P}^* that is determined in the FORM. The related $H_{IS}(\mathbf{x})$ reads as:

$$H_{IS}(\mathbf{x}) = f_j(\mathbf{x} - \mathbf{X}_{\mathbf{P}^*}) \quad (2-11)$$

where $\mathbf{X}_{\mathbf{P}^*}$ is the point obtained by transforming back the design point \mathbf{P}^* to the original input space. Indeed, this IS PDF is similar to the original joint PDF $f_j(\mathbf{x})$ but with the mean replaced by the point $\mathbf{X}_{\mathbf{P}^*}$.

2.1.3.3 Subset Simulation (SS)

The SS, also known as adaptive multilevel splitting, consists in solving a series of simpler reliability problems with intermediate failure thresholds (Au and Beck, 2001) in order to estimate the probability of a rare event. The considered failure event E_{SS} is decomposed into a sequence of intermediate events $[E_{SS_1}, E_{SS_2}, \dots, E_{SS_m}]$, each of which is associated with a larger probability of occurrence, and therefore easier to estimate than the original Pf . The estimation of the final Pf in the SS can be written as (Li and Cao, 2016):

$$Pf = P(E_{SS}) = P(E_{SS_1}) \prod_{i=2}^m P(E_{SS_i} | E_{SS_{i-1}}) \quad (2-12)$$

where $P(E_{SS_i} | E_{SS_{i-1}})$ is the conditional Pf of the event $E_{SS_i} | E_{SS_{i-1}}$. Given an initial threshold, $P(E_{SS_1})$ can be easily estimated from a crude MCS with N_{SS} samples. The remaining conditional probabilities can be estimated similarly, but the generated samples should be within the associated intermediate event. The latter can be accomplished by using the modified Metropolis-Hastings Markov Chain Monte Carlo sampling (MCMC) (Au and Beck, 2001; Papaioannou et al., 2015). In practice, the intermediate failure thresholds are selected so that the conditional failure probabilities are equal to P_{SS} which is suggested to be chosen in the range [0.1, 0.3] (Zuev et al., 2012).

As a summary and illustration, Figure 2.3 plots the distribution of the samples generated by the three sampling methods (MCS, IS and SS) for the 'R-S' problem that treated in Marelli et al. (2019). The MCS samples are centered on the mean point and show a great population (i.e. a large number of model evaluations). In the IS, the $H_{IS}(\mathbf{x})$ is defined as Eq. (2-11). As a result, the IS samples are located around the point \mathbf{X}_P^* . The SS samples show clear a 3-level searching process. The first level is indeed a small MCS as shown by the blue samples.

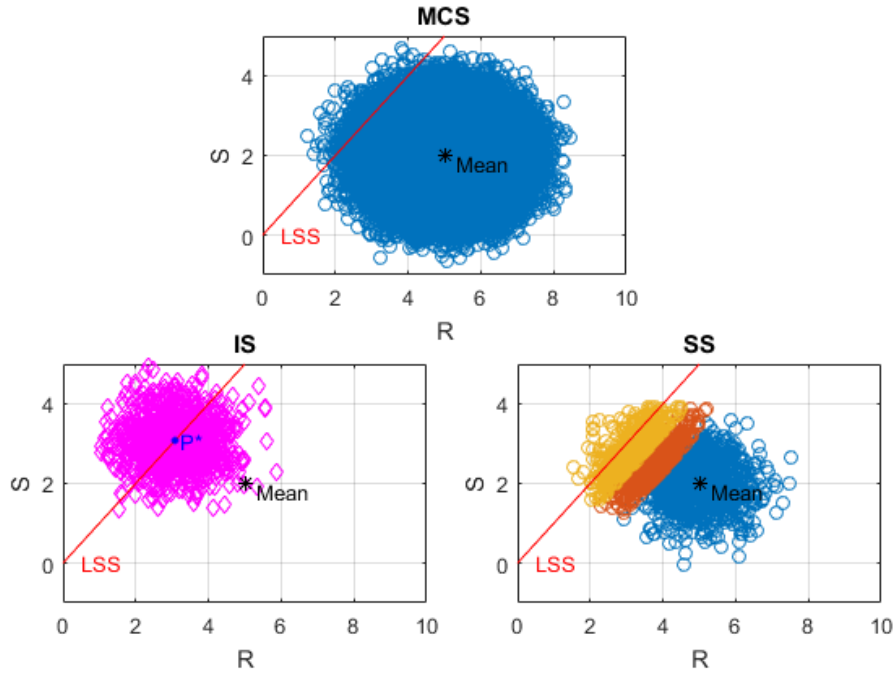


Figure 2.3 Distribution of the samples generated by three reliability methods for a 'R-S' problem

2.1.3.4 Moment methods (MM)

The MM uses the statistical moments of a RV to approximate its distribution (Zhao and Ono, 2001). Once the distribution is determined, the reliability index and failure probability can be obtained easily by assuming a threshold value. A well-known MM is the second moment approximation (abbreviated as MM-2). It assumes that the random model response follows a normal distribution and uses the first two moments to estimate the reliability index which reads as (Babu et al. 2007):

$$\beta_{MM-2} = \frac{\mu_{PF}}{\sigma_{PF}} \quad (2-13)$$

where β_{MM-2} is the reliability index estimated by the MM-2, μ_{PF} and σ_{PF} is respectively the mean and the standard deviation of the $g(\mathbf{x})$ values.

In this work, a fourth moment approximation (noted as MM-4) is also used to perform the reliability analysis since it can give more accurate results compared to the MM-2 (Napa-García et al. 2017). The adopted MM-4 is given as follows (Zhao and Ono, 2001):

$$\beta_{MM-4} = \frac{3(\alpha_{4G} - 1)\beta_{MM-2} + \alpha_{3G}(\beta_{MM-2}^2 - 1)}{\sqrt{(9\alpha_{4G} - 5\alpha_{3G}^2 - 9)(\alpha_{4G} - 1)}} \quad (2-14)$$

where β_{MM-4} is the reliability index estimated by the MM-4, α_{3G} and α_{4G} are respectively the third and fourth central moment of the $g(\mathbf{x})$ values. Eq. (2-14) is obtained by relating the standardized variable of $g(\mathbf{x})$ with the standard normal random variable RV_s through Eq. (2-15) in the context of high-order moment standardization method (Zhao and Ono, 2001).

$$RV_s = \frac{\alpha_{3G} + 3(\alpha_{4G} - 1)g_s(\mathbf{x}) - \alpha_{3G}(g_s(\mathbf{x}))^2}{\sqrt{(5\alpha_{3G}^2 - 9\alpha_{4G} + 9)(1 - \alpha_{4G})}} \quad (2-15)$$

where $g_s(\mathbf{x})$ is the standardized variable of $g(\mathbf{x})$ and is expressed as $g_s(\mathbf{x}) = (g(\mathbf{x}) - \mu_{PF})/\sigma_{PF}$. Once the reliability index is obtained, the associated Pf can be estimated by Eq. (2-3). The required statistical moments ($\alpha_{iG}, i = 1,2,3,4$) in the MM-2 and MM-4 can be determined by a crude MCS which involves repeatedly running the deterministic model for different sets of input parameters until all the desired moments are converged. Alternatively, improved sampling techniques (Napa-García et al., 2017) can be used which focus on estimating the statistical moments in the outcome space by intelligently sampling in the input space. Also, the First-order second-moment (FOSM) (Dolinski, 1982) provides a solution to estimate the first two moments of a model response with a limited number of model evaluations.

2.1.4 Surrogate modelling techniques

The principle of a surrogate-based reliability analysis is to firstly construct a surrogate model (also known as meta-model) with limited calls to the deterministic model, and then to perform a crude MCS (Guo and Dias, 2020) or any other sampling methods (Huang et al. 2016) on the obtained meta-model. The main objective is to reduce the total computational time of a reliability analysis especially for the cases with costly-to-evaluate models or small failure probability. There are several mathematical tools

which are able to build such approximation models with a given set of samples. For structural reliability analysis, the most common methods are based on the three following techniques (Hu and Mahadevan, 2016): the Kriging, the Polynomial Chaos Expansion and the Support Vector Machine. These three surrogate modelling techniques are briefly presented in the following sections. Besides, the active learning process which can further enhance the performance of these techniques in estimating Pf is introduced and commented. In addition to these three techniques, the quadratic polynomial-based Response Surface Methodology (RSM) (Mollon et al. 2009) and the Artificial Neural Network (ANN) (Cho, 2009) can also provide approximations to the LSF of a computational model. However, the RSM requires defining the polynomial forms *a priori*, and the ANN usually relies on a large size of training samples. Therefore, they are not presented in this work.

2.1.4.1 Kriging

The Kriging model is based on the assumption that the performance function $g(\mathbf{x})$ is a realization of a Gaussian Process (GP). It predicts the value of $g(\mathbf{x})$ at unknown points by a combination of $g(\mathbf{x})$ at known points with a random function, which includes a regression part and a stochastic process as follows (Echard et al. 2011):

$$g(\mathbf{x}) = \mathbf{f}_r(\mathbf{x})^T \boldsymbol{\beta}_{AK} + \epsilon(\mathbf{x}) \quad (2-16)$$

where $\boldsymbol{\beta}_{AK}$ is a vector of unknown coefficients, $\mathbf{f}_r(\mathbf{x})$ is a vector of regression functions, $\mathbf{f}_r(\mathbf{x})^T \boldsymbol{\beta}_{AK}$ is the trend of prediction or mean of the GP, and $\epsilon(\mathbf{x})$ is assumed to be a GP with zero mean and covariance $Cov[\epsilon(\mathbf{x}^{(i)}), \epsilon(\mathbf{x}^{(j)})]$:

$$Cov[\epsilon(\mathbf{x}^{(i)}), \epsilon(\mathbf{x}^{(j)})] = \sigma_\epsilon^2 R(\mathbf{x}^{(i)} - \mathbf{x}^{(j)}, \boldsymbol{\theta}_K) \quad (2-17)$$

where σ_ϵ^2 is the constant variance of the GP, $\boldsymbol{\theta}_K$ is a vector of unknown parameters, and $R(.,.)$ is the correlation function which describes the spatial correlation between observations and new points. A valid correlation function needs to satisfy two

conditions, saying that the $R(.,.)$ should be symmetric and positive semi-definite. There are many functions which have been proven effective for these two conditions such as the constant, Gaussian and Matérn functions (Lataniotis et al. 2018).

For the construction of a Kriging surrogate model, a set of experimental design (ED) should be provided for the estimation of the hyper-parameters which can be achieved by an optimization procedure (e.g. Genetic algorithm) performed on the cross-validation error (Lataniotis et al., 2018). The term ED refers to a number of input samples and their corresponding model responses, which are used to determine a surrogate model in the field of metamodeling.

2.1.4.2 Support Vector Machine (SVM)

The SVMs are a class of learning techniques which are able to classify the random model responses into a desired number of classes. Particularly, the binary classification is of great interest for reliability analyses since it may label safety and failure domains (Bourinet, 2018). Let us consider firstly the case where the data are linearly separable in the original space of the input random variables. An infinite number of hyperplanes that separate the data may be identified. Considering a possible hyperplane (the SVM decision function) (Pan and Dias, 2017a):

$$f_{svm}(\mathbf{x}) = \boldsymbol{\omega}^T \mathbf{x} + b = 0 \quad (2-18)$$

where $\boldsymbol{\omega}$ is perpendicular to the hyperplane and b is a scalar factor. The optimal hyperplane is the one that has the largest distance to the nearest training samples (maximum margin). The margin can be calculated by $2/\|\boldsymbol{\omega}\|$ (Bourinet, 2018). Then, it consists in maximizing the margin which in turn equivalent to the following equation:

$$\min_{\boldsymbol{\omega}} 0.5\|\boldsymbol{\omega}\|^2 \quad (2-19)$$

$$\text{Subject to: } y_i (\boldsymbol{\omega}^T \mathbf{x}^{(i)} + b) - 1 \geq 0, i = \{1, 2, \dots, N_{ED}\}$$

where N_{ED} is the number of training samples (i.e. size of the ED) and $y_i = \{-1, 1\}$ indicates the class of each training point. The optimization constraint of Eq. (2-19) ensures that there is no training sample existing inside the margin. For data which are non-linearly separable, the solution is to map them into a higher dimensional space (also known as feature space). The optimal separating hyperplane can then be determined in this space. This operation is carried out through a kernel function which is constructed under some rules so as to guarantee the existence of an underlying mapping (Moustapha et al., 2018).

The SVM was firstly introduced in the context of the binary classification as discussed above. It was later extended to regression by using the ϵ -insensitive loss function (Vapnik et al. 1997). Readers can refer to Bourinet (2018) for more details about the SVM used in regression.

2.1.4.3 Polynomial Chaos Expansions (PCE)

In PCE, the meta-model is built by expanding the system response on a suitable basis which is a series of multivariate polynomials. By definition, a model response, having a finite variance, can be expanded as follows (Blatman and Sudret, 2010):

$$Y \cong \sum_{\alpha \in \mathbb{N}^M} \mathbf{k}_\alpha \Psi_\alpha(\boldsymbol{\xi}) \quad (2-20)$$

where $\boldsymbol{\xi} = \{\xi_1, \xi_2, \dots, \xi_M\}$ are independent RVs, $\Psi_\alpha(\boldsymbol{\xi})$ are multivariate polynomials, \mathbf{k}_α are unknown coefficients to be computed and $\boldsymbol{\alpha} = \{\alpha_1, \dots, \alpha_M\}$ is a multidimensional index. The multivariate polynomial $\Psi_\alpha(\boldsymbol{\xi})$ is the tensor product of univariate orthonormal polynomials $\psi_{\alpha_i}(\xi_i)$. There are several families for the orthogonal univariate polynomials such as the Legendre polynomials and the Hermite polynomials (Sudret, 2014).

In practice, the representation of Eq. (2-20) needs to be truncated to a finite number of terms. The standard truncation scheme consists in selecting all the multivariate polynomials whose total degree $|\alpha|$ are less than a given p . The related formula reads as:

$$A^{M,p} = \left\{ \alpha \in \mathbb{N}^M : |\alpha| = \sum_{i=1}^M \alpha_i < p \right\} \quad (2-21)$$

Once the truncated basis is selected, the coefficients $\{k_\alpha\}_{\alpha \in A^{M,p}}$ shall be computed using the Least Angle Regression (LAR) method introduced in Blatman and Sudret (2011). The accuracy of the PCE can be estimated by the empirical mean-square residual error and the leave-one-out error ε_{LOO} (Blatman and Sudret, 2011).

2.1.4.4 Adaptive algorithms for surrogate modelling

It is found that constructing a surrogate model with only one set of ED is not enough in the sense that the region of interest is difficult to be covered except if a big sample size is given to the ED . Such a region refers to the vicinity of the LSS in a reliability analysis and usually corresponds to a low probability. In light of this, the idea of building a surrogate model by gradually enriching an initial ED was come out. In the past decade, various algorithms were developed under this idea to enhance the efficiency and accuracy of surrogate-based reliability analysis. Examples can be found in Echard et al. (2011), Marelli and Sudret (2018) and Pan and Dias (2017a) for respectively the Kriging, PCE and SVM.

All the developed algorithms share a same procedure in principle and can be illustrated by Figure 2.4. There are two important elements for an adaptive surrogate-based reliability analysis: learning function and stopping condition. The former consists in finding the next sample to be added in the current ED so that the meta-model can be improved in estimating the Pf . The latter is used to stop the ED enrichment process when the current surrogate model is accurate enough.

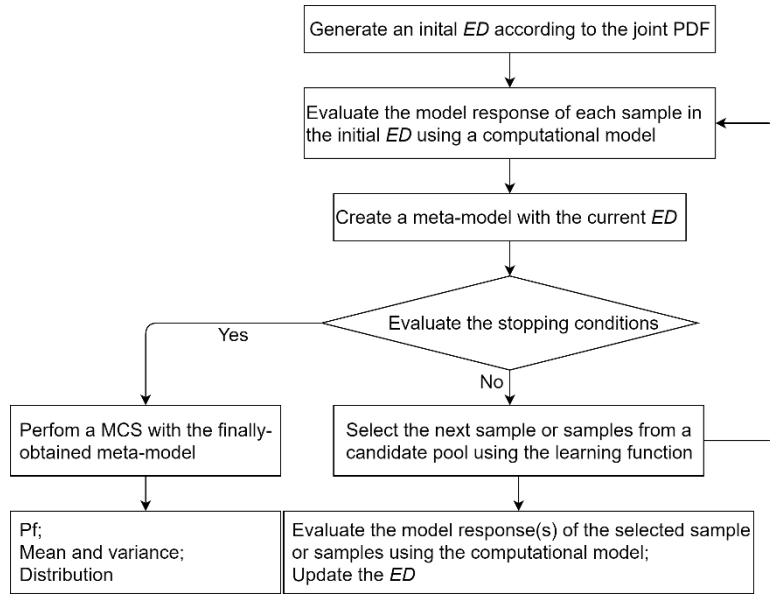


Figure 2.4 Flowchart of an adaptive surrogate modeling combined with MCS for reliability analysis

2.2 Detailed presentation of the methods employed in this work

This section aims to present in detail the probabilistic methods employed in this thesis. It starts with the PCE which is used, in different forms, throughout the work for the dam reliability analysis. Then, the Sobol-based Global Sensitivity Analysis (GSA) is introduced, which is utilized to identify the input parameters having a significant impact on the variance of the dam safety factor (FoS) values. It is followed by the RF generation methods. Three techniques are presented for three kinds of RFs which will be used in CHAPTER V. At the end, other techniques, including the iso-probabilistic transformation, the Latin Hypercube Sampling and the variogram analysis, that also contribute to the present work, are presented and discussed.

2.2.1 PCE, SPCE and adaptive SPCE

2.2.1.1 Basic concepts of the PCE

As presented before, the PCE approximates a model response by means of a series of multivariate polynomials $\Psi_{\alpha}(\xi)$ which are orthonormal with each other so that they can form a basis in the Hilbert space (Sudret, 2014). The random response can be completely determined by its coordinates (i.e. k_{α} in Eq. (2-20)) in this basis. The $\Psi_{\alpha}(\xi)$

is formed by univariate orthonormal polynomials $\psi_{\alpha_i}(\xi_i)$. Table 2.1 gives a summary of the common $\psi_{\alpha_i}(\xi_i)$ families and their associated distribution type for the input RVs. Concerning the truncation scheme on the PCE terms, the standard method shown in Eq. (2-21) is inefficient especially for high dimensional problems. In order to tackle this problem, another technique, called as the hyperbolic truncation scheme, was proposed by Blatman and Sudret (2011). It defines a so-called q -quasi-norm and requires the norm to be smaller than the maximum degree p . The corresponding truncated PCE set reads as:

$$A^{M,p,q} = \left\{ \boldsymbol{\alpha} \in \mathbb{N}^M : |\boldsymbol{\alpha}|_q = \left(\sum_{i=1}^M \alpha_i^q \right)^{\frac{1}{q}} < p \right\} \quad (0 < q < 1) \quad (2-22)$$

The case $q = 1$ corresponds to the standard truncation set $A^{M,p}$ of Eq. (2-21). As shown in Blatman and Sudret (2011), the size of the hyperbolic truncation set $A^{M,p,q}$ may be smaller by 2-3 orders of magnitude than the one of the standard truncation scheme.

The unknown coefficients $\{\mathbf{k}_{\boldsymbol{\alpha}}\}_{\boldsymbol{\alpha} \in A^{M,p,q}}$ can be computed using a regression approach. Based on the least-square regression method, the unknown coefficients can be given by (Blatman and Sudret, 2010):

$$\hat{\mathbf{k}} = (\Phi^T \Phi)^{-1} \Phi^T \hat{\mathbf{Y}} \quad (2-23)$$

where $\hat{\mathbf{k}}$ represents the column vector of the unknown coefficients $\{k_1, \dots, k_L\}^T$, $\hat{\mathbf{Y}}$ is the model evaluations of the input random vectors $\{\mathbf{x}^{(1)}, \dots, \mathbf{x}^{(N_{ED})}\}$ in the ED , and Φ is a PCE-independent data matrix of dimension $N_{ED} \times L$. It is defined by (Blatman and Sudret, 2010):

$$\Phi_{ij} = \left(\Psi_{\alpha_j}(\mathbf{x}^{(i)}) \right)_{\substack{i=1, \dots, N_{ED} \\ j=0, \dots, L-1}} \quad (2-24)$$

The accuracy of the truncated PCE can be assessed by computing the coefficient of determination R^2 and the Q^2 indicator. The former is related to the empirical error Err_e using the model responses already existing in the ED , and can be expressed as:

$$R^2 = 1 - \frac{Err_e}{Var[\hat{Y}]} \quad (2-25)$$

where $Var[\hat{Y}]$ is the variance of the full model responses in the ED . The Q^2 is obtained with the leave-one-out (LOO) cross-validation technique. The idea consists in using each sample in the ED as a single validation point for the meta-model constructed with the remaining $N_{ED} - 1$ samples. Computation of the Q^2 is given as follows:

$$Q^2 = 1 - \frac{\frac{1}{N_{ED}} \sum_{i=1}^{N_{ED}} [\hat{Y}^{(i)} - M^{PCE \setminus i}(\mathbf{x}^{(i)})]^2}{Var[\hat{Y}]} \quad (2-26)$$

where $M^{PCE \setminus i}(\mathbf{x}^{(i)})$ represents the prediction at the sample $\mathbf{x}^{(i)}$ made by the PCE which is built by the ED excluding the $\mathbf{x}^{(i)}$. For efficient solutions of estimating the Q^2 , readers can refer to Blatman (2009).

Table 2.1 Classical families of univariate orthogonal polynomials (Sudret, 2014)

RV distribution	Orthogonal polynomials	Hibertian basis
Uniform	Legendre $P_k(x)$	$\frac{P_k(x)}{\sqrt{\frac{1}{2k+1}}}$
Gaussian	Hermite $H_{e_k}(x)$	$\frac{H_{e_k}(x)}{\sqrt{k!}}$
Gamma	Laguerre $L_k^a(x)$	$\frac{L_k^a(x)}{\sqrt{\frac{\Gamma(k+a+1)}{k!}}}$
Beta	Jacobi $J_k^{a,b}(x)$	$\frac{J_k^{a,b}(x)}{\mathfrak{S}_{a,b,k}}$

2.2.1.2 Sparse PCE

The Sparse PCE (SPCE) is an extension of the PCE methodology. It was proposed by Blatman and Sudret (2008, 2010, 2011) for the purpose of further reducing the number of the involved $\Psi_\alpha(\xi)$ after the truncation operation when dealing with a high

dimensional stochastic problem. The idea came from the fact that the non-zero coefficients in the PCE form a sparse subset of the truncation set obtained by the hyperbolic truncation scheme (Sudret, 2014). Thus, it consists in building a suitable sparse basis instead of computing useless terms in the expansions that are eventually negligible. Figure 2.5 shows an example of the PCE coefficients in the truncated set $A^{M,p}$ with a max degree of 14 for the *Ishigami* problem (Marelli and Sudret, 2019). Clearly, a large number of coefficients are negligible since their ratios to the mean are rather small ($<10^{-14}$). The significant coefficients (e.g. ratio $>10^{-8}$) form indeed a sparse basis of the $A^{M,p}$.

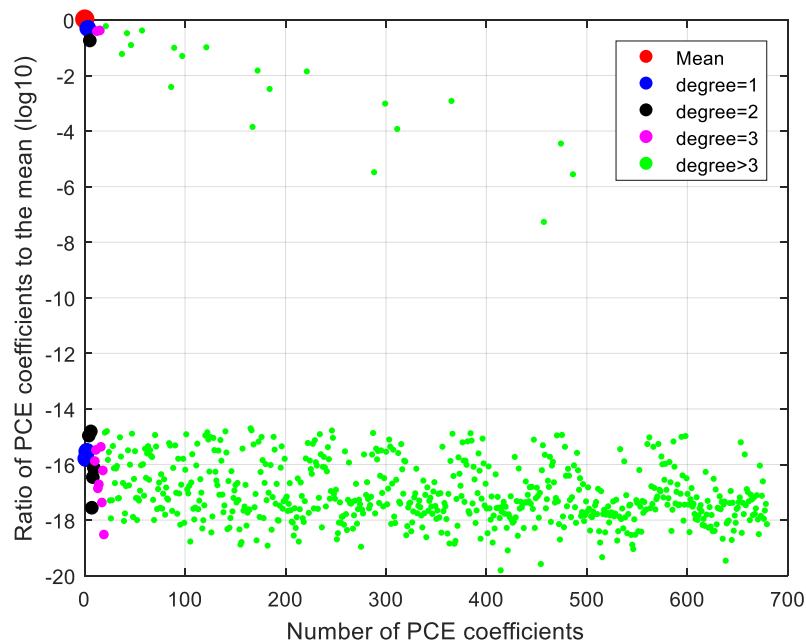


Figure 2.5 PCE coefficients in $A^{M,p}$ with a max degree of 14 for *Ishigami* problem (Marelli and Sudret, 2019)

The procedure for building a SPCE proposed by Blatman and Sudret (2010) is based on an iterative procedure to reach a minimal number of unknown coefficients. This procedure is described in Table 2.2. For other approaches of determining a sparse subset of PCE, readers can refer to (Papaioannou et al. 2019; Tipireddy and Ghanem 2014; Tsilifis et al. 2020).

Table 2.2 The procedure of obtaining a sparse representation of the PCE

Step	Description
1	Select an initial experimental design χ and collect the model evaluations \hat{Y} by performing the deterministic model at each sampling point.
2	Prescribe a target accuracy Q_{tg}^2 , the maximal PCE degree P_{max} and the cut-off values $\varepsilon_1, \varepsilon_2$.
3	For any $p \in \{1, \dots, p_{max}\}$: <div style="margin-left: 2em;">Forward step: compute the increase in the determination coefficient R^2 by adding each candidate $\Psi_\alpha(\xi)$ from a PCE basis set ($A^{M,p}$ or $A^{M,p,q}$). Retain eventually those candidate terms that lead to a significant increase in R^2, i.e. greater than ε_1. Let $A^{p,+}$ be the final truncation set at this stage.</div> <div style="margin-left: 2em;">Backward step: compute the decrease in R^2 by removing each candidate term in $A^{p,+}$ of degree not greater than p. Discard eventually from $A^{p,+}$ those terms that lead to an insignificant decrease in R^2, i.e. less than ε_2. Let A^p be the final truncation set.</div>
3-1	
3-2	
3-3	If $Q_{A^p}^2 \geq Q_{tg}^2$, stop

2.2.1.3 The adaptive SPCE for reliability analysis

The accuracy indicators R^2 and Q^2 mentioned above can be used to measure the global behavior of the obtained PCE model. However, it lacks a local error estimate which can provide statistics (e.g. variability or confidence bounds) for each PCE predictions. Kriging-based methods can rely on the Kriging variance for this task, but PCEs do not provide a natural equivalent (Marelli and Sudret, 2018). To address this issue, the bootstrap resampling technique was implemented into the PCE by Marelli and Sudret (2018) to derive a local error estimator. The rationale can be briefly presented as follows.

Firstly, a reference experimental design is generated from the input space. It includes N_{ED} vectors of \mathbf{x} and is noted as $ED^{(ref)}$. The corresponding model responses are evaluated by a computational model and are represented by a vector of \hat{Y} . Secondly, B new ED s are generated based on the $ED^{(ref)}$ by the bootstrap resampling technique. This is achieved by randomly assembling B times N_{ED} realizations of $\mathbf{x}^{(i)}$ ($i = 1 \dots N_{ED}$) and the relating $\hat{Y}^{(i)}$. For one of the new ED s, it is possible to have a same

input vector for zero, one or more times. It is noted that the $\hat{\mathbf{Y}}^{(i)}$ in the B new EDs are already available since the $\mathbf{x}^{(i)}$ is selected from the reference one ($ED^{(ref)}$). Finally, B different PCEs can be constructed with the new EDs . For the points which are not included in the $ED^{(ref)}$, it exists then B possible predictions by the PCEs. Therefore, empirical quantiles can be employed to provide local error bounds on the PCE prediction for such points. In the case of SPCE, performing B times sparse least-square analysis can be time-consuming. Marelli and Sudret (2018) proposed a fast bootstrap-PCE for this problem. It assumes that the sparse polynomial basis identified by the $ED^{(ref)}$ is effective for all the new EDs . The sparse least-square analysis is performed thus only one time and the bootstrapping is applied only to the unknown coefficient ($\hat{\mathbf{k}}$) estimation which is based on a classic ordinary least-square. This assumption was checked by several academic examples and found effective (Marelli and Sudret, 2018). For the sake of clarity, the bootstrap-based SPCE is noted as bSPCE in this work.

As discussed in section 2.1.4, the metamodeling-based reliability analysis can be enhanced by an adaptive experimental design algorithm. The introduced local error estimates by the bootstrap technique provide a solution for the learning function and the stopping condition that could be used in an active learning SPCE. In this work, the stopping condition proposed by Marelli and Sudret (2018) is adopted, which focuses on the stability of the Pf values estimated by the B SPCE models at each iteration. The formula is as follows:

$$\frac{P_f^+ - P_f^-}{P_f} \leq \varepsilon_{Pf} \quad (2-27)$$

where ε_{Pf} is an acceptance threshold with a range between 0.05 and 0.15 for typical usage scenarios (Marelli and Sudret, 2018), Pf is the failure probability estimated with the SPCE which is based on the full set of the $ED^{(ref)}$, and P_f^+ and P_f^- is respectively the maximum and minimum of the Pf values provided by the B different SPCE models.

Marelli and Sudret (2018) suggested stopping the active learning procedure when the condition of Eq. (2-27) is satisfied for two continuous iterative steps. The learning function (Marelli and Sudret, 2018) adopted in the work is based on the probability of misclassification of a candidate sample. For the sample $\mathbf{x}^{(i)}$ ($i = 1 \dots N_{mc}$), the value of its learning function can be represented as follows:

$$LF_{bSPCE}(\mathbf{x}^{(i)}) = \left| \frac{Num_S(\mathbf{x}^{(i)}) - Num_F(\mathbf{x}^{(i)})}{B} \right| \quad (2-28)$$

where B is the number of the bootstrap SPCE models, while $Num_S(\mathbf{x}^{(i)})$ and $Num_F(\mathbf{x}^{(i)})$ represent respectively the number of safe and failure for the B different estimates at the sample $\mathbf{x}^{(i)}$. The ‘best’ next sample to be added into the ED can be identified by finding the sample which can minimize the value of the learning function. Table 2.3 provides a full procedure of the adaptive SPCE (termed as AbSPCE) for reliability analysis.

Table 2.3 The procedure of a reliability analysis performed by the AbSPCE

Step	Description
1	Generate a Monte Carlo population in the input space using the Latin Hypercube sampling. It is noted as \mathbf{S}_{MC} and composed of N_{mc} samples.
2	Generate an initial experimental design ED_{ini} with N_{ini} samples using Latin Hypercube sampling. Then, evaluate the corresponding model responses \hat{Y} by a computational model.
3	Construct an SPCE surrogate model based on the current experimental design.
4	Evaluate the failure probability Pf by performing an MCS with the current SPCE model.
5	Generate B sets of new EDs and construct B SPCE models.
6	Evaluate the stopping condition of Eq. (2-27) for the adaptive experimental design algorithm. If the condition is not satisfied, continue to next step. Otherwise, directly go to step 8.
7	Choose the 'best' next sample from \mathbf{S}_{MC} according to the learning function of Eq. (2-28). Update the current ED with the selected sample and the corresponding model response. Return to step 3.
8	Compute the uncertainty related to the estimated Pf by Eq. (2-9). If the CoV_{Pf} is smaller than 5%, continue to next step. Otherwise, enrich the MC population \mathbf{S}_{MC} with N_{add} samples and return to step 4.
9	Post-processing on the MCS results to obtain the PDF and statistics of the model response

2.2.2 Sobol-based global sensitivity analysis

In a probabilistic analysis, it is also of interest to quantify how each input RV contributes to a given quantity of interest (QoI). The Global Sensitivity Analysis (GSA), which focuses on assessing the sensitivity of the QoI with respect to each RV over its entire varying range, is a powerful tool to achieve this purpose. Among many methods for performing a GSA, the Sobol' indices have received much attention since they can give accurate results for most models (Sudret, 2008), and are adopted in the present work. This section is intended to present the Sobol-based GSA and provide two solutions for estimating the Sobol indices: one within the framework of MCS and the other appeals to the PCE.

The Sobol index is based on the variance decomposition of the model output. The decomposition formula reads as (Iooss and Lemaître, 2015):

$$\begin{aligned} \mathcal{F}(x_1, \dots, x_M) = & \mathcal{F}_0 + \sum_{i=1}^M \mathcal{F}_i(x_i) \\ & + \sum_{i<j}^M \mathcal{F}_{ij}(x_i, x_j) + \dots + \mathcal{F}_{1,\dots,M}(x_1, \dots, x_M) \end{aligned} \quad (2-29)$$

where $\mathcal{F}(\cdot)$ is the computational model, M is the number of the input variables, \mathcal{F}_0 is a constant and equals to the expectation of $\mathcal{F}(\mathbf{x})$ and $\mathcal{F}_i(x_i)$ is a function only concerned with the variable x_i and by the analogy for others (e.g. $\mathcal{F}_{ij}(x_i, x_j)$). Eq. (2-29) expands indeed the model $\mathcal{F}(\cdot)$ to a series of functions which are related to one or more variables from (x_1, \dots, x_M) . The total variance of the model output is given as:

$$V_t = \int \mathcal{F}(\mathbf{x})d\mathbf{x} - \mathcal{F}_0^2 \quad (2-30)$$

Analogously, this total variance can be decomposed as follows:

$$V_t = \sum_{i=1}^M V_i(Y) + \sum_{i<j}^M V_{ij}(Y) + \dots + V_{1,\dots,M}(Y) \quad (2-31)$$

where $Y = \mathcal{F}(x_1, \dots, x_M)$ is the model output, $V_i(Y) = Var[\mathbb{E}(Y \parallel x_i)]$, $V_{ij}(Y) = Var[\mathbb{E}(Y \parallel x_i, x_j)] - V_i(Y) - V_j(Y)$ and so on for higher order interactions (Iooss and Lemaître, 2015). For the $Var[\mathbb{E}(Y \parallel x_i)]$, the inner expectation operator $\mathbb{E}(\cdot)$ is the mean of Y considering all possible $x_{\sim i}$ values while keeping x_i constant; the outer variance $Var(\cdot)$ is taken over all possible values of x_i . Then, the first-order Sobol index is given:

$$S_i = \frac{V_i(Y)}{V_t} \quad (2-32)$$

The S_i is a measure about the effect of the variable x_i alone. By replacing the term $V_i(Y)$ of Eq. (2-32) by $V_{ij}(Y)$ or others, higher-order Sobol indices can be obtained which take into account the interaction effects among different variables. There is also the total Sobol index for a variable x_i , which represents the sum of all the Sobol indices involving this variable. The definition can be written as:

$$S_{Ti} = S_i + \sum_{i \neq j} S_{ij} + \dots S_{1,\dots,M} \quad (2-33)$$

The following sections provide two numerical approaches to estimate the first-order and total Sobol indices.

2.2.2.1 Sobol index obtained from the crude MCS

The first approach is within the framework of MCS. The idea is to evaluate the conditional moments (e.g. $Var[\mathbb{E}(Y \parallel x_i)]$) with sampling on the input joint PDF.

Consider two independent sampling matrices \mathbf{A} and \mathbf{B} , with a_{ji} and b_{ji} as generic elements. Each of them contains N_s numbers of input vectors \mathbf{x} , so N_s rows and M colomuns. A new matrix $\mathbf{A}_B^{(i)}$ is introduced which means that all the columns are from the \mathbf{A} except the i -th column which is from the \mathbf{B} . Then, the computation of the first-order and total Sobol indices can be derived from the following equations which estimate the desired conditional moments (Saltelli et al., 2010).

$$\begin{aligned} V_i &= \frac{1}{N_s} \sum_{j=1}^{N_s} \mathcal{F}(\mathbf{B})_j \mathcal{F}(\mathbf{A}_B^{(i)})_j - \mathcal{F}_0^2 \\ V_{\sim i} &= \frac{1}{N_s} \sum_{j=1}^{N_s} \mathcal{F}(\mathbf{A})_j \mathcal{F}(\mathbf{A}_B^{(i)})_j - \mathcal{F}_0^2 \end{aligned} \quad (2-34)$$

where V_i is the model output variance induced only by the variable x_i and $V_{\sim i}$ represents the variance without considering the x_i variation. Then, the first order Sobol

index can be simply calculated by Eq. (2-32). For the one of total effect, it can be estimated as $S_{Ti} = 1 - S_{\sim i} = 1 - V_{\sim i}/V_t$. It is observed that all the desired results (S_i and S_{Ti}) could be available with a triplet of matrices \mathbf{A} , \mathbf{B} and $\mathbf{A}_B^{(i)}$. Therefore, the total model evaluation number is $N_s \cdot (M + 2)$. The N_s should be large enough in order to have accurate estimates. At least the N_s should be equal to 500 according to Saltelli et al. (2010), while Iooss and Lemaître (2015) suggested to use a N_s of 10 000 which is associated with an uncertainty of 10%.

2.2.2.2 PCE-based Sobol index

The second approach to estimate the Sobol indices is based on the PCE meta-model. The idea was proposed by Sudret (2008) for a purpose of reducing the total computational time of a Sobol-based GSA. It is achieved by post-processing on the PCE coefficients to estimate the Sobol indices. Once a PCE model is available, no further deterministic calculation is needed. For example, the first-order Sobol index is given as follows:

$$S_i = \frac{\sum_{\alpha \in A_i} (k_j)^2 \mathbb{E}[(\Psi_\alpha)^2]}{\sum_{\alpha \in A} (k_j)^2 \mathbb{E}[(\Psi_\alpha)^2]} \quad (2-35)$$

where k_j are the PCE coefficients, A is the truncation set ($A^{M,p,q}$), A_i is a subset of A in which the multivariate polynomials are only functions of the random variable x_i and $\mathbb{E}[(\Psi_\alpha)^2]$ is the expectation of $(\Psi_\alpha)^2$. For the computation of high-order and total Sobol indices, readers can refer to Sudret (2008). In summary, once the PCE coefficients are determined, the complete list of Sobol indices are available analytically. The main computational burden of this approach lies in constructing an accurate PCE model.

2.2.2.3 Correlated variables

The above-presented Sobol decomposition holds only for independent variables. Extra efforts are required to generalize the Sobol-based GSA for correlated variables. Xu and

Gertner (2008) proposed to divide the variance contribution of x_i into two parts: one considers only the independent variation while the other includes the contribution due to the correlation with other variables. Kucherenko et al. (2012) proposed to directly decompose on the output variance by considering the conditional samples. The MCS estimation techniques are also available for the Kucherenko indices.

2.2.3 Random-fields generation

The RF theory is widely used for describing the soil spatial variability in geotechnical engineering. Theoretically, an accurate RF can be represented by an infinite set of RVs. In practice, the RF domain should be discretized into a grid in order to allow a representation by a finite set of RVs. There are mainly three groups of methods for RFs discretization: point discretization, average discretization and series expansions (Sudret and Der Kiureghian, 2000).

For a stationary Gaussian RF, it can be completely described by its mean μ , variance σ^2 and an autocorrelation function $\rho(\mathbf{x}, \mathbf{x}')$ (Baecher and Christian, 2005) such as the exponential one which is expressed below:

$$\rho(\mathbf{x}, \mathbf{x}') = \exp\left(-\frac{|x - x'|}{L_x} - \frac{|y - y'|}{L_z}\right) \quad (2-36)$$

where (x, y) and (x', y') are the coordinates of two arbitrary points in the RF space, L_x and L_z are respectively the horizontal and vertical autocorrelation length. The autocorrelation length is defined as the distance which can lead to a decrease from 1 to $1/e$ for the autocorrelation function.

The objective of this section is to present the methods that are used in CHAPTER V to generate the three kinds of RFs: generic, conditional and nonstationary RFs.

2.2.3.1 *Generating stationary unconditional RFs by the Karhunen-Loève expansion*

The Karhunen-Loève expansion (K-L) method is part of the third group mentioned above: series expansions, and has been widely used in geotechnical problems such as slopes (S. Cho, 2009), tunnels (Pan and Dias, 2017b) and foundations (Ahmed and Soubra, 2014). According to Sudret and Der Kiureghian (2000), the methods in this group can lead to the minimal number of RVs involved in the discretization, which is an attractive feature for reliability analysis since the input dimension is limited.

The K-L method is based on the spectral decomposition of the autocovariance function $C(\mathbf{x}, \mathbf{x}')$ which is the autocorrelation function $\rho(\mathbf{x}, \mathbf{x}')$ multiplied by the standard deviation $\sigma(\mathbf{x})$ and $\sigma(\mathbf{x}')$. This function, being symmetrical and positive definite, by definition, has all its eigenfunctions mutually orthogonal, and they form a complete orthogonal basis of Ω . Any realization of $H(\mathbf{x}, \theta)$ in Gaussian distribution can thus be expanded over this basis as follows (Sudret and Der Kiureghian, 2000):

$$\begin{aligned}
 H(\mathbf{x}_{RF}, \theta) &= \mu + \sigma \sum_{i=1}^{\infty} \sqrt{\lambda_i} \phi_i(\mathbf{x}_{RF}) \xi_i(\theta) \\
 &\cong \mu + \sigma \sum_{i=1}^{S_{KL}} \sqrt{\lambda_i} \phi_i(\mathbf{x}_{RF}) \xi_i(\theta)
 \end{aligned}
 \tag{2-37}$$

where \mathbf{x}_{RF} is the point location in the RF domain, $\{\xi_i(\theta), i = 1, \dots\}$ denotes the coordinates of the realization θ of the RF in the expanded space, λ_i and ϕ_i are the eigenvalues and eigenfunctions of the autocovariance function respectively and S_{KL} is the size of the series expansion. The term $\xi_i(\theta)$ is, in fact, a set of uncorrelated standard normal variables as long as the realization of the RF is fixed. The value of S_{KL} strongly depends on the desired accuracy, the autocorrelation length and the RF size. It can be determined by evaluating the error estimation of the truncated series expansion. The

error estimate based on the variance of the truncated error for a K-L expansion with S_{KL} terms is given by (Phoon, 2008):

$$\varepsilon = \frac{1}{\Omega} \int_{\Omega} \left[1 - \sum_{i=1}^{S_{KL}} \lambda_i \phi_i^2(\mathbf{x}_{RF}) \right] d\Omega \quad (2-38)$$

where Ω is the RF domain.

For the cases of non-Gaussian RFs, one can obtain them by performing an isoprobabilistic transformation, which will be presented later in section 2.2.4, on the Gaussian RFs of the K-L expansions as shown in Eq. (2-37). The cross-correlation between different RFs can also be accounted for as discussed in Al-Bittar (2012).

For the sake of illustration, Figure 2.6 presents two standard normal RFs generated by the K-L expansions for a 20m×20m site. The left one is an isotropic RF with $L_x = L_z = 10m$ while the right one is anisotropic with $L_x = 5m$ and $L_z = 1m$. They require respectively 150 and 1800 RVs to reach an error of around 5%. These numbers are determined by using Eq. (2-38) and represent indeed the size of the series expansions S_{KL} . It can be observed that the left RF is more homogeneous than the right one. Besides, there are some zones with relatively uniform or slightly varied values in the isotropic RF. In contrary, the stochastic values vary rapidly even within short distances for the right RF. The anisotropic character is also clearly demonstrated by this RF.

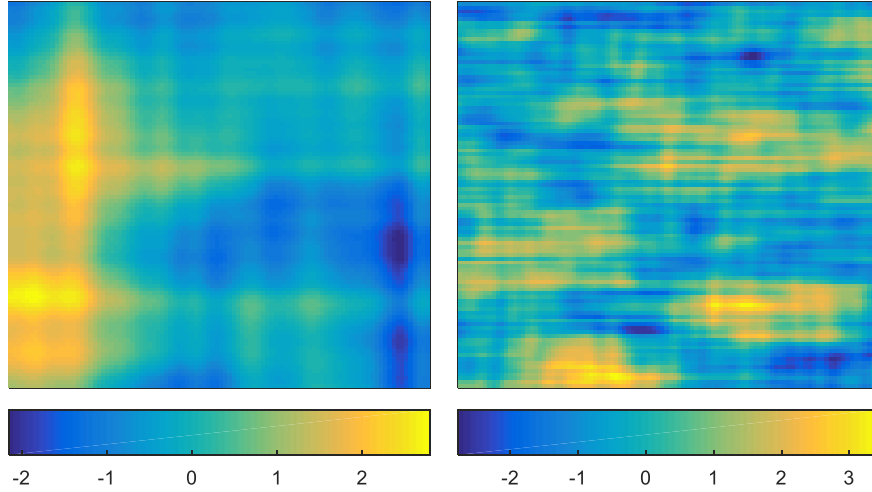


Figure 2.6 Two standard normal RFs generated by the K-L expansions with different autocorrelation distances (left: $L_x=10\text{m}$, $L_z=10\text{m}$; right: $L_x=5\text{m}$, $L_z=1\text{m}$)

2.2.3.2 Kriging-based conditional RFs

The generated RFs by the K-L expansions are all unconditional which means that the measured data and their location information are not taken into account. Geo-localized measurements are commonly encountered in geotechnical engineering and are project-specific. This section presents a method which can generate the RFs conditioned on known data.

Suppose that the random field $RF(x, y)$ has been measured at the points $[(x_1, y_1), (x_2, y_2), \dots, (x_{\mathcal{P}}, y_{\mathcal{P}})]$ and should be simulated at points $[(x_{\mathcal{P}+1}, y_{\mathcal{P}+1}), (x_{\mathcal{P}+2}, y_{\mathcal{P}+2}), \dots, (x_n, y_n)]$. The aim of conditional RF simulations is then to produce $RF(x, y)$ realizations which exactly match the data at \mathcal{P} points and are randomly generated at the remaining $(n - \mathcal{P})$ points. In this work, the algorithm proposed by Griffiths and Fenton (2007) is adopted to achieve this purpose. Application of the algorithm in geotechnics can be found in Liu et al. (2017b) and Lloret-Cabot et al. (2012). This algorithm combines the Kriging model and the theory of unconditional RFs. The procedure is given in Table 2.4 for a conditional RF of one soil property. It can be seen that the final conditional RF ($RF_c(x, y)$) exactly matches with the measured

data at the known locations with zero variance. This means that the measurements errors are ignored in the produced conditional RF. For the unknown locations, the term $[RF_{un}(x, y) - RF_{k-un}(x, y)]$ represents a random deviation which increases with the separation distance between the unknown and known points. In this algorithm, it is assumed to use a same autocorrelation structure for the three component RFs (RF_k , RF_{un} and RF_{k-un} in Table 2.4). This can be improved by determining the correlation length in the Kriging RF with an optimization process and estimating the autocorrelation structure of the third RF for each simulation with a variogram analysis (presented later). Obviously, extra computational efforts are required for this solution so the initial assumption is kept. Then, the Kriging type (e.g. simple or ordinary) also needs to be selected by users. A discussion on this issue is provided in section 5.3.2.

The best linear unbiased estimates (BLUE), that is involved in Table 2.4, is an approach to provide a best estimate of the soil properties between known data (locations of measurements). The basic idea is to estimate the values of a $RF(x, y)$ at any point using a weighted linear combination of the observations. Suppose that $[X(x_1, y_1), X(x_2, y_2), \dots, X(x_p, y_p)]$ are known data of the RF. Then, the BLUE of $RF(x, y)$ is given by:

$$RF(x_i, y_i) = \sum_{j=1}^p \beta_j^i * X(x_j, y_j) \quad (2-39)$$

where the vector of weight coefficient β^i is to be determined. The goal is to find the best estimate at a particular point. It seems reasonable that if the point (x_i, y_i) is close to one of the known locations, saying (x_k, y_k) , then the weight coefficient β_k^i would be high. The covariance between the two points is thus employed to determine the weights in Eq. (2-39). In the case where the mean and the standard deviation are constant for the whole field, the system equations of BLUE can be written as follows,

$$\begin{aligned}
& \begin{bmatrix} \mathbf{K} & \mathbf{I} \\ \mathbf{I}^T & 0 \end{bmatrix} \begin{bmatrix} \boldsymbol{\beta} \\ \lambda \end{bmatrix} = \begin{bmatrix} \mathbf{k} \\ 1 \end{bmatrix} \\
& \mathbf{K} = \begin{bmatrix} K_{11} & K_{12} & \cdots & K_{1p} \\ K_{21} & K_{22} & \cdots & K_{2p} \\ \vdots & \vdots & \cdots & \vdots \\ K_{p1} & K_{p2} & \cdots & K_{pp} \end{bmatrix} \\
& \boldsymbol{\beta} = [\beta_1^i \quad \beta_2^i \quad \cdots \quad \beta_p^i]^T \\
& \mathbf{k} = [K_{i1} \quad K_{i2} \quad \cdots \quad K_{ip}]^T, (i \in [p+1, n])
\end{aligned} \tag{2-40}$$

where \mathbf{K} is the Kriging covariance matrix; \mathbf{I} is a column vector of all ones with a length of \mathcal{P} ; $\boldsymbol{\beta}$ is the vector of weights of the known data; \mathbf{k} is the vector of covariance between the estimated point and the known points; and λ is a Lagrange multiplier. It is noted that K_{ij} is the covariance between any two points, which can be determined by an autocorrelation function.

Table 2.4 Procedure of the adopted conditional RFs generator

Step	Description
1	Determine the probabilistic distributions and statistics (e.g., means, standard deviations, and autocorrelation structure) of the soil property.
2	Collect the information of the measured data, including the values of soil properties and the corresponding data locations. Then, transform the collected data to standard Gaussian samples by using the iso-probabilistic method (Lebrun and Dutfoy, 2009a).
3	Compute the BLUE of the field at the unknown points according to the measured data. This is a Kriging estimate and is called here as $RF_k(x, y)$.
4	Generate a standard Gaussian unconditional random field $RF_{un}(x, y)$ using the autocorrelation structure determined in step 1 with the K-L expansions.
5	Compute the BLUE of the unknown points by regarding the $[RF_{un}(x_1, y_1), RF_{un}(x_2, y_2), \dots, RF_{un}(x_p, y_p)]$ as known data. That is to say, a BLUE field $RF_{k-un}(x, y)$ from the generated unconditional RF is produced.
6	Produce the standard Gaussian conditional RF by combining the three fields: $RF_c(x, y) = RF_k(x, y) + [RF_{un}(x, y) - RF_{k-un}(x, y)]$.
7	Transform the standard Gaussian conditional RF to the desired distribution type using the iso-probabilistic method with the distribution and statistics of step 1.

2.2.3.3 Modelling of nonstationary RFs

It is well known that natural soil properties often exhibit non-stationary characteristics (Wu et al., 2019), such as linearly increasing mean value with depths for the undrained cohesion. In those cases, using non-stationary RFs is more appropriate for describing soil variability than stationary RFs. A non-stationary RF means that the mean, standard deviation or auto-covariance is not constant for the whole RF domain, but depends on its location. The most commonly used non-stationary RF is the one with a linearly increasing mean along depth. For generating such RFs, the algorithm proposed for the Lognormal distribution (Zhu et al., 2017) is given in Table 2.5. It was then modified by Jiang and Huang (2018) to consider the uncertainty in the increasing rate t_{non} . It can also be extended to other kinds of distributions by replacing the scaling factor of step 2 with an iso-probabilistic process.

Table 2.5 Procedure for generating non-stationary random fields (Zhu et al., 2017)

Step	Description
1	Determine the linear trend with depth z_{non} according to the available measurements. The trend is defined by the mean at the ground surface μ_{non_0} and an increasing rate t_{non} .
2	Generate initially a stationary RF with the μ_{non_0} and other stationary parameters. Call this field as RF_{non_0} .
3	The values at grid points of the RF_{non_0} are adjusted in order to account for the variation of mean by using a scaling factor and the obtained RF reads as: $RF_{non} = \left(\frac{\mu_{non_0} + t_{non} \cdot z_{non}}{\mu_{non_0}} \right) \cdot RF_{non_0}$

2.2.4 Other techniques related to the performed probabilistic analysis

This section presents some other techniques that are also implemented in the probabilistic analysis of the present work.

2.2.4.1 Latin Hypercube Sampling (LHS)

In a probabilistic analysis, one needs to draw a number of samples from a specific distribution. This is related to sampling strategies such as the true random sampling

(also called as standard Monte Carlo) and the Latin Hypercube Sampling (LHS) (Helton and Davis, 2003) which is adopted in the present work.

The LHS was first proposed by McKay et al. (1979) and has been widely used in recent years for the uncertainty propagation. It can be viewed as a combination between the true random sampling and the stratified sampling (Helton and Davis, 2003) since many desirable features of the two sampling techniques are included in the LHS. In a first step of the LHS, the range of each RV is exhaustively divided into N_{LHS} , with N_{LHS} being the desired sample size, disjoint intervals of equal probability. Then, one value is randomly selected from each interval for the variable x_1 . What comes to next is to pair the N_{LHS} values of x_1 , at random, with the N_{LHS} values obtained identically for the x_2 . This process is continued until a set of N_{LHS} M -tuples is formed with M being the variables' number. These tuples constitute the Latin Hypercube samples. The above-presented procedure is effective for independent variables. For the cases of correlated variables, the method developed by Iman and Conover (1982) in the context of LHS can be used.

Compared with the true random sampling, the LHS performs better in space-filling and thus can avoid missing some important subsets of the input space which have low probability but high impacts on the analysis of uncertainty (Helton and Davis, 2003). Additionally, it has been demonstrated by previous studies (Olsson and Sandberg, 2002; Sandberg and Olsson, 1999) that the LHS is efficient for estimating mean values and standard deviations in stochastic structural analysis. Above all, the LHS is of great interest for the probabilistic analysis which involves small sample size, such as the surrogate modelling. Figure 2.7 compares the LHS with the true random sampling (MC) for drawing 50 samples from the 'R-S' problem (Marelli et al., 2019). It can be seen that some samples in MC are highly close with theirs neighbours. This phenomenon is unfavourable for uncertainty analysis since two similar samples usually give similar

outputs which are not good for capturing the model global behaviour. In contrary, using the LHS can avoid such issue. There are also some limitations for the LHS such as the aspects of correlation and variance reduction (Shields and Zhang, 2016). However, the LHS is widely used in the field of reliability analysis and can provide reasonable estimates for most cases.

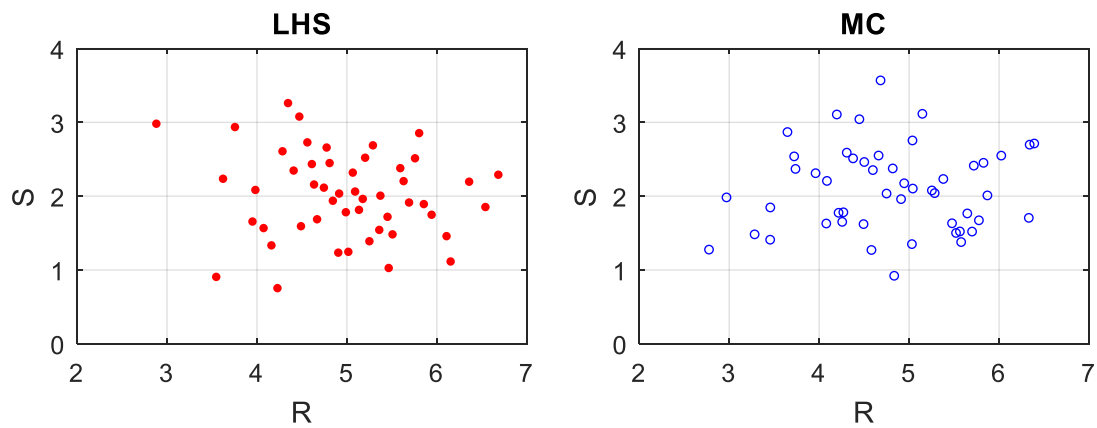


Figure 2.7 50 samples drawn by the LHS and the MC for the ‘R-S’ problem

2.2.4.2 Iso-probabilistic transformation

In some cases, there is a need of transforming the input variables into a specific space defined by a desired joint distribution. For example, it is required to work in the independent standard Gaussian space in the FORM.

For uncorrelated marginal distributions, it can be achieved by a simple iso-probabilistic transformation expressed as follows:

$$u_i = uCDF_i^{-1}(xCDF_i(x_i)) \quad (2-41)$$

where x_i and u_i is respectively the value before and after the transformation for the i -th variable, $xCDF_i$ and $uCDF_i$ is respectively the cumulative density function (CDF) of the original and desired distribution for the i -th marginal and $uCDF_i^{-1}$ means the inverse CDF. In the case of dependent variables, the Nataf or Rosenblatt transformation

should be used to properly transform a sample to the desired space (Lebrun and Dufloy, 2009a, 2009b).

2.2.4.3 Variogram analysis

A variogram is a function which provides a description of how data are spatially correlated. The first step of a variogram analysis is to construct an experimental variogram which describes the correlation between any two values of the observation data separated by a distance h . The experimental semi-variogram γ^* is defined as (Baecher and Christian, 2005):

$$\gamma^*(h) = \frac{1}{2N_h} \sum_h (Va_i - Va_j)^2 \quad (2-42)$$

where $Va_i - Va_j$ represents all the possible pairs of samples which are separated with a distance of h , and N_h is the number of the pairs of $Va_i - Va_j$. This calculation should be repeated for as many different values of h as the observation data will support. Then a mathematical model is applied to the experimental semi-variogram in order to represent an autocorrelation structure over the whole study area and to estimate the autocorrelation distances. One of the most common variogram models is the exponential one, which is used in this study and its equation is (Baecher and Christian, 2005):

$$\gamma(h) = C[1 - e^{-(3h/a)}] \quad (2-43)$$

The parameter a represents the range of the variogram (also called autocorrelation distance), and C is the sill value at which the variogram levels off. The nugget is the intercept of the variogram and represents the small-scale variability of the data which can include, to some content, the measurement error. Figure 2.8 shows the characteristics of a variogram analysis. It provides a solution to estimate the autocorrelation distance defined as the length beyond which the spatial correlation is

only slightly remarked. This can be translated as the distance (or larger than it) leads to significant scattered data in space, e.g. the maximum variance shown in Figure 2.8.

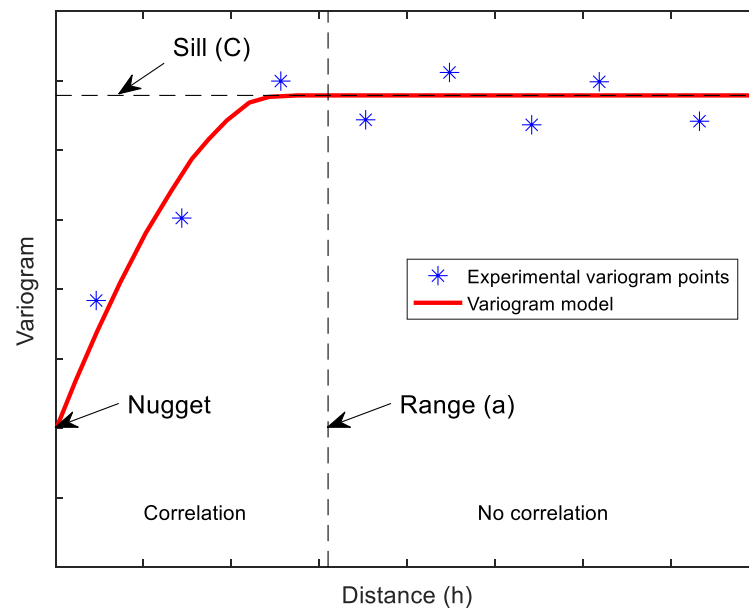


Figure 2.8 Characteristics of a variogram analysis

2.3 Previous studies about probabilistic analysis of earth dams

This section aims to provide a general review of the existing studies dealing with earth dam problems in a probabilistic framework. The concerned studies are divided into three groups corresponding to three major research topics within earth dams: (1) Stochastic seepage analysis; (2) Dam reliability analyses regarding its stability; (3) Probabilistic analysis of dams' failure due to internal erosion. Besides, other studies that do not belong to any of the three groups are presented as well in this section.

2.3.1 Stochastic flows

The first group focuses on stochastic flows inside earth dams by considering the variabilities of soil hydraulic parameters. Fenton and Griffiths (1996) statistically studied the free surface flow in earth dams accounting for the spatial soil permeability variability. The statistics of the flow rate and free surface drawdown were estimated within an MCS framework. Besides, an empirical approach was proposed to predict the mean and variance of the flow rate in order to avoid performing a large number of flow

calculations. The same authors (Fenton and Griffiths, 1997) continued their works on investigating stochastic flows inside earth dams and focused on the variation of hydraulic gradients. Two homogeneous dams with a horizontal filter drain were considered. The results showed that the flow exit point was conservatively estimated in a deterministic analysis. The authors also suggested installing a filter drain which is longer than $\frac{1}{4}$ of the dam base and has a permeability value 120 times the one of the dam body, in order to ensure that the dam inner flows are insensitive to the permeability variations. Ahmed (2009) studied the free surface flow through earth dams using a finite element model with a focus on quantifying the flow rate statistics. The soil hydraulic conductivity (K_s) was modelled by lognormal RF. It was observed that increasing the horizontal scale of fluctuation led to increase in the flow. Le et al. (2012) modelled the soil porosity (correlated with K_s and water retention) of an earth embankment by lognormal RFs and investigated its effects on the flow rate and time to reach steady state in an unsaturated context. They found that increasing the standard deviation or correlation length of the porosity RF can lead to a decrease of the mean value of the time to reach steady state and to an increase of the mean value of flow rate. Cho (2012) performed a series of probabilistic seepage analyses on a homogeneous earth dam by modelling the K_s as RFs. The results revealed that the influence of the autocorrelation distances on the seepage behaviour was dependent on the dominant component of the flow vector. For example, the horizontal autocorrelation distance effect is significant for the mean flow rate, since the dominant flow is horizontal in the dam body. Besides, it was found that assuming two layers (i.e. two independent RFs) for the dam body led to smaller mean and standard deviation estimates of the flow rate compared to a single layer. Calamak et al. (2012) investigated the variation of the free flow surface inside a homogeneous earth dam due to the K_s spatial variability. Four coefficients of variation for the K_s were considered and four locations, which represent different distances to the upstream hydrostatic loading, were observed for the statistical representation of the flow head. The authors concluded that the free surface variation increased in the flow

direction, and the probability distribution of the phreatic head may not be Gaussian especially for highly variable K_s . Calamak et al. (2013) continued working on the K_s spatial variability but treated a zoned earth dam within an unsaturated flow condition. It showed that the flow rate passing through a zoned dam is mostly affected by the K_s in the core part. If the mean K_s of the core is low enough, the uncertainty in the flow rate will be insignificant. Liu et al. (2017) compared different autocorrelation functions (ACF) for a seepage problem through an embankment. They concluded that the single exponential ACF may underestimate the seepage flow rate while the results provided by the squared exponential one are conservative. Overall, the differences between different ACFs are not significant according to this study. Mouyeaux et al. (2019) established a RF representation of the K_s for a real earth dam by exploiting field data with a geostatistical manner. It was then coupled in a random finite element framework to estimate the probabilistic distribution of the pore water pressure and phreatic surface. As an illustration, Figure 2.9 shows a result obtained by Calamak et al. (2013). It shows the free surface and contours of the water head for a stochastic soil with spatially varying K_s . The considered K_s variation in the Core zone is higher than the one of the Shell. Therefore, it leads to an irregular phreatic surface in the clay zone as shown in the figure.

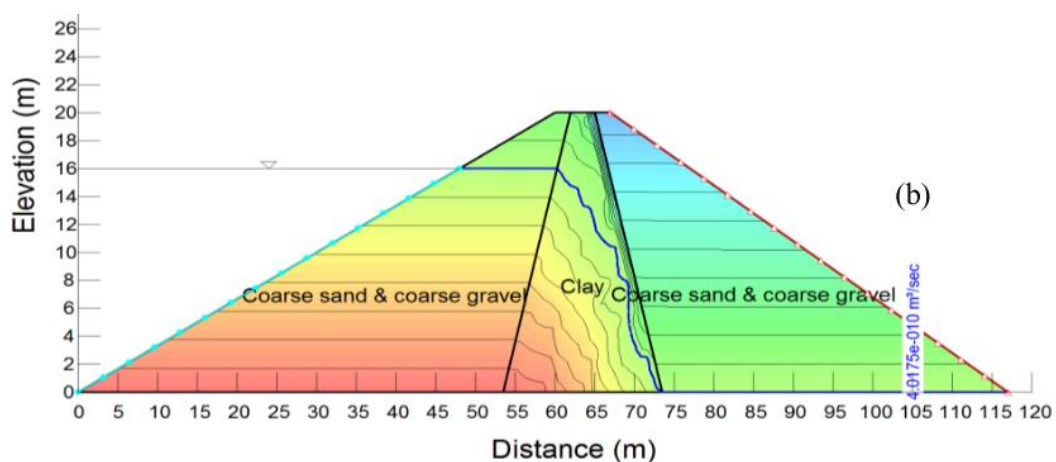


Figure 2.9 Water head contour in a zoned dam considering spatially varying K_s (Calamak et al., 2013)

2.3.2 Slope stability of dams

The second group deals with the slope stability issue of earth dams in the context of reliability analysis. Liang et al. (1999) proposed an algorithm combining the FOSM and Fellenius limit equilibrium method to theoretically derive the reliability index. They applied this approach to the King Talal embankment dam to assess the dam reliability with respect to the stability of the upstream and downstream slopes under different loading conditions (e.g. rapid drawdown). Gui et al. (2000) studied the effects of the K_s variability on the slope stability of a homogeneous embankment dam. The MCS and the FOSM were used for respectively performing the probabilistic analysis and estimating the dam reliability index. Al-Homoud and Tanash (2004) investigated the Karameh dam reliability using the proposed probabilistic 3D slope stability analysis model (based on the FOSM). The uncertainties in the soil shear strength parameters and pore water pressure were considered by analysing the monitoring data. Ghanem et al. (2007) applied the polynomial chaos representation method to a benchmark problem related to earth dams. A strict safe condition was adopted for estimating the dam failure probability, saying that the failure was considered to occur if at least one point of the dam body satisfied the Mohr-Coulomb criterion. Preziosi (2008) presented a reliability analysis of a small earth-fill dam with respect to its stability (upstream and downstream slopes). In addition to the soil variabilities, the uncertainties of the dam geometry (height and crest width) and the upstream hydraulic loadings were also taken into account for the reliability analysis which was based on the FOSM. Babu and Srivastava (2010) investigated the reliability of four rehabilitated earth dams, by using the RSM in combination with the FORM. They found that the variabilities in the geotechnical parameters, in peak ground acceleration value and in the full reservoir water level, had a significant influence on the estimates of the dam reliability index. Nishimura, et al. (2010) presented a reliability-based design of an earth dam by using the MCS. The spatial variability of the soil strength parameters was determined by considering the measurements. An improvement for the design was evaluated in a reliability context

and the failure costs were estimated. Chen and Chang (2011) probabilistically examined the stability condition of a 314m-high earth dam, the Shuangjiangkou dam which is currently under construction and will be the highest embankment dam in the world. A critical slip surface was firstly determined and then a MCS was used to estimate the dam reliability index under different design scenarios with or without considering some of the following factors: spatial variability of the soil shear strength parameters, fluctuation of the phreatic line inside the dam, normal reservoir water level and upstream slope. Calamak and Yanmaz (2014) conducted a probabilistic stability analysis on a homogeneous earth dam regarding its instability of both upstream and downstream slopes by using the MCS in combination with the Limit Equilibrium Method (LEM). The uncertainties of the soil hydraulic conductivity and shear strength parameters were accounted for. They found that using a deterministic seepage flow model leads to higher P_f estimates. The results also shown that the Janbu method (Janbu, 1973) was the most conservative one giving the lowest reliability indices, whereas the Morgenstren-Price (Morgenstern and Price, 1965) is the least conservative. Mouyeaux et al. (2018) presented a probabilistic stability analysis of an earth dam using field data. They focused on quantifying the FoS statistics of the dam by considering three proposed calculation configurations.

In addition to earth dams, extensive research papers are available in literature for the probabilistic stability analysis of slopes. Examples include those in which the uncertainties of soil shear strength parameters (Cho 2007; Griffiths et al. 2009), the rainfall effects (Cho 2014; Yuan et al. 2019), or the seismic loadings (Burgess et al. 2019; Rathje and Saygili 2008) were implemented. These studies also provided useful information and results for the slope problem of earth dams. For an illustration, Figure 2.10 presents two failure mechanisms of a slope that were obtained in Griffiths et al. (2016) within a MCS with stochastic shear strength parameters.

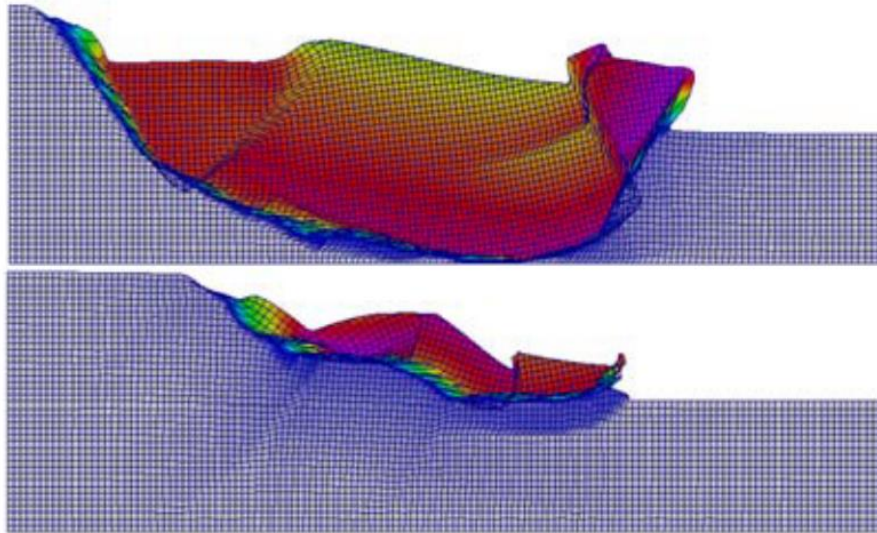


Figure 2.10 Two failure mechanisms of a slope considering stochastic parameters (Griffiths et al., 2016)

2.3.3 Internal erosion

The third group investigates the dam failure due to internal erosion (sometimes called as piping) which refers to the loss of soil particles by seepage forces (Zhang et al., 2016). Four different mechanisms can be identified for internal erosion: concentrated leak erosion, backward erosion, soil contact erosion, and suffusion (Zhang et al., 2016). Foster et al. (2000b) introduced a method (termed as UNSW) for estimating the likelihood of failure of earth dams due to piping in a preliminary assessment stage. The UNSW was based on adjusting the historical piping failure frequency with weighting factors which can be determined by the geometry, soil properties and monitoring data of the studied dam. A summary about the occurred piping failures in embankment dams was given. Mínguez et al. (2006) assessed the filter system reliability, a way of preventing internal erosion in dams, by regarding different empirical criteria. The variability of base material and filter particle sizes was considered by means of FORM. Schweckendiek et al. (2014) proposed a method for updating the uncertainty modelling of resistance parameters and the failure probability estimates related to uplift and piping. The field performance observations during historical loadings, was considered by the Bayesian Inference to conduct the updating. Andreini et al. (2016) developed probabilistic models for two soil erosion parameters, the critical shear stress and the

coefficient of erosion. The non-cohesive and cohesive contributions were both considered. The proposed models were further calibrated using laboratory testing data within a Bayesian framework. An application of the models was shown via the reliability analysis of a typical earth dam. The probabilities of the erosion initiation and no-detection for the dam were estimated considering two probabilistically-simulated erosion parameters. Liang et al. (2017) conducted a probabilistic study on the piping considering the spatial variability of three parameters (the void ratio, K_s and content of the movable particles) by using the MCS. An index describing the probability of seepage instability was proposed and further extended to develop a risk rating system. Andreini et al. (2019) proposed probabilistic models for the concentrated leak erosion in earth dams. A Bayesian approach combined with an IS simulation was implemented into the models for calibrating the model parameters using laboratory and in-situ data. According to Foster et al. (2000b), a failure induced by piping involves mainly three stages: initiation of piping, backward erosion and breach mechanism (e.g. settlement leading to overtopping). Figure 2.11 demonstrates these three stages in a homogeneous dam.

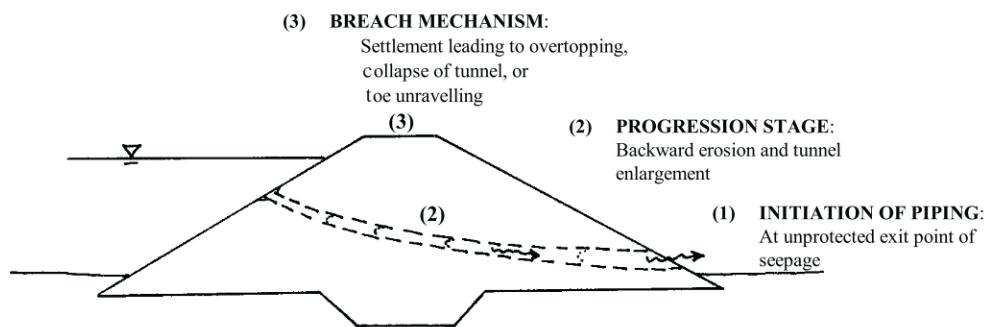


Figure 2.11 Three stages for a failure by piping (Foster et al., 2000b)

2.3.4 Other existing studies

As mentioned before, some existing studies cannot be classified into any of the three former groups. Therefore, they are collected herein and briefly described as follows. Foster et al. (2000a) provided an overall statistical analysis of failures in embankment dams constructed before 1986. The results showed that the embankment zoning have a

significant impact on the occurrence of piping and slope instability. In general, the dams of homogeneous earth-fill, earth-fill with filter, or concrete face earth-fill have experienced more problems associated with the two aforementioned failure modes. U.S. Army Corps of Engineers (2006) provided a guidance for reliability analysis and risk assessment of embankment dams. The failure modes related to seepage (e.g. piping and heave) and slope instability were considered. Carvajal et al. (2009) proposed a probabilistic model for modelling the floodwater level in a dam reservoir. It permitted to generate numerous hydrological scenarios close to the reality of observed hydrological events, and to consider the seasonal variabilities in the headwater level. Having such a model could be useful to incorporate the variation of the hydraulic loadings into a reliability analysis of dams. Kartal et al. (2011) focused on the crack of the upstream slab in a concrete-faced rockfill dam (CFRD) from a probabilistic point of view. The RSM, based on a quadratic function without mixed terms, in combination with the MCS was adopted to perform the probabilistic analysis. It was found that the deterministic and probabilistic results were comparatively close each other for the empty reservoir condition. Pang et al. (2018) evaluated the seismic performance of high CFRDs considering stochastic ground motions. The generalized probability density evolution method combined with the spectral representation-random function method was used to assess the CFRDs with respect to three aspects: deformation, slope stability and face-slab safety.

As the present study focuses on the stability of an earth dam, the probabilistic analysis of concrete dams is not included in the review. Readers can refer to (Hariri-Ardebili, 2018; Hariri-Ardebili and Sudret, 2019) in which reviews on concrete dams are available.

2.4 Conclusion

The commonly used reliability analysis methods are reviewed at first in this chapter. The approximation methods (F/S-ORM) have been widely used in practical engineering due to their efficiency and ease of implementation such as in a spreadsheet environment (Low and Tang, 2007). However, they may fail in giving accurate Pf estimates if the LSS is complex (e.g. highly non-linear). In contrast, the sampling methods perform better in giving accurate results but require much more computational efforts. The third category of reliability methods (meta-modelling) can potentially address the above-encountered issues if a satisfied surrogate model can be obtained. The efficiency and accuracy of these methods in estimating Pf can be further improved by an adaptive experimental design algorithm.

In a second part, the probabilistic methods that are used in this work are presented in detail. Firstly, the PCE technique is presented for different forms: basic PCE, sparse PCE and adaptive sparse PCE. These techniques are used in CHAPTERs IV, V and VI, combined with the MCS, to perform the dam reliability analyses. Secondly, the Sobol-based GSA is introduced. It allows quantifying the contribution of each soil property on the variance of the dam FoS as shown in CHAPTERs IV and VI, and reducing the input dimension as in CHAPTER V. Thirdly, the RFs generators which are used in CHAPTER V are described to produce three kinds of RFs: generic, conditional and nonstationary. At the end, three techniques that have also been used in the following chapters are presented. The LHS is adopted in the work to draw samples for the MCS and the PCE meta-model construction. The iso-probabilistic method serves at transforming samples between different distribution types, while the variogram analysis is used in CHAPTER III to estimate the autocorrelation distance of the soil dry density according to the measurements.

Besides, a review on the previous studies of earth dam probabilistic analyses is given. Three major issues, seepage, slope stability and piping, were considered. The number of the conducted works is limited (around 30) regarding the great population of earth dams in the world and the importance of such structures for economy and human safety. Additionally, most of the studies were based on a simple homogenous dam with hypothetical data, and used the traditional reliability methods (e.g. MCS or FORM) for the uncertainty propagation. Global sensitivity analysis, 3D probabilistic analysis and spatial modelling by different types of RFs were seldom performed for dams, as discussed in *Introduction*. The present work is partially motivated by these facts to present a probabilistic analysis (reliability and sensitivity) of the stability of a real zoned dam by using various reliability methods and different kinds of RFs with exploiting the available field data.

3 CHAPTER III: Soil variability modelling and computational model development

This chapter aims to present the necessary elements required for the probabilistic stability analysis of the considered dam: input uncertainty representation and deterministic model. Firstly, the studied dam is briefly described. A horizontal pseudo-static acceleration is introduced for the calculation scenario in order to account for seismic loading effects on the dam. Then, the uncertainties of the soil properties are quantified by analysing the available measurements. Three soil parameters (density γ_d , cohesion c' and friction angle ϕ'), which are highly relevant to the dam stability, are modelled with means of RVs or RFs. The Beta and Truncated normal distributions are selected to describe the soil variabilities due to their nature of bounding extreme values. At the end, three computational models are developed for estimating the dam FoS values. The two first models are based on the strength reduction method and are combined respectively with finite element and finite difference method. The last one employs the limit equilibrium method and genetic algorithm to estimate the dam FoS.

3.1 Presentation of the studied dam

The studied dam, constructed in 1998, is a 23.8 m high earth-filled dam located in the west of France. The width is around 140 m and the length in the 3rd dimension is 170 m for the crest. The dam closes a valley covered with alluvial deposits and can retain a reservoir of about 5×10^6 m³. The normal and maximal reservoir water level is respectively 20 and 21.6 m. This work focuses on the dam stability under steady state flow conditions and the reservoir water level is fixed at a level of 20m. The soil is assumed to be saturated. Such an assumption is based on the two following reasons: (1) quantifying the variability in the soil unsaturated parameters is a difficult task given that there is no enough support data; (2) considering a saturated flow instead of an unsaturated one would lead to lower FoS estimates thus give conservative Pf results.

Figure 3.1 presents the main cross section of the dam. It can be seen that the dam is formed by three different zones including a core constituted with sandy silts and two

backfill zones constituted with gravelly sands in respectively the upstream and downstream part of the core. These three zones are respectively named as Core, Shell-1, and Shell-2 in this work. A vertical and an horizontal drain were installed in the downstream part in order to collect the water flows and to lower the phreatic surface inside the dam. In the foundation, a waterproof grout curtain was realized with a depth of around 15 m.

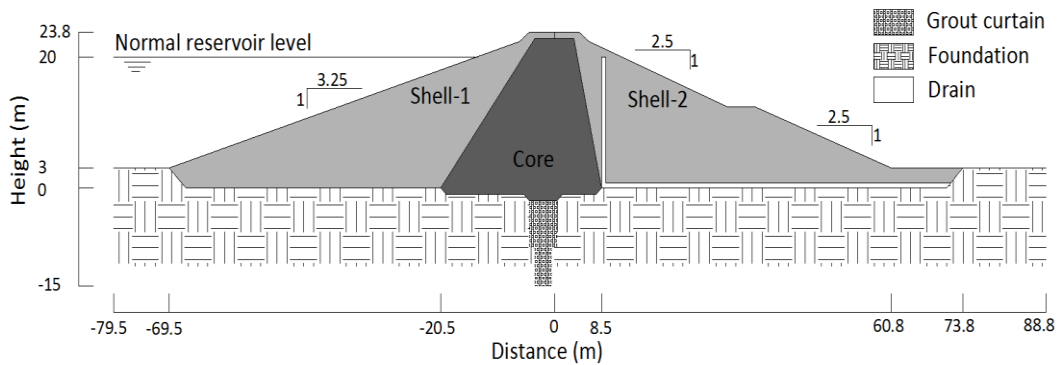


Figure 3.1 The main cross section of the studied dam

The materials constituting the dam were collected from the vicinity of the dam site. Two different types of soils can be identified in the valley. The first type is gravelly sands resulting from the alteration of shales on slopes and uplands which dominate the valley. The foundation of the dam is considered as gravelly sands according to the site investigation. This material is used for the construction of the Shell zone. The second soil type, the sandy silts, can be found on the bottom of the valley and on the slopes. It was used for the construction of the Core zone. Figure 3.2 presents the maximum, average and minimum granulometry for these two soil types. The curves in Figure 3.2 are based on 37 particle size analyses for the gravelly sands and 27 analyses for the sandy silts. For the latter, the average curve gives about 20% of elements smaller than 2 μm and 28% of coarse elements (grain size bigger than 2 mm). For the gravelly sands, the average curve presents much more coarse elements with a percentage of 75% and only 5% of elements smaller than 2 μm .

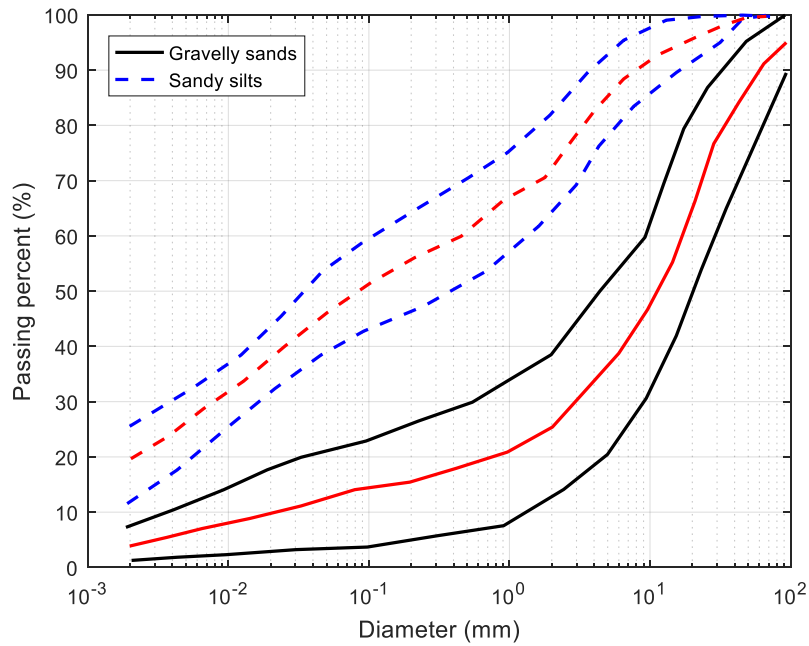


Figure 3.2 Maximum, average (red lines) and minimum granulometry for the two soil types

A horizontal pseudo-static acceleration is considered in this work in order to take into account, by a simple way, the seismic loading conditions for the dam reliability analyses. The value of the acceleration is set to $2.4\text{m}\cdot\text{s}^{-2}$, which corresponds to around $0.24g$ (g : gravity acceleration). It is determined as a product of a reference maximum acceleration for the rock and two coefficients (Loudière et al., 2014). The reference value is equal to $2.4\text{m}\cdot\text{s}^{-2}$, and is selected according to the location of the considered dam with respect to the seismic zones in France and the category of the dam (Loudière et al., 2014). The two coefficients are the coefficients of soil amplification and the pseudo-static method. They are respectively equal to 1.5 and $2/3$ for the studied case. The seismic acceleration used in the calculation is considered to be related with a return period of 5000 years.

3.2 Soil variability modelling

Different data are available for the dam in several phases: design studies, construction controls and structure monitoring. This work focuses on the field data which are highly relevant to the dam stability analysis under steady state flows: dry density measurements collected during the construction and the results of the triaxial tests

performed in laboratories. The former is directly related to the γ_d and the latter allows estimating c' and ϕ' . This section aims at presenting the statistical representation of the three soil properties by means of RVs and RFs using the measurements. For each soil property, the related measurements are firstly presented and followed by the variability modelling which consists in determining the parameters required for the RV distribution and for the RF autocorrelation structure.

3.2.1 Variability modelling of the γ_d

3.2.1.1 The available measurements

During the construction, the dry density and the soil water content after compaction were monitored in-situ using a gammadensimeter. This leads to a large number of γ_d data. In total, about 1200 representative measurements of the γ_d were collected, including 469 measurements for the Core zone and 709 measurements for the Shell zone. The average dry density for the Shell zone is close to 2 g.cm^{-3} , and is smaller for the Core zone (1.83 g.cm^{-3}). As an illustration, the histogram of the dry density measurements in the Shell zone is presented in Figure 3.3.

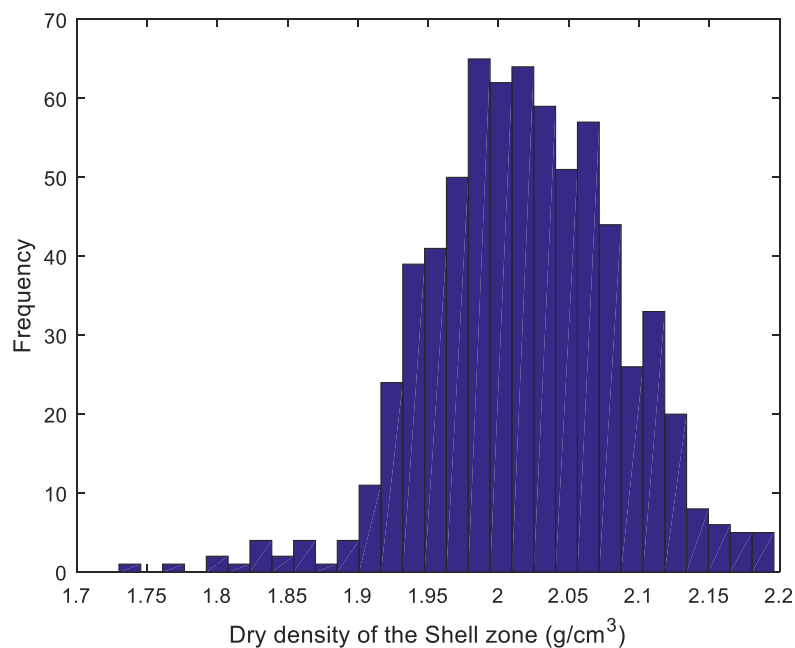


Figure 3.3 Histogram of the dry density measurements in the Shell zone

An advantage of these data is that they were collected following a grid monitoring system. This makes it possible to localize the measurements in space (along three axes). The grid system consists of 10 profiles in the longitudinal direction (Y axis) and 13 profiles in the transversal direction (X axis). Such a grid system allows determining the location of the measurements on an X-Y plan and the knowledge of the construction layer gives the elevation of the measurements along the Z axis. Finally, the number of effective geo-localized γ_d measurements is 381 for the Core zone, 248 for the Shell-1 zone and 272 for the Shell-2 zone. Figure 3.4 gives a plan view of the dam contour with the grid system and the location of the measurements.

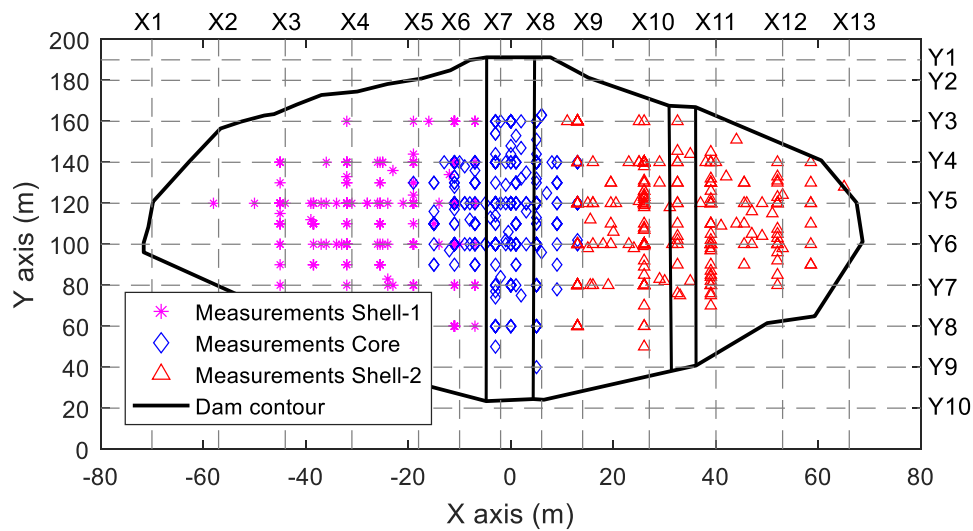


Figure 3.4 The collected measurements of γ_d with the grid system

3.2.1.2 Random variables

By fitting the measured data with an assumed probabilistic distribution, the γ_d variability can be described by means of RVs. The physical range of the soil property value, i.e. minimum and maximum values, should be considered when RVs are used to model the soil variability, in order to avoid generating unreasonable values (Phoon and Kulhawy, 1999a). For this reason, the Truncated normal and Beta distributions are adopted. Figure 3.5 presents the histogram and cumulative density function (CDF) of the γ_d measurements in the Shell zone, together with the fitted CDF curves by a Beta and a Truncated normal distribution. The minimum and maximum values are derived

from StructX (2015) and Phoon and Kulhawy (1999a, 1999b) according to the soil type. The fitted CDFs are in good agreement with the one of raw data, which indicates that the two chosen distribution types can describe well the variability of the γ_d measurements. The fitted parameters of the two distributions types are determined using the maximum likelihood estimation method and are given in Table 3.2 in section 3.2.3.

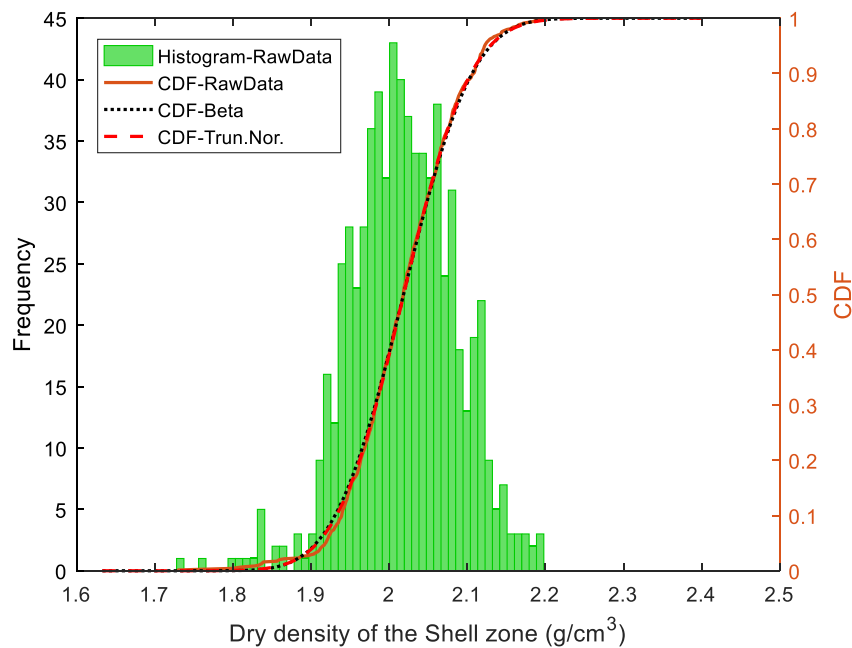


Figure 3.5 Histogram and CDF of the dry density measurements in the Shell zone

3.2.1.3 Random fields

Representing soil variabilities by means of RVs does not take into account the spatial variability of soil properties. Using the RF theory for soil variability modeling can address this issue. A RF can be considered as a collection of a series of RVs located at different stochastic discretization points. By considering a stationary RF, all the RVs follow a same probabilistic distribution (Beta or Truncated normal determined previously) and they are correlated with an autocorrelation structure. This part aims at determining the autocorrelation structure of the γ_d measurements for the purpose of modelling γ_d as RFs. It could be achieved by a variogram analysis on the geo-localized γ_d measurements as presented in section 2.2.4. Taking the Shell-2 zone as an example,

an experimental semi-variogram is firstly obtained by applying Eq. (2-42) to all the γ_d measurements of this zone. Then, the autocorrelation distances can be estimated by fitting a mathematical model (exponential one in this work which is also commonly used in literature (Cho 2014; Li et al. 2017; Li et al. 2015; Wang et al. 2019)) to the experimental semi-variogram. Figure 3.6 shows the experimental semi-variogram of the Shell-2 zone together with the fitted exponential model for both horizontal and vertical directions. It can be observed that the variance between two measurements increases with the increase of its separation distance. The variance roughly reaches a constant value after the distance beyond 5-7m for the horizontal directions. For the vertical direction, it converges when the distance is bigger than 1.5m. The black points in Figure 3.6 represent the points which reach 95% of the sill value. It is considered that the abscissa of these points is the autocorrelation distance. For the cases in Figure 3.6, the horizontal and vertical distances are respectively 4.9 m and 1.9 m. It indicates that the soil is less homogeneous in the vertical direction than in the horizontal direction. This finding is consistent with the observations of Lumb (1970) and Tang et al. (2012). By repeating the same procedure to the γ_d measurements in the other two zones Core and Shell-1, all the necessary autocorrelation distances are obtained and presented in Table 3.4.

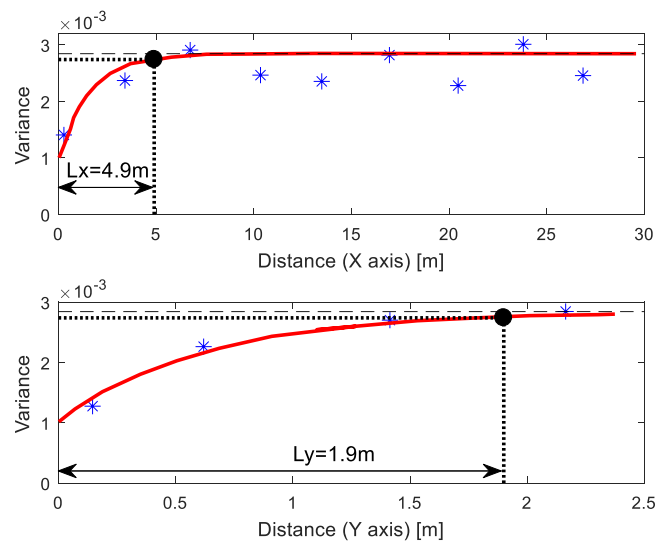


Figure 3.6 Variogram analysis for the γ_d measurements in the Shell-2 zone

3.2.2 Variability modelling of the c' and ϕ'

3.2.2.1 The available measurements

For a long-term stability analysis of earth dams, the effective cohesion c' and friction angle ϕ' are required. The shear strength parameters can be determined by triaxial shear tests. In total, 8 consolidated-undrained triaxial shear tests with pore water pressure measurement are available for the considered dam. Among the 8 tests, 5 tests are for the Shell zone and the other 3 for the Core zone. By plotting the Mohr circles of the effective stress at failure, the values of c' and $\tan\phi'$, that determine the Coulomb line, can be estimated using the Kf line (Figure 3.7) with Eqs. (3-1, 3-2). Using this method, the results of each test can be exploited to compute the values of c' and ϕ' . According to the 8 available tests, the average of c' is estimated to be equal to 9.4 kPa for the Shell zone and to 10 kPa for the Core zone. For ϕ' , a value of 34.2° was obtained for the Shell zone and of 34.3° for the Core zone. It is noted that these average values are estimated with the 8 triaxial tests, thus may be different from the mean values used in the probabilistic analysis which are obtained using a statistical method proposed by Mouyeaux et al. (2018). It can be found that the shear strength parameters for long term of the two soils are very close to each other. In fact, the two materials are relatively similar as they derive from the schist alteration composing the bedrock. The considered dam is actually a pseudo-zoned earth dam.

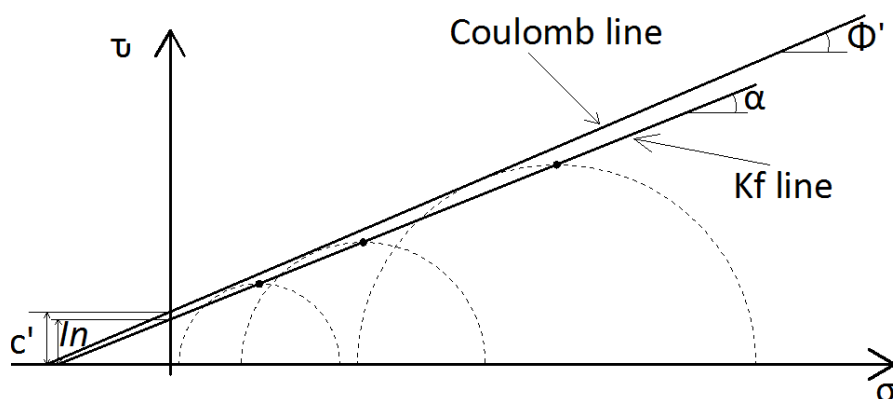


Figure 3.7 Interpretation of the triaxial shear test results using the method in (Aigouy et al., 2015)

$$\sin\phi' = \tan\alpha \quad (3-1)$$

$$c' = \frac{In}{\cos\phi'} \quad (3-2)$$

3.2.2.2 Random variables

The 8 available tests correspond to the test number typically performed for an earth dam design. However, it doesn't allow to carry out a statistical study for the c' and ϕ' distribution due to the low quantity of data. The method presented in Figure 3.7 provides a possibility to generate a large number of artificial data for c' and ϕ' . The idea was introduced in the work of Mouyeaux et al. (2018) and it consists in using the first two statistical moments of In and $\tan\alpha$ obtained when doing a regression analysis, to generate a large number of these two parameters and then compute the corresponding c' and ϕ' values following Eqs. (3-1, 3-2). The procedure is given in Table 3.1.

Table 3.1 The procedure of generating artificial data for c' and ϕ'

Step	Description
A	Determination of the extreme values for the regression parameters (In and $\tan\alpha$)
A.1	Determination of the physical range for c' and ϕ' values according to the soil type and the reference values recommended in StructX (2015) and Phoon and Kulhawy (1999a, 1999b),
A.2	Computation of the extreme values for In and $\tan\alpha$ using Eqs. (3-1, 3-2) with the determined physical range of c' and ϕ' .
B	Generation of 10^6 samples for the parameters In and $\tan\alpha$ between the extreme values,
B.1	Plot the peak points of all the Mohr circles in the $\sigma - \tau$ plan,
B.2	Determine the Kf line by performing a simple linear regression. The mean and standard deviation of the two regression parameters (In and $\tan\alpha$) can be obtained (as shown in Figure 3.8),
B.3	Assume a normal distribution for both In and $\tan\alpha$ with the previously defined mean and standard deviation,
B.4	Generate randomly 10^6 samples respectively for In and $\tan\alpha$ following the PDF of the normal distribution,
C	Computation of the c' and ϕ' value corresponding to each pair of In and $\tan\alpha$.

Figure 3.8 presents the 16 peak points of the Mohr circles obtained from the 5 triaxial tests for the Shell zone and the regression line. The mean and the standard deviation of the two regression parameters are also provided. Based on the two parameters, 10^6 artificial samples for c' and ϕ' are obtained as mentioned in Table 3.1. Figure 3.9 presents the histogram and CDF of the generated values (termed as 'RawData' in the figure) for c' and ϕ' in the Shell zone. It is observed that the variable c' are not symmetric around the peak, but are skewed. The peak is found near the lower end of the scale. The artificial data of c' and ϕ' are also fitted to a Beta distribution and a Truncated normal distribution. The minimum and maximum values for c' and ϕ' are derived from StructX (2015) and Phoon and Kulhawy (1999a, 1999b) according to the soil type. From Figure 3.9, it seems that the Beta distribution describes better the variability of c' data, than the Truncated normal distribution. The fitted parameters of the two distributions types are determined using the maximum likelihood estimation method and are given in Table 3.2 in section 3.2.3.

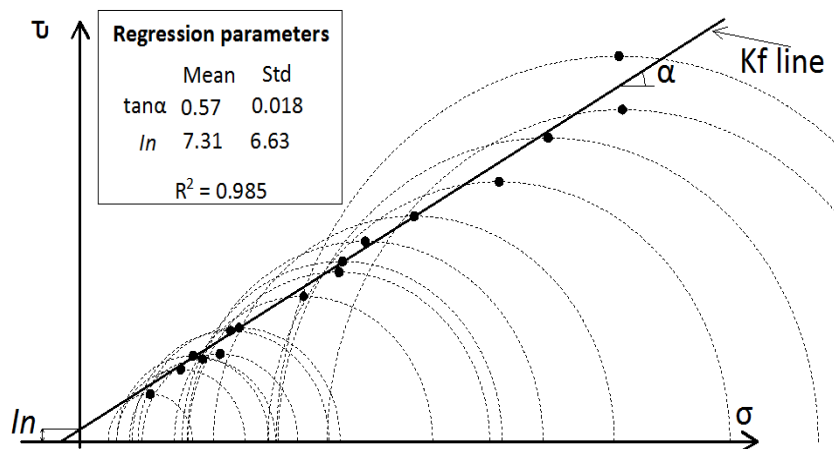


Figure 3.8 Mohr circles of the tests in the Shell zone (Std: standard deviation)

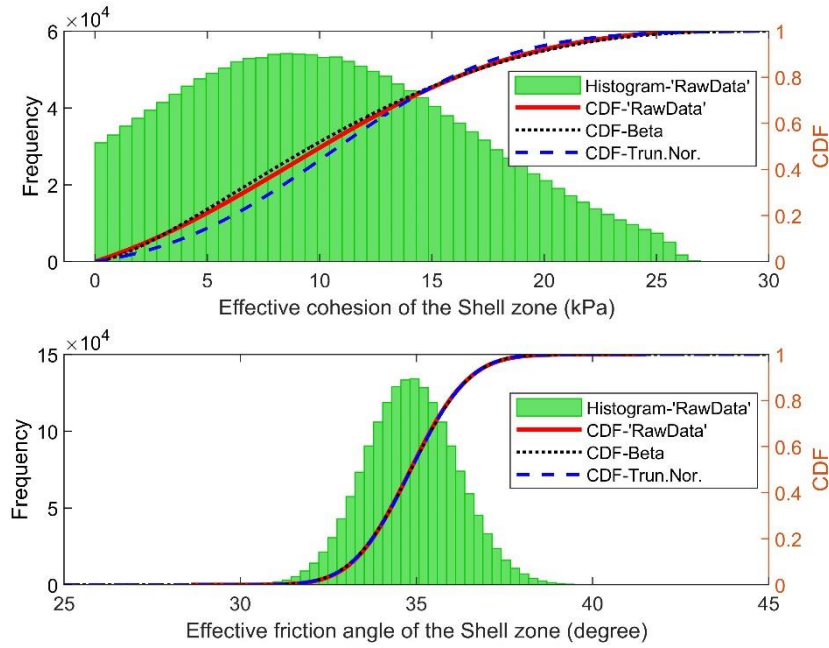


Figure 3.9 Histogram and CDF of the generated c' in the Shell zone

3.2.2.3 Random fields

The method of Mouyeaux et al. (2018) adopted for generating values of c' and ϕ' cannot provide the location information. Therefore, it is not possible to estimate the autocorrelation structure for these two soil properties with the 8 triaxial tests. However, one can use physical or empirical relations to obtain c' or ϕ' RFs by transforming the ones of γ_d . The Caquot's relation, expressed in Eq. (3-3), is adopted here to obtain the ϕ' RFs since it links the friction angle with the soil void ratio e (thus indirectly with dry density). The parameter k is a constant for a given material; its value is respectively equal to 0.25, 0.32 and 0.22 for the Shell-1, Core and Shell-2 zones. These values, treated as deterministic, are obtained using Eq. (3-3) for each zone with the corresponding friction angle and dry density mean values (Table 3.2). The uncertainties in the parameter k are difficult to be estimated due to the lack of data. A theoretical study could be conducted in future in order to investigate the effect of these uncertainties occurred in a transformation model. No effective transformation equations exist for estimating c' from γ_d (Li et al., 2014; Mouyeaux et al., 2018). For this reason, the c' variability is only represented by RVs.

$$e \cdot \tan(\phi') = k \quad (3-3)$$

3.2.3 Summary of the soil parameters

Table 3.2 presents a summary of the distribution parameters determined in the previous sections with the maximum likelihood estimation method. The abundant number of γ_d measurements in both the upstream and downstream Shell zones allows estimating dependent distribution parameters for the two zones (Shell-1 and Shell-2). On the contrary, only a global representation of the Shell zone is available for the variables c' and ϕ' . Besides, the method introduced by Mouyeaux et al. (2018) for determining the distribution parameters of c' and ϕ' assumes that the intermediate parameters (In and $\tan\alpha$ in Eqs. 3-1 and 3-2) are two uncorrelated normal variables. Therefore, the correlation between the generated artificial c' - ϕ' pairs is supposed to be very weak and thus negligible according to Eq. 3-2. This is further checked by estimating the correlation coefficient between the abundant artificial c' - ϕ' values which leads to a correlation coefficient close to 0 for the data of both the two zones (Shell and Core). In this work, the correlation between c' - ϕ' is not considered at a first time (CHAPTERS IV and V) and will be investigated later in CHAPTER VI.

Table 3.2 Distribution parameters for the random variables of γ_d , c' and ϕ'

Soil property	Zone	Beta		Truncated normal		Extreme values	
		$a^{(1)}$	$b^{(1)}$	Mean	CoV ⁽²⁾ (%)	Min	Max
γ_d (g/cm ³)	Shell-1	15.7	18.0	1.99	3.21	1.63	2.40
	Shell-2	26.7	22.2	2.05	2.65	1.63	2.40
	Shell (all)	15.6	15.5	2.02	3.30	1.63	2.40
	Core	22.4	27.5	1.83	3.33	1.44	2.32
c' (kPa)	Shell	1.48	2.78	10.55	57.63	0	30
	Core	4.07	5.22	13.23	34.21	0	30
ϕ' (°)	Shell	28.71	29.61	34.85	3.72	25	45
	Core	231.16	192.28	34.11	2.48	15	50

Note: ⁽¹⁾Beta distribution parameters; ⁽²⁾Coefficient of variation

Table 3.3 presents the deterministic values of all necessary soil parameters for a dam stability analysis under steady state flow conditions. The mean values shown in Table 3.2 are used for the γ_d , c' and ϕ' . The others are determined according to the measurements or laboratory test results. For vertical and horizontal drains, the hydraulic conductivity is set as isotropic considering a deterministic value of 10^{-4} m/s. The foundation is composed of altered schists whose superficial layers have been purged. Its location is very close to the Shell zone according to the site investigation and granulometric analyses. Therefore, same values as the Shell zone are assigned to the mechanical parameters of the foundation. All the soils are assumed to follow a linear elastic perfectly plastic behaviour characterized by the Mohr Coulomb shear failure criterion in this work.

Table 3.3 Deterministic value of the soil properties

Soil parameters	Shell-1	Core	Shell-2	Foundation
γ_d (g/cm ³)	1.99	1.83	2.05	2.02
c' (kPa)	10.55	13.23	10.55	10.55
ϕ' (°)	34.85	34.11	34.85	34.85
$K_y^{(1)}$ (m/s)	5×10^{-6}	5×10^{-9}	5×10^{-5}	1×10^{-6}
$K_x/K_y^{(2)}$ (m/s)	2	3	2	1
Porosity	0.26	0.32	0.26	0.26
Dilatancy angle ψ (°)	12	12	12	12
Young Modulus E (MPa)	45	40	45	45
Poisson coefficient ν	0.33	0.33	0.33	0.33

Note: ⁽¹⁾Verical hydraulic conductivity; ⁽²⁾Ratio between horizontal and vertical hydraulic conductivity

Table 3.4 presents the autocorrelation distances estimated by fitting the geo-localized γ_d measurements to an exponential model. Table 3.4 indicates that a considerable homogeneity can be found in the Shell-1 zone, while the γ_d in the Shell-2 and Core is

likely to have more remarkable spatial variation due to the small values of L_x and L_z . This difference can be explained by the better selection of the material composing the upstream zone and the greater attention which has given to its construction. The nugget effect corresponds to about a half of the variance for the upstream shoulder and to a slightly lower fraction for the downstream shoulder and the core. The nugget effect can be attributed to the mixture of the materials during their excavation from the borrow pits. In our case, it is considered as a short dimension structure whose scale is less than the sampling step.

Table 3.4 Results of the geostatistical analysis for the γ_d measurements

Zones	Autocorrelation distance (m)		Nugget effect
	Horizontal (L_x)	Vertical (L_z)	
Shell-1	78.1 m	7.8 m	1.6×10^{-3}
Core	13.0 m	1.5 m	8.6×10^{-4}
Shell-2	4.9 m	1.9 m	1.0×10^{-3}

3.3 Development of the deterministic models

Three deterministic models in 2D are developed in this work. The objective of the considered deterministic models is to estimate the dam safety factor (FoS) under steady flow conditions with or without a pseudo-static acceleration, once the input soil parameters are fixed. The first two models are based on the strength reduction method (SRM) (Dawson et al. 1999; Griffiths and Lane 1999; Smith et al. 2015; Zienkiewicz et al. 1975), combined respectively with finite element method (FEM) and finite difference method (FDM). These two models were compared with a previous study (Mouyeaux, 2017) considering its calculation configuration (unsaturated flows without a pseudo-static acceleration) in a deterministic framework. The computational model developed in Mouyeaux (2017) is based on the code Cast3M (FEM). Good agreements were obtained in terms of the provided FoS and the located failure surfaces among the three models. Such a cross comparison allows a first validation on the two models

developed in this work. The third one combines the limit equilibrium method (LEM) and genetic algorithm (GA). Particularly, a two-step search procedure is proposed for the third model in order to optimize and locate the non-circular critical slip surface. Table 3.5 gives a summary of the three models. The following sections present in detail the three developed deterministic models. As each model has its own positive and negative features, it is thus worth developing more than one deterministic model especially for a big project so that different models can be selected to address different problems. For example, it is better to use the *LEM_GA* (Table 3.5) if one needs fast estimates on the dam reliability at a preliminary stage. However, the *LEM_GA* has difficulties of accounting for the uncertainties of soil hydraulic parameters. In this case, the *SRM_FEM* is more appropriate. Additionally, having more than one models permits to compare the results made by different models in both deterministic and probabilistic frameworks. It is noted that the defects mentioned in Table 3.5 for the *SRM_FEM* are only associated with the used platform (Plaxis) and should not be considered as general remarks to the FEM. There are several FEM codes in which random fields can be easily implemented. In this work, the Plaxis platform is selected since it is fast in hydraulic calculations and has a very user-friendly interface which can facilitate the modelling procedure especially in 3D for a complex geometry.

Table 3.5 Summary of the three deterministic models developed for the present work

Model	Name	Platform	Remarks
1	<i>SRM_FEM</i>	Plaxis (Brinkgreve et al. 2015)	<ul style="list-style-type: none"> * Fast in hydraulic calculations * Difficult to implement random fields * An assumption imposed to modify pore water pressure during a pseudo-static analysis
2	<i>SRM_FDM</i>	Flac (Itasca, 2011)	<ul style="list-style-type: none"> * Slow in hydraulic calculations * Easy to implement random fields * Well-established coding environment
3	<i>LEM_GA</i>	Matlab (Mathworks, 2015)	<ul style="list-style-type: none"> * Very fast in estimating the dam FoS * Some assumptions are required for locating the critical slip surface * Easy to implement random fields

3.3.1 The model *SRM_FEM*

The *SRM_FEM* model is a numerical one developed using a finite element code Plaxis (Brinkgreve et al., 2015). Figure 3.10 shows the adopted mesh which includes 4175 15-noded plane elements and 33799 nodes. It is determined by a mesh refinement parametric study. A further reduction of the element size compared to the one shown in Figure 3.10 has a negligible effect on the computed FoS value. The effects of using a coarse mesh will be discussed later in CHAPTER VI. The mechanical boundary conditions used in this model are the following ones: the displacements are blocked following the horizontal and vertical axis on the base of the model; the horizontal displacements are blocked on the lateral edges of the model. Table 3.6 presents the procedure used to perform a stability analysis with the model.

It is noted that the function ‘Remote Scripting’ available in Plaxis is used for the *SRM_FEM*. This function allows building models and modifying soil parameters by typing commands which are based on the Python language. It is thus possible to

automate the operations (e.g. start a calculation and read results) and to link the model with the reliability methods developed with other tools. Such a technique can reduce significantly the computational time of a probabilistic analysis by avoiding manual operations.

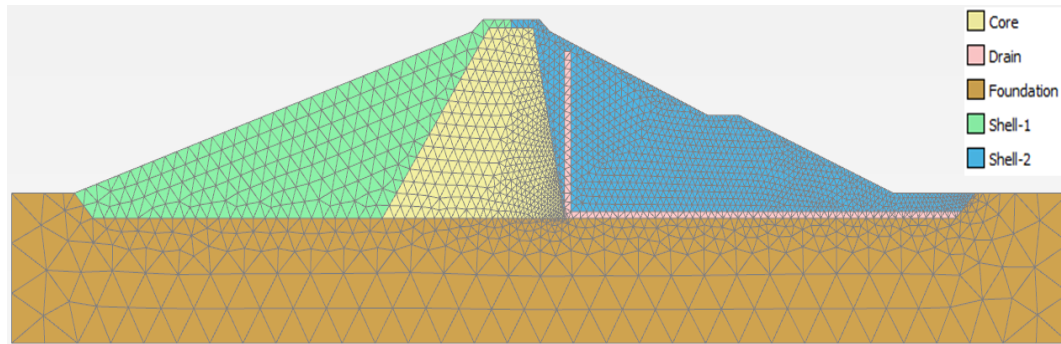


Figure 3.10 The model *SRM_FEM* and its mesh condition

Table 3.6 Procedure of a stability analysis using the *SRM_FEM*

Step	Name	Description
1	Initial equilibrium calculation	Once the mesh is realized, the soil parameters are assigned and the boundary conditions are fixed, a mechanical calculation of the initial stress state is performed under the loading of the soil's own weight.
2	Flow calculation only	A hydrostatic head of 20m (normal reservoir water level) is applied on the upstream slope and the pore water pressure distribution is obtained under steady state flow conditions.
3	Effective stress calculation	A mechanical calculation is performed with the pore pressure distribution determined by the step 2. This step permits to calculate the effective stress state of the soil. A pseudo-static acceleration could be added in this step.
4	Stability analysis	The FoS is determined using the strength reduction method in this step.

3.3.2 The model *SRM_FDM*

The *SRM_FDM* is also a numerical model and is created using the finite difference code Flac2D (Itasca, 2011). Figure 3.11 shows the mesh which consists of 18000 4-node quadrilateral plane elements with 18894 nodes. It is determined by a mesh sensitivity

parametric study as for the *SRM_FEM* but additionally refined in the dam body in order to satisfy a condition when RFs are mapped into the mesh. The condition requires that the largest element of the deterministic mesh in a given direction (horizontal or vertical) should not exceed 0.5 times the autocorrelation distance in that direction (Der Kiureghian and Ke, 1988). The boundary conditions are the same to the one of *SRM_FEM* and it follows also the procedure of Table 3.6 to perform a stability analysis. The model is defined with the FISH commands in Flac and is further linked with Matlab by using the function ‘*system*’ for the purpose of automating the probabilistic analysis.

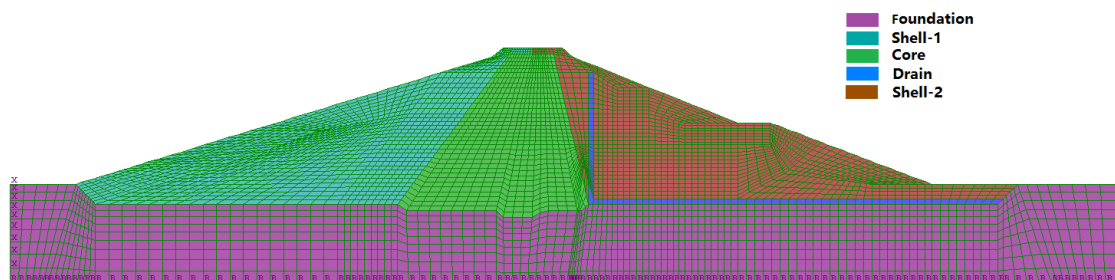


Figure 3.11 The model *SRM_FDM* and its mesh condition

3.3.3 The model *LEM_GA*

The third model *LEM_GA* is developed in Matlab. The pore water pressure field used in this model is determined using the ones obtained by a numerical simulation. The *LEM_GA* is based on the combination of the LEM and the genetic algorithm (GA). The principle is to generate a number of trial slip surfaces as an initial population at first, and then to search the minimum FoS value by simulating natural process along generations including reproduction, crossover, mutation and survivors’ selection. The FoS of a given slip surface is computed by using the procedure of Zhu et al. (2005) which is based on the Morgenstern Price method, and the slip surface generation method described in Cheng et al. (2008) is adopted which allows generating non-circular slip surfaces. Compared to the two previous models, more details are given in the subsequent sections for this model since the *LEM_GA* combines various techniques and shows original contributions (e.g. the two-stage search procedure) to efficiently estimate the dam FoS. The *SRM_FDM* and *SRM_FEM* are based on the conventional

slope stability analysis solution (SRM with REM or FDM). They are thus briefly presented.

3.3.3.1 Generation of trial slip surfaces

It is required to generate a number of slip surfaces as initial population in GA. The slip surface generation method described in Cheng et al. (2008) is adopted. A brief description is given as follows.

Consider a slip surface with four slices and five vertices as shown in Figure 3.12. The ground surface is represented by $y = y_g(x)$ and the bedrock is given by $y = R(x)$. The trial failure surface can be described by eight control variables as: $x_1, x_5, \beta_1, \beta_5, \delta_5, \delta_6, \delta_7$ and δ_8 . The vector $V = (x_1, x_5, \beta_1, \beta_5, \delta_5, \delta_6, \delta_7, \delta_8)$ can thus represent the slip surface mathematically, where $\delta_5, \delta_6, \delta_7, \delta_8$ are random variables with a range (0, 1) and x_1 (x_5) represents the x-coordinate of the vertice V_1 (V_5). The trial slip surface as shown in Figure 3.12 with solid lines is identified by using the vector $V = [x_1, x_5, \beta_1, \beta_5, 0.5, 0.5, 0.5, 0.5]^T$. Once the values of first four variables in V are given, two vertices V_1, V_5 and temporary vertices V_6 are obtained. The x-coordinate of the vertices V_2 can then be computed as:

$$X_{V_2} = \delta_5 * (X_{V_6} - X_{V_1}) + X_{V_1} \quad (3-4)$$

Another temporary vertice V_7 is then determined as:

$$X_{V_7} = \delta_6 * (X_{V_5} - X_{V_6}) + X_{V_6} \quad (3-5)$$

Similar to V_2 and V_7 , we can locate V_3 and V_4 using respectively δ_7 and δ_8 . The procedure will continue until the specified number of vertices is generated. In summary, the trial slip surfaces of n segments and $n + 1$ vertices can be obtained by using the presented procedure with the vector $V = (x_1, x_{n+1}, \beta_1, \beta_{n+1}, \delta_5, \dots, \delta_{2n})$ easily.

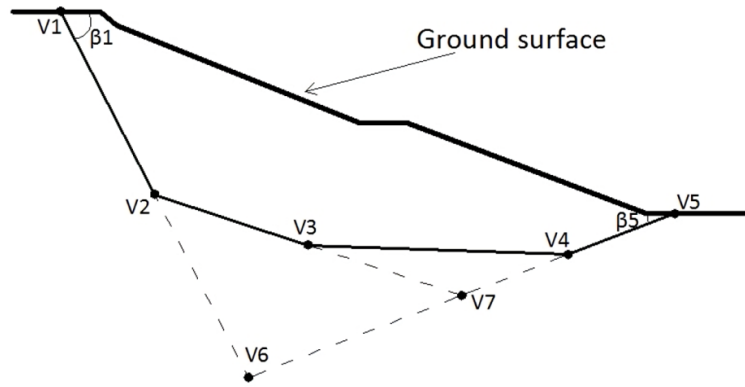


Figure 3.12 The adopted generation method for the trial slip surface

3.3.3.2 Formulation of the problem

Since the slip surface can be described by the vector V , the FoS is then regarded as being a function of V , when the soil property and slope geometry are fixed.

$$FoS = f(V) = f(x_1, x_{n+1}, \beta_1, \beta_{n+1}, \delta_5, \dots, \delta_{2n}) \quad (3-6)$$

The process of locating the critical slip surface can thus be mathematically formulated as an optimization problem of minimizing the objective function FoS with respect to the vector V .

Usually, some constraints should be considered in performing an optimization procedure. For the problem of locating the critical slip surface, the following geometrical and kinematical compatibility constraints should be respected (Li et al., 2010):

1. The x-coordinate of the vertices must be monotonically increasing or decreasing and the two end vertices must be on the slope surface.
2. All the segment lines determined by two adjacent vertices must be within the solution domain. Any segment line which passes through the ground surface or bedrock is permitted.
3. The slip surface should be concave upward in order to be kinematically admissible.

The constrain 1 and 3 are automatically satisfied if the slip surfaces are generated by the presented method (Cheng et al., 2008). However, the constrain 2 should be paid attention by eliminating the slip surfaces which break the slope or the bedrock. For the first four variables of V , the bound values can be specified by the users according to slope geometry and soil property (Li et al., 2010).

3.3.3.3 The two-step genetic algorithm

The GA is a search technique used to find approximate solutions of an optimization problem. It is a particular class of evolutionary algorithm that uses techniques inspired by evolutionary biology Zolfaghari et al. (2005). The main idea of GA is to first create an initial population and then model the evolution along generations until an optimal solution is converged. The natural processes such as reproduction, crossover, mutation and survivors' selection are repeated for each generation.

Typically, the potential solution (named chromosome in GA) is represented in binary as strings of 0s and 1s. Li et al. (2010) proposed a real-value representation of chromosome for GA and applied it in searching the critical slip surface. Here, the vector $V = (x_1, x_{n+1}, \beta_1, \beta_{n+1}, \delta_5, \dots, \delta_{2n})$ can be used to represent a $2n$ variables real-value solution as a chromosome.

It is found that applying directly the GA proposed by Li et al. (2010) on the studied dam may lead to a local minimum. The result is strongly dependent to the initial population. For this reason, a two-step strategy is proposed to reinforce the GA of Li et al. (2010). This strategy allows avoiding local minima in the searching process and can always lead to the global optimization result. In fact, the studied dam presents a complex geometry with a multi-stage slope (with berms) in the downstream part. Cheng

et al. (2007) reported that it may exist several local minima of FoS for such slopes. Complementary efforts should thus be made to overcome this problem.

The following flowchart (Figure 3.13) presents the procedure of the proposed two-step GA. It is started by a diversified initial population and it contains two steps in the searching process. The first step, named as Global search, aims at locating the most potential failure region at the slope surface. The second step, named as Local focus, focuses on the region found previously to locate precisely the critical slip surface. The first step is performed by considering a large mutation probability and a large generation size. These two parameters are decreased in the second step in order to focus on the obtained failure region and to accelerate the searching. After the flowchart, some specific features of the proposed two-step GA are explained in Table 3.7 and the adopted GA parameters are given in Table 3.8. For more details about the GA principles, readers are referred to Zolfaghari et al. (2005).

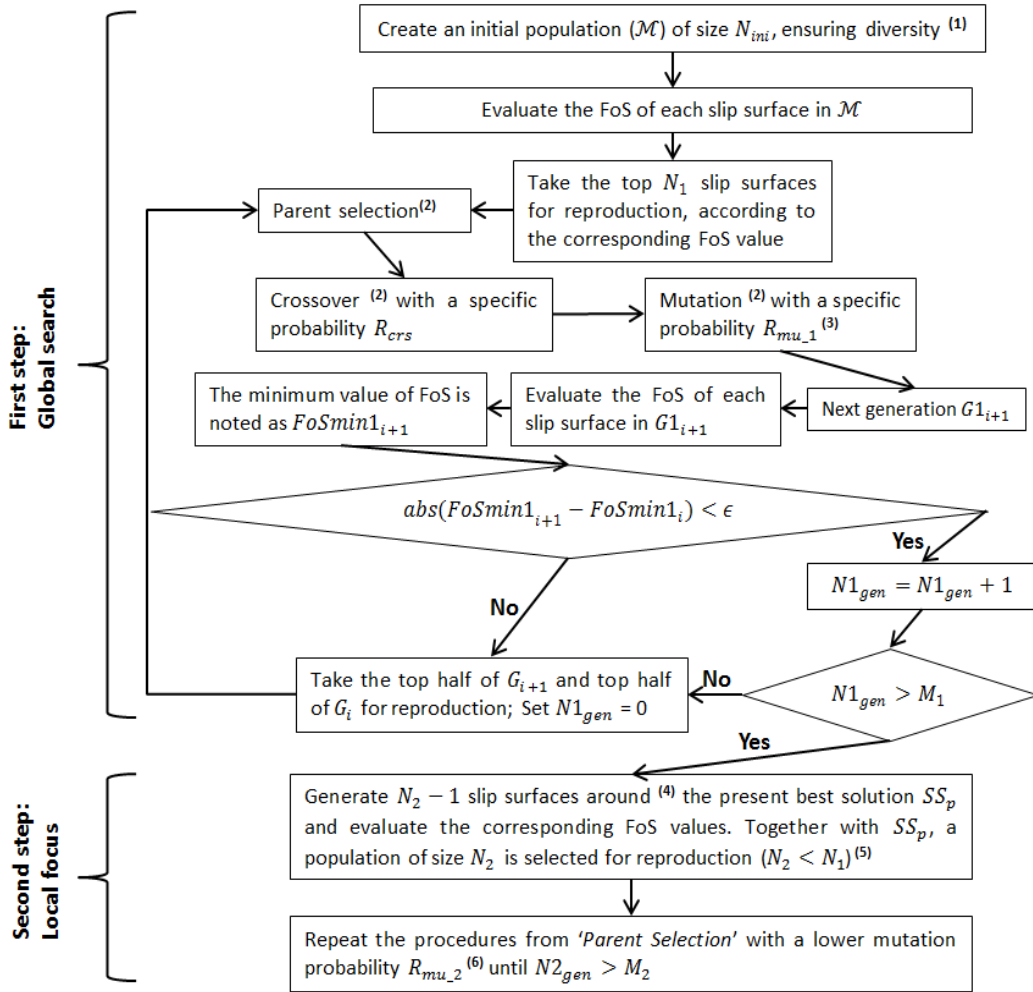


Figure 3.13 Flowchart of the proposed two-step GA

Table 3.7 Specific features of the proposed two-step GA (notes related to Figure 3.13)

Note number in Figure 3.13	Description and remarks
(1)	Population diversity is one of the most important factors in GA. Usually, it is ignored for the GA application on searching the critical slip surface and the initial slip surfaces are generated randomly. As several local minima exist for the studied dam, it is worth ensuring the diversity in the initial population. This is realized by dividing the slope surface into 5 regions ((1), (2), (3), (4) and (5)), as shown in Figure 3.14, and by generating an identical number of slip surfaces within each possible combination of regions to constitute the initial population. The possible combination is determined by selecting two reasonable regions as the range for the first and last vertices. For example, the first vertices can be limited between the points F and E if the region (1) is selected, and a combination (1)-(5) means that the end-vertices can only be generated within these two regions.
(2)	The techniques adopted in the paper for parent selection, crossover and mutation are respectively linear ranking selection, single arithmetic crossover and uniform mutation (Eiben and Smith, 2003).
(3)	A relatively large value (e.g. 0.5) is set to the mutation probability in the first step. For all evolutionary algorithms, the key point is to find a balance between ‘exploration’ and ‘exploitation’. The former is given by mutation process in GA while the latter is given by crossover process. Giving more possibility to ‘exploration’ can prevent the search from falling into local minimum early.
(4)	The second step focuses on the regions of the best solution determined by the first step. We assume that the critical slip surface SS_c is located in the vicinity of the present best solution SS_p and SS_p should be moved to find the SS_c . Therefore, we kill all the chromosomes, except the SS_p after the first step, and generate randomly ($N_2 - 1$) slip surfaces within the regions to constitute an initial population of size N_2 for the second step.
(5)	As we have found the most potential failure regions, the generation size can be decreased compared to the first step in order to accelerate the searching.
(6)	A relatively small value (e.g. 0.1) is set to the mutation probability R_{mu_2} in the second step since there is no need to lay more emphasis on ‘exploration’ when the most potential failure region is found.

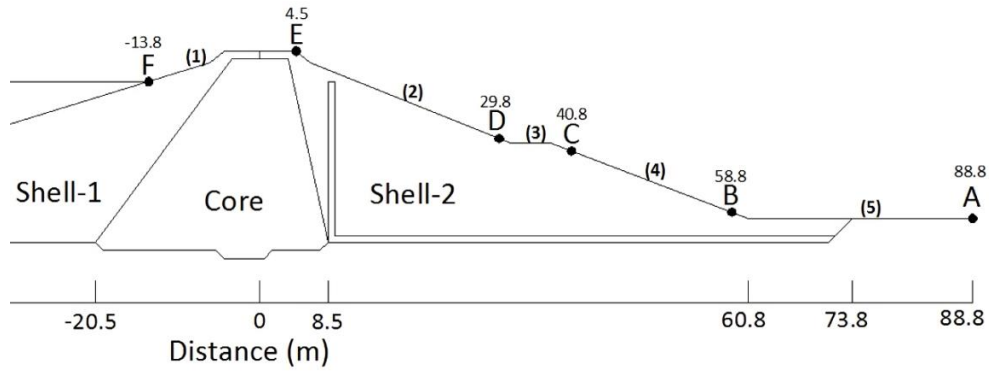


Figure 3.14 Division of the slope surface (the value at top of the point is the relating x-coordinate)

Table 3.8 Values used in this work for the two-step GA parameters

	First step	Second step
Size of one generation	$N_1 = 40$	$N_2 = 20$
Crossover probability		$R_{crs} = 0.8$
Mutation probability	$R_{mu_1} = 0.5$	$R_{mu_2} = 0.1$
Specified relative difference		$\epsilon = 5 \times 10^{-5}$
Minimum number of generations before termination	$M_1 = 30$	$M_2 = 120$

3.4 Conclusion

This chapter presents the studied dam which is a zoned earth dam composed of two shoulders and a low-permeable core. The reservoir height in the dam upstream is fixed to the normal level (20m) in this work and a horizontal pseudo-static acceleration of 0.24g is considered under seismic conditions.

Then, the statistical modelling of the soil variabilities by using the available measurements is presented. For γ_d , the quantity of the related data allows meaningful estimates of its statistics and of the autocorrelation distances which are determined by performing a variogram analysis on the geo-localized measurements. It will thus be possible to simulate γ_d by both RVs or RFs. For the shear strength parameters (c' and ϕ'), a large number of artificial values are generated by using the method of Mouyeaux et al. (2018) with the results of 8 available triaxial tests. Then, the distribution

parameters of c' and ϕ' are estimated with respect to the artificial values using the maximum likelihood estimation method. A transformation equation (Caquot's relation) which links γ_d and ϕ' is adopted to obtain the ϕ' RFs. The c' values are only modelled by RVs due to the lack of enough geo-localized data and of effective transformation equations from γ_d (Li et al., 2014; Mouyeaux et al., 2018). It is noted that the Truncated normal and Beta distribution types are chosen to represent the soil variabilities since they can avoid generating unrealistic values by giving two bounds. A summary of the obtained values for representing soil properties is then presented. The soils are assumed to follow a linear elastic perfectly plastic behavior characterized by the Mohr Coulomb shear failure criterion.

In the last part of this chapter, the three computational models developed in this work are presented. A two-step search procedure is proposed for the optimization of the third model in order to avoid local minima FoS values. Using three different deterministic models permits a comparative study of different slope stability analysis methods (SRM and LEM) in a probabilistic framework. Having more than one model allows also a better selection of the appropriate model for specific purposes.

4 CHAPTER IV: Probabilistic stability analysis with the random-variables approach

This chapter aims to present the dam probabilistic stability analysis in the context of the random-variables (RVs) approach which assumes the soils to be homogeneous in one deterministic simulation but varies certain properties for different simulations according to a joint probability distribution. Obviously, the soil spatial variability cannot be explicitly modelled in the RVs approach. However, it is simple and easy to be implemented in practical applications, and permits to provide fast estimates of reliability results. Moreover, having a large number of geo-localized data for determining the RFs parameters is rare in practice. Above all, the RVs approach is adopted in this chapter to conduct the dam probabilistic stability analysis which consists of, in general, two stages: (1) a sensitivity analysis to identify the soil properties to be modelled as RVs; (2) a reliability analysis to estimate the dam failure probability (P_f) and obtain a probabilistic distribution of the dam FoS. Two exploitation conditions (normal and seismic) are considered in the dam probabilistic analysis. The pseudo-static method is adopted to perform the seismic stability analysis, and an acceleration of $0.24g$ with a return period of 5000 years is considered as said in section 3.1.

4.1 Sensitivity analysis

4.1.1 Introduction

A global sensitivity analysis (GSA) is first performed. It considers the uncertainties of both the soil geo-mechanical and hydraulic parameters. The objective is to investigate the effects of the variabilities related to the soil hydraulic conductivity, which was not explored in CHAPTER III, on the dam stability condition. The obtained GSA results allow understanding the contribution of each soil property on the dam FoS variation, and validating the assumption of ignoring the variabilities of the hydraulic parameters.

Two parameters (vertical hydraulic conductivity K_v and anisotropy coefficient R_k), which are relevant with the steady-state flow simulations, are introduced for the GSA compared to the RVs defined in Table 3.2. The R_k is the ratio between the horizontal

and vertical hydraulic conductivity. The K_v is assumed to follow a Lognormal distribution by using the mean values given in Table 3.3 issued from the in-situ permeability tests. The CoV is estimated by assuming that the inverse CDF at 5% is equal to a low value which is determined from a great number of predicted K_v data. The available measurements of γ_d are used in combination with the following equation proposed by Chapuis and Aubertin (2003) to obtain the predicted K_v values.

$$\log(K_v) = 0.5 + \log \left[\frac{e^3}{(1 + e)G_s^2 S_s^2} \right] \quad (4-1)$$

where e is the void ratio, G_s is the specific weight of solids and S_s is the specific surface. This model is adopted since its input parameter e is linked with the γ_d data thus a large number of K_v predictions can be obtained. More details about the K_v predictions for the studied dam can be found in Mouyeaux et al. (2019). Concerning the anisotropy, there is no relevant measurements available to estimate the R_k statistical parameters. The values used in Mouyeaux et al. (2019) are thus directly taken for the present study. Table 4.1 gives a summary of the 4 introduced hydraulic RVs together with the 6 geo-mechanical RVs already defined in Table 3.2. It can be seen that the Shell K_v mainly varies between 2×10^{-5} and 1×10^{-4} m/s while the Core K_v is basically bounded between 1×10^{-9} and 2×10^{-8} m/s. The lower limit (unit in Table 4.1) for the R_k permits to ensure that the horizontal hydraulic conductivity is always higher than the vertical one, while the upper limit can avoid excessive contrasts according to Smith and Konrad (2011). Assuming $R_k > 1$ is logical for earth dams because these structures are usually constructed by layers and each layer should be vertically compacted. Finally, 10 RVs are considered in the sensitivity analysis.

Performing directly a GSA by the MCS is time-consuming as mentioned in section 2.2.2, given that the total number N_{md} of deterministic evaluations in a GSA is highly related to the input dimension N_{in} (Iooss and Lemaître, 2015; Saltelli et al., 2010). In

light of this, the PCE-based Sobol indices (section 2.2.2), are employed to investigate the importance of the 10 RVs for the dam stability. Particularly, an adaptive algorithm is proposed to reinforce the performance of the PCE for estimating the sensitivity indices. The proposed algorithm is described in the following section and the obtained results are presented. It is noted that the *SRM_FEM* model is selected to conduct the deterministic calculations in the GSA because the *SRM_FEM* is more efficient than the *SRM_FDM* for flow simulations.

Table 4.1 Input probabilistic model considered for the sensitivity analysis

Zone	RV	Distribution	Mean	CoV (%)	Min	Max
Shell	γ_d (g/cm ³)	Beta	2.02	3.30	1.63	2.40
	c' (kPa)	Beta	10.55	57.63	0	30
	ϕ' (°)	Beta	34.85	3.72	25	45
	K_v ($\times 10^{-5}$ m/s)	Lognormal	5	50.2	2.05 ⁽¹⁾	9.75 ⁽²⁾
	R_k	Beta	2	50	1	15
Core	γ_d (g/cm ³)	Beta	1.83	3.33	1.44	2.32
	c' (kPa)	Beta	13.23	34.21	0	30
	ϕ' (°)	Beta	34.11	2.48	15	50
	K_v ($\times 10^{-9}$ m/s)	Lognormal	5	73.8	1.36 ⁽¹⁾	11.9 ⁽²⁾
	R_k	Beta	5	50	1	15

Notes: ⁽¹⁾inverse CDF of 5%; ⁽²⁾inverse CDF of 95%.

4.1.2 An adaptive PCE for GSA

As aforementioned, an adaptive algorithm is proposed for the PCE-based Sobol indices. The algorithm adds gradually training samples, by space-filling sampling techniques, to improve the PCE meta-model and ends the procedure by regarding three conditions: (1) the PCE model accuracy indicated by the Q^2 of Eq. (2-26); (2) the stability of the estimated principal Sobol indices; (3) the PCE order q_{PCE} . The idea is to improve the PCE global approximation performance by adding a sample which can help the current experimental design (*ED*) to better cover the whole input space, and to stop the

enrichment procedure once satisfying results are obtained so that unnecessary deterministic evaluations can be avoided.

Table 4.2 describes the proposed algorithm step by step. The advantages over the existing algorithms are the following ones: (1) the PCE order is determined by a comparison test instead of being imposed by users. It is achieved by testing a range of PCE orders and selecting the one (q_{opt}) which leads to the maximum Q^2 . The q_{opt} is then considered as the optimal order for the current ED and used for the PCE model construction. (2) the ED size is determined by an adaptive process. Users are not required to specify the ‘proper sample size’ for a given probabilistic analysis which is usually unknown *a priori*. One can start a simulation with a small ED and then enrich it until the stopping conditions are met. (3) the convergence of the obtained Sobol indices is guaranteed. An error estimate ε_{iSA} which measures the stability of the Sobol indices is proposed. To compute the ε_{iSA} , the RVs which have non-negligible contribution to the model response variance are selected at first. For example, the variable whose current total Sobol index (at iteration i) is higher than 1% of the global sum can be chosen. For each selected variable, a vector of size N_{SA} is formed using its Sobol index from the iteration $(i - N_{SA} + 1)$ to the current iteration i . Then the absolute error of all possible pairs for each vector is calculated. The maximum error for all pairs of all vectors is considered as the error estimate ε_{iSA} . When ε_{iSA} is lower than a small value (e.g. 5%), the convergence of the Sobol indices is reached and it means that further adding training samples leads to insignificant improvement for the GSA results.

Concerning the sampling strategy, the LHS is used to generate the initial ED and is enriched with new samples by using the technique introduced in Lataniotis et al. (2019) which is similar to the one of Sheikholeslami and Razavi (2017). The LHS aims to spread the sample points more evenly across all possible values with the concept of

Latin square as mentioned in section 2.2.4. The generated samples are ‘space-filling’ and can be considered as a good representation of the whole variability domain compared to the MC samples. The LHS enrichment technique (Lataniotis et al., 2019; Sheikholeslami and Razavi, 2017) adds samples such that the progressive *ED* can better capture the global information of the whole input space. In other words, it preserves the desired distributional properties of the LHS while the sample size grows during the analysis.

Table 4.2 Description of the proposed adaptive PCE for GSA

Step	Description
1	Generate an initial $ED^{(1)}$ according to the input joint distribution using the LHS
2	Evaluate the model response of the samples in the ED using a deterministic model
3.1	Construct a sparse PCE ⁽²⁾ with the current ED using the method presented in section 2.2.1. The PCE order q_{opt} is determined by testing a range of values (2: $q_{mSA}^{(3)}$). The PCE accuracy indicator is noted as Q_{ISA}^2 .
3.2	Estimate the Sobol index (first-order and total effect) of each input variable with the PCE coefficients using the method presented in section 2.2.2.
3.3	Stop condition 1: if $q_{opt} \geq q_{tSA}^{(4)}$ continue to next step, otherwise, go to step 3.6.
3.4	Stop condition 2: if $Q_{ISA}^2 \geq Q_{tSA}^2^{(5)}$ continue to next step, otherwise, go to step 3.6.
3.5	Stop condition 3: if $\varepsilon_{ISA} \leq \varepsilon_{tSA}^{(6)}$ go to the step 4, otherwise, go to step 3.6.
3.6	Enrich the current LHS samples by adding a new one with the technique described in (Lataniotis et al., 2019; Sheikholeslami and Razavi, 2017). Evaluate the model response of the added sample using a deterministic model and update the current ED . Then go back to step 3.1.
4	Collect the results (Sobol indices, q_{opt} and Q_{ISA}^2) of the current iteration; the Sobol index of each input variable is obtained.

Notes:⁽¹⁾a small size (30 in this work) can be used for the initial ED ; ⁽²⁾Hermite polynomials are used in this work; ⁽³⁾the PCE order is tested between 2 and 10 in this work; ⁽⁴⁾the minimum PCE order is set as 4; ⁽⁵⁾the target accuracy is 0.98; ⁽⁶⁾the tolerance error is 5% and the N_{SA} is set as 10.

4.1.3 Numerical results

This section presents the GSA results of the dam for two design scenarios: normal and seismic. The latter refers to a pseudo-static acceleration of $0.24g$ applied to the dam. The method of Table 4.2 is employed to investigate the contribution of the ten RVs defined in Table 4.1 with respect to the dam stability. Two sparse PCE meta-models are finally obtained to estimate the Sobol indices for the two scenarios. For the normal condition, 109 deterministic calculations are performed according to Table 4.2 and an 8-order sparse PCE with a Q^2 of 0.9898 is adopted at the last iteration. As for the seismic condition, the total number of deterministic calculations is 126 and the obtained PCE is a 5-order one with a Q^2 of 0.9808. Figure 4.1 presents the GSA results estimated by the coefficients of the two PCE models. The first-order and total Sobol indices are both shown in this figure. As a reminder to section 2.2.2, the first-order Sobol index gives the influence of each variable taken alone while the total one evaluates the total effects of one variable by accounting for possible interaction effects with others.

By observing Figure 4.1, one can have an insight into the contribution of each variable on the dam FoS variance. Firstly, it can be concluded that the c' of the Shell takes the first place among the 10 parameters and has the most important influence on the FoS variance with a Sobol index higher than 0.8. This is not surprising since nearly all the slip surfaces take place in the downstream part of the dam under steady-state flow conditions and the variable c' in the Shell zone has the biggest variability ($CoV = 57.63\%$) among the 10 variables, as shown in Table 4.1. The next most important parameter is the Shell ϕ' with a Sobol index varied between 0.1 and 0.2. The other variables have a lower influence on the FoS variability since their Sobol indices (even the total one) are all smaller than 0.01. This finding is consistent with previous studies (Fenton and Griffiths, 1997; Wu, 2013): Wu (2013) remarked that the dry density has very limited impacts on the variability of slope stability analysis results; Fenton and Griffiths (1997) found that the variability of soil permeability did not significantly add

variability to the phreatic surface for the dams equipped with filter drains as long as the drain permeability is high enough and the effective filter length is long enough. The computed total Sobol indices show that the hydraulic parameters (K_v and R_k) are not influential even if possible iterations with other variables are considered. Therefore, the variabilites of the soil hydraulic parameters are ignored in the following studies for the sake of simplicity.

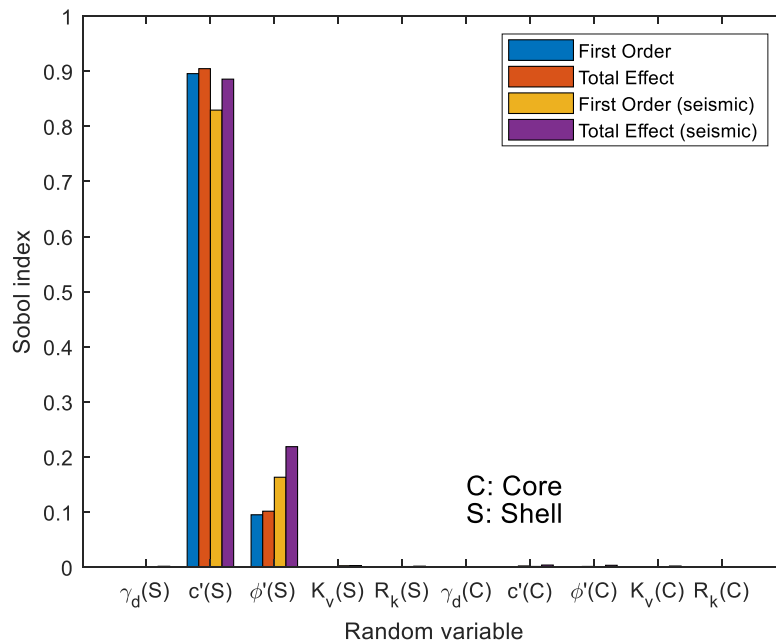


Figure 4.1 First-order and Total Sobol indices of the ten parameters

4.2 Reliability analysis results

The reliability analyses in this chapter are performed by using the SPCE-based MCS. It consists in constructing a SPCE model as an approximation to a computational model, then performing a crude MCS with the surrogate model. Once an SPCE model is available, the Sobol indices can also be derived as shown in the previous section. Therefore, this approach allows obtaining more results (e.g. Pf , FoS distribution and GSA results) than other reliability methods such as the SS, IS and FORM which focus on evaluating the Pf . The PCE, also called as stochastic response surface method by some researchers, is selected to construct the surrogate model since it has been widely used in the field of geotechnical reliability analysis for tunnels (Mollon et al. 2011; Pan

and Dias 2017b), dams (Ghanem et al., 2007; Hariri-Ardebili and Sudret, 2019), foundations (Al-Bittar and Soubra, 2014, 2013) and slopes (Li et al. 2011; Pan et al. 2017). The SPCE is an improvement to the original PCE by limiting the number of involved multivariate polynomials and thus reducing the number of required deterministic calculations. The following values are adopted for the user-defined parameters which are necessary for the procedure of Table 2.2: the target accuracy $Q_{tg}^2 = 0.99$, the maximal polynomial degree $P_{max} = 5$, the cut-off values $\varepsilon_1 = \varepsilon_2 = 5 \times 10^{-5}$ and the q-quasi-norm $q = 0.7$. These values are consistent with the ones adopted in existing studies (Al-Bittar and Soubra, 2013; Pan and Dias, 2017b).

Concerning the soil variability modelling, all the variables are firstly assumed to follow a Beta distribution with the parameters given in Table 3.2. The effect of using a different distribution type (Truncated normal) for input variables will be discussed in a second time. For each exploitation condition (normal and seismic), two reliability analyses are performed using respectively the *SRM_FDM* and the *LEM_GA* as the deterministic model for a purpose of comparing the two slope stability analysis methods (SRM and LEM) in a probabilistic framework. Comparison between the SRM and the LEM within deterministic calculations has been widely reported. However, evaluating and comparing the performance of the two methods in reliability analyses are seldom performed in literature. This study attempts to provide first insights into this issue. Particularly, the *SRM_FDM* instead of *SRM_FEM* is chosen to represent the SRM since the latter has an assumption during a pseudo-static analysis which does not permit it to be directly compared with the LEM. The assumption, imposed by Plaxis (Brinkgreve et al., 2015), increases the pore water pressure and the hydrostatic loadings with a ratio related to the pseudo-static acceleration in order to take into account the hydrodynamic overpressure.

4.2.1 Normal exploitation condition

This section presents the reliability analysis results of the dam under normal exploitation condition. Figure 4.2 gives the PDF of the FoS, and Table 4.3 presents the reliability results including failure probability, mean and standard deviation of the FoS. Plotting the PDF allows having a global idea on the FoS distribution and its major variation range. The results in Table 4.3 are derived from the SPCE-based MCS estimates, i.e. a large number of FoS values. The results based on the FoS evaluation by the *SRM_FDM* and the *LEM_GA* model are both provided. By post-processing the SPCE coefficients, the sensitivity index of each input variable can be determined and are presented in Figure 4.3.

From Figure 4.2, one can observe that the PDFs of the dam FoS are not symmetric. The two curves are considered to be negatively skewed with a relatively bigger tail at the left. Thus, more data in the left tail, i.e. more small values of FoS, would be expected than a normal distribution. It can be explained by the fact that the distribution of the input variables is not symmetric and that some variables have more small values, such as c' in the Shell zone as shown in Figure 3.9. The PDF curve obtained with the numerical model – *SRM_FDM* (PDF_{srm}) is more skewed to the right side than the one obtained with the analytical model – *LEM_GA* (PDF_{lem}). An interpretation of this point will be given later in section 4.3.1.

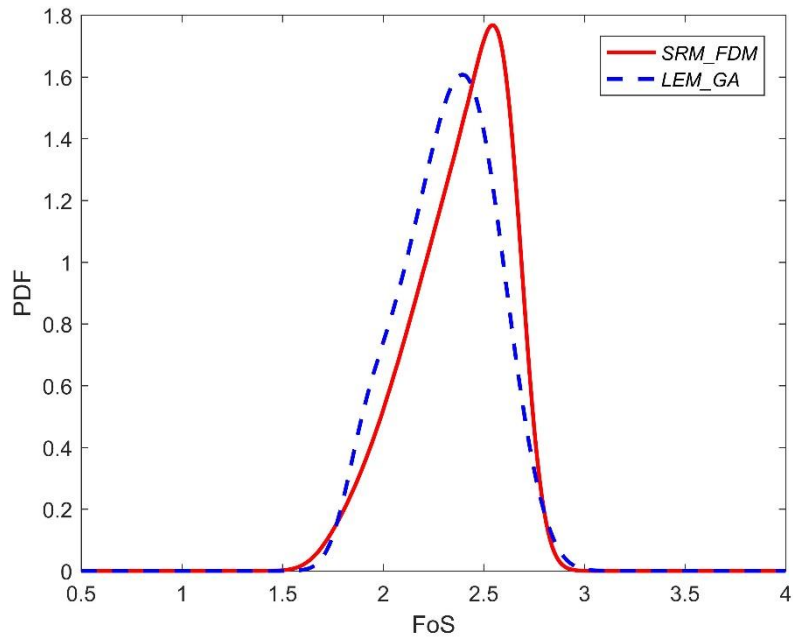


Figure 4.2 PDF of the studied dam FoS under normal exploitation condition

According to Table 4.3, the failure probability of the considered dam is estimated to be 6.5×10^{-6} or 2.7×10^{-6} by the two models. The *SRM_FDM* leads to a slightly higher failure probability than the *LEM_GA*. Concerning the first two statistical moments of FoS, the *LEM_GA* gives a smaller mean value and a smaller standard deviation. The differences are not significant.

Table 4.3 Summary of the reliability results (normal exploitation condition)

Model	P_f	$Mean_{FoS}$	Std_{FoS}	CoV_{FoS}
<i>SRM_FDM</i>	6.5×10^{-6}	2.37	0.245	10.3%
<i>LEM_GA</i>	2.7×10^{-6}	2.32	0.242	10.5%

The GSA results shown in Figure 4.3 are in good agreement with Figure 4.1. It is observed that the Shell c' and ϕ' contribute more to the variance of the dam FoS while other variables are not influential since their Sobol indices are all smaller than 0.005. Another remark is that the results obtained by the two deterministic models are consistent with each other.

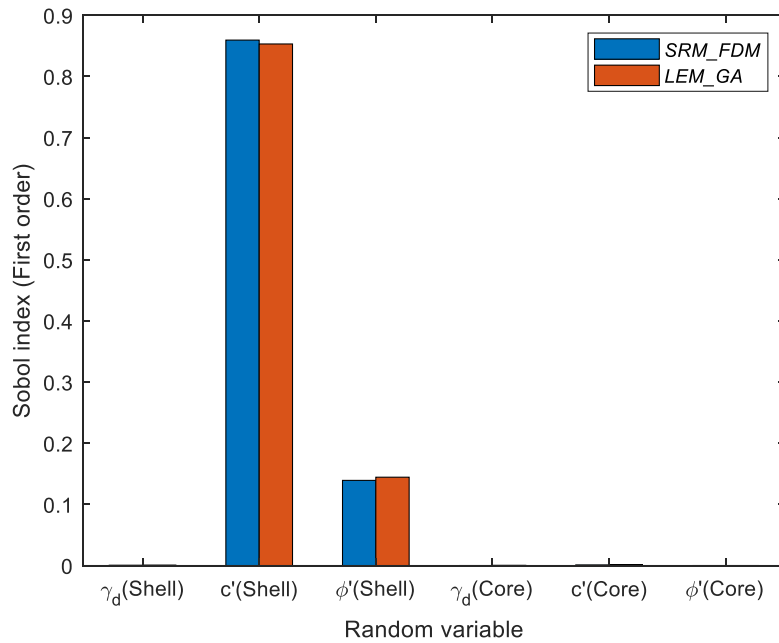


Figure 4.3 Sobol indices of each variable (Normal exploitation condition)

4.2.2 Exploitation under seismic loading condition

This section presents the reliability analysis results of the dam under seismic loading conditions. A pseudo-static acceleration of $0.24g$ with a return period of 5000 years is considered. Figure 4.4 gives the PDF of the FoS, and Table 4.4 presents the reliability results. The results based on the FoS evaluation by the *SRM_FDM* and the *LEM_GA* model are both provided. Additionally, a direct MCS and a direct GSA with respect to the *LEM_GA* are performed. The aim is to evaluate the accuracy of the reliability and sensitivity results provided by the SPCE meta-model.

According to Figure 4.4, the observations made in the previous section for the FoS distribution under normal exploitation condition remain valid. The PDF curves obtained with the two deterministic models are both not symmetric and are negatively skewed. The PDF_{srm} is more skewed to the right side than the PDF_{lem} .

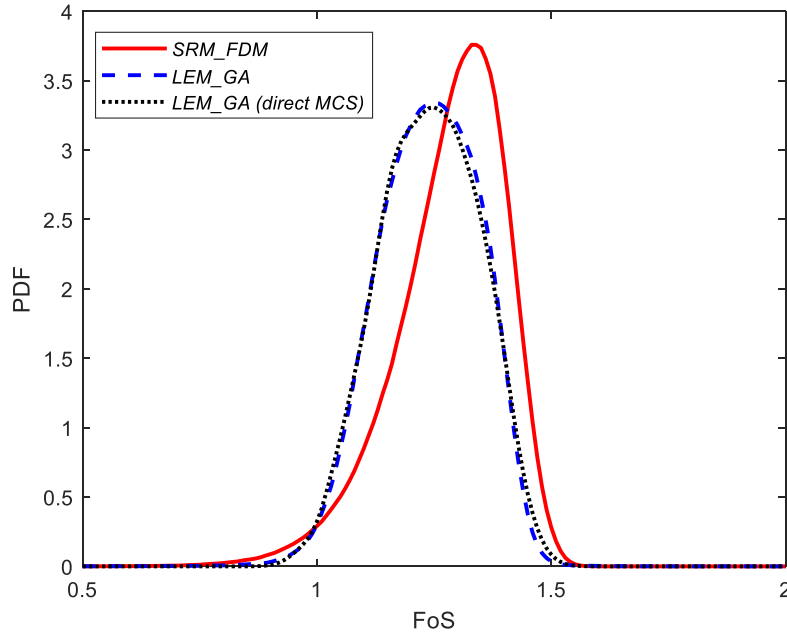


Figure 4.4 PDF of the studied dam FoS under seismic loading conditions

In Table 4.4, two kinds of Pf are given: Pf_{con} and Pf_{sce} . The first one is obtained directly by the AbSPCE procedure (or a direct MCS) and represents the structure reliability under the considered seismic loading (a pseudo-static acceleration of $0.24g$). Therefore, it is a failure probability (i.e. $Pr(DamFailure|0.24g)$) conditioned on the loading and termed as Pf_{con} in this work. Then, the probability of the analyzed scenario $Pr(DamFailure \cap 0.24g)$, termed as Pf_{sce} , can be assessed with the following formula using the conditional probability theory: $Pf_{sce} = Pf_{con} \times Pr(0.24g)$ in which $Pr(0.24g)$ is the occurrence probability of the seismic event having a maximum acceleration of $0.24g$. The Pf_{sce} involves the occurrence of both of the two events: the dam failure and an earthquake of $0.24g$. According to the recommendations given in Loudière et al. (2014), the considered pseudo-static loading ($0.24g$) corresponds to a return period of 5000 years for the dam site. This means, by the definition of the return period, that the probability of having a seismic event exceeding the considered loading (i.e. $0.24g$) is $1/5000$ in any one year. Then, it is assumed in this work to adopt simply the value of $1/5000$ for the $Pr(0.24g)$. Therefore, the failure probability of the analyzed scenario (Pf_{sce}) can be approximated by $Pf_{con} \times 1/5000$. Assuming a

$Pr(0.24g)$ of 1/5000 leads to a higher estimate on the Pf_{sce} so conservative results. Using a more sophisticated approach for the $Pr(0.24g)$ estimation is beyond the scope of this work and could be of interest for a future study by having more information on the dam site seismic records. Then, for obtaining a total failure probability of the dam in which all the possible seismic events are considered, one option is to prepare the dam fragility curve (Pf_{con} with respect to different seismic loadings) and estimate the occurrence probability of each possible seismic event. With the introduced reliability method (SPCE), it seems feasible to carry out such a study in future and the total computational time is expected to be acceptable. From Table 4.4, the Pf_{con} is estimated to 2.4×10^{-2} by the *SRM_FDM* model, and to 1.4×10^{-2} by the *LEM_GA* model. These values are then multiplied by a coefficient of 1/5000 and respectively become equal to 4.7×10^{-6} and to 2.8×10^{-6} . They are in the same order of magnitude of the dam Pf under normal exploitation condition, and are all quite small. Concerning the first two statistical moments of FoS, the *LEM_GA* model gives a smaller mean value and a smaller standard deviation compared to those of the *SRM_FDM*. The differences are not significant.

Table 4.4 Summary of the probabilistic results (seismic)

Model	Method	Pf_{con}	Pf_{sce}	$Mean_{FoS}$	Std_{FoS}	CoV_{FoS}
<i>SRM_FDM</i>	SPCE-MCS	2.4×10^{-2}	4.7×10^{-6}	1.28	0.119	9.2%
<i>LEM_GA</i>	SPCE-MCS	1.4×10^{-2}	2.8×10^{-6}	1.24	0.108	8.7%
<i>LEM_GA</i>	Direct MCS	1.2×10^{-2}	2.4×10^{-6}	1.24	0.106	8.6%

According to Figure 4.5, the main conclusions related to the GSA remain the same compared to Figures 4.1 and 4.3: (1) the sensitivity analysis results obtained by the two deterministic models are in good agreement with each other; (2) the variables c' and ϕ' in the Shell zone are the most two important variables for the FoS variance with a sum of Sobol index around 0.99; (3) the dry density has almost no impact on the FoS variability.

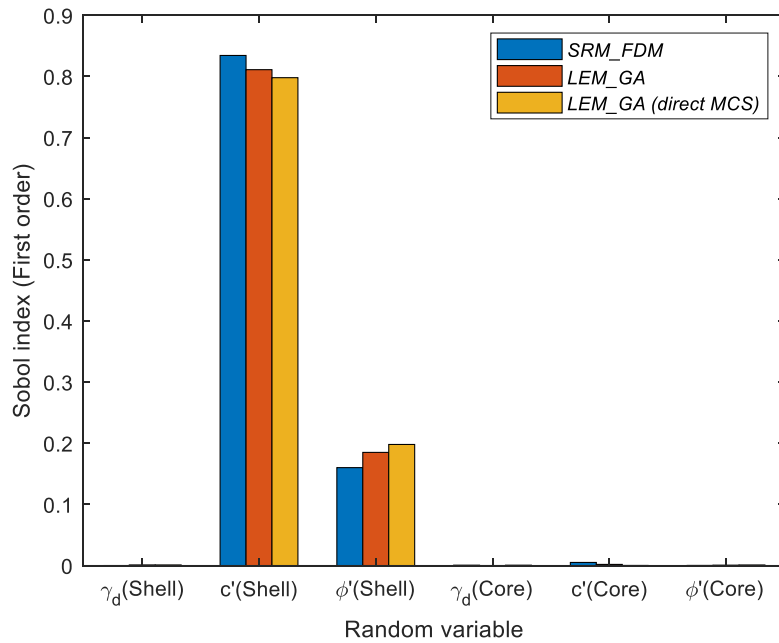


Figure 4.5 Sobol index of each variable (Seismic loading conditions)

As mentioned before, a direct MCS and a direct GSA using the *LEM_GA* are performed in this section in order to validate the reliability and sensitivity results issued from the SPCE. 15 000 deterministic calculations are performed in the direct MCS, ensuring that the *CoV* of the estimated *Pf* is lower than 8%. For the direct GSA, 8 000 simulations on the *LEM_GA* are conducted. It is found in Figure 4.4 that the PDF_{lem} is almost superposed with the PDF obtained by the direct MCS. This indicates that the surrogate model constructed by the SPCE can replace well the original model to predict the dam FoS values. Then, the results in Table 4.4 show that the Pf_{con} values by the SPCE-MCS is very close to the reference ones (direct MCS), and the FoS statistics are almost identical between the two methods. These findings show a good accuracy of the SPCE-MCS in estimating reliability results. Additionally, it is observed in Figure 4.5 that the Sobol indices based on the SPCE coefficients are very similar to those obtained with a direct GSA. This permits to validate the SPCE in estimating the sensitivity analysis results for the considered dam. The idea of constructing a surrogate model in a probabilistic analysis is to reduce the computational time. Following the procedure of Table 2.2, it needs around 200 deterministic simulations to obtain a satisfied SPCE

meta-model. Then, the running time of an MCS or a GSA based on the meta-model is negligible. The total computational time of performing an SPCE-based reliability and sensitivity analyses with the *LEM_GA* is about 35 mins on an Intel Xeon CPU E5-1620 3.5 GHz PC. On the contrary, it requires around 42 hours for a direct MCS and 24 hours for a direct GSA using the *LEM_GA*. Such a comparison highlights the advantage of using SPCE in this work. In summary, the employed SPCE method can provide accurate estimates for reliability and sensitivity results with a greatly reduced calculation time.

4.3 Discussions

This section discusses two issues which are not explained in detail (comparison between the SRM-LEM) or not considered (effect of distribution type for input variables) in the previous sections.

4.3.1 Comparison between the two deterministic models

According to the previous sections, it can be concluded that the two deterministic models can give similar results in terms of Pf , mean value, standard deviation and sensitivity indices. The obtained PDF curves have also a similar shape. These findings are consistent with the comparison between the two methods (SRM and LEM) in a deterministic framework, as pointed out by Cheng et al. (2007). However, some differences between the two methods in a probabilistic framework are highlighted as well in the study.

The *SRM_FDM* model leads to a slightly higher failure probability compared to the *LEM_GA*, and the PDF_{srm} is more skewed to the right side than the PDF_{lem} . According to Figures 4.2 and 4.4, the right part to the peak point of the PDF_{srm} has less variability than the PDF_{lem} one. It means that the *SRM_FDM*, compared to the *LEM_GA*, is less sensitive to the variation of the input variables when they varied within great values. An interpretation of this phenomenon is the following one. For the FoS computation

using the *SRM_FDM*, the SRM is adopted. It reduces the shear strength parameters (c' and $\tan(\phi')$) by a factor and re-calculates the stress of each element. This process is repeated for different values of reduction factor until the model becomes unstable. As the same reduction factor is applied to both the strength parameters each time, the parameter with a relatively small value is thus the crucial parameter which defines the final reduction factor (i.e. FoS) since it is easier to reach its critical value which can lead to an instability. For the encountered problem, the variable $\tan(\phi'_{shell})$ becomes the crucial parameter when great values are set to the input variables. Because the ϕ'_{shell} has a lower variance than the one of c'_{shell} . It is more probable to generate a high value for c'_{shell} such as 25 kPa which is over two times than its mean value, than for ϕ'_{shell} which varies mainly between 32° and 38° (Figure 3.9). As a result, the PDF_{srm} has a very small variability for its right part. For the *LEM_GA*, the negative skewness of the PDF_{lem} is simply due to the fact that the c'_{shell} , which is the most important variable for FoS variance, has much more small values. Therefore, the right part of the PDF_{srm} peak point has a lower variability than the PDF_{lem} one.

An advantage of using the *LEM_GA* is that it can reduce considerably the computation time of a reliability analysis. The time required to perform one deterministic simulation using the *SRM_FDM* is about 20 minutes on an Intel Xeon CPU E5-1620 3.5GHz PC, while it is just 10 seconds for the *LEM_GA*. Then, the time of performing a direct MCS, coupled with the *LEM_GA*, is acceptable (2~3 days) for the cases with a relatively high Pf ($> 10^{-2}$). The surrogate model (e.g. SPCE) can be used optionally for a further time reduction (e.g. reduced to 30 mins as showed in section 4.2.2) and obtaining more results (e.g. sensitivity indices). However, for the cases with a lower Pf ($< 10^{-3}$), it seems necessary to appeal to the surrogate modelling technique or other methods since the time of a direct MCS could be several weeks or months if the target CoV_{Pf} is 10%, even an efficient deterministic model (i.e. 10 seconds for one simulation) is used.

4.3.2 Effect of the distribution type for input variables

In the previous section, all the variables are assumed to follow Beta distributions. Although it seems that this type of distribution can describe better the soil variability of the studied dam according to Figure 3.9, the effect of using another distribution type for input variables on the reliability results is investigated.

In this section, all the variables are assumed to follow Truncated normal distributions instead of Beta distributions. The results are compared to those obtained in section 4.2. The statistical parameters are taken from Table 3.2. Only the *LEM_GA* model is used for this study since it can provide similar results to the *SRM_FDM* and is faster. The aim is to study the effect of distribution type on the probabilistic results.

Figure 4.6 compares the PDFs of the FoS under two exploitation conditions obtained by assuming two distribution types for the RVs, and Table 4.5 presents the reliability results. For the sensitivity indices, they are presented in Figure 4.7.

It can be observed from Figure 4.6 that the PDF curve obtained by truncated normal distributions (PDF_N) is taller and narrower than the one of beta distribution (PDF_B), for both the two exploitation conditions. For the part left to the peak point of the PDF curve, the PDF_B presents a higher variability and a higher value of probability density than the PDF_N . It indicates that using a Beta distribution gives a higher probability to obtain a small FoS value. This is because the probability of generating a small value of c' in the Shell zone drawn from the fitted Beta distribution is higher than the Truncated normal distribution, as presented in Figure 3.9. Please note that the variable c' in the Shell zone has the most important influence on the FoS variance which is evidenced by the GSA results. In addition, the four curves are negatively skewed. The reason has been given in the previous section.

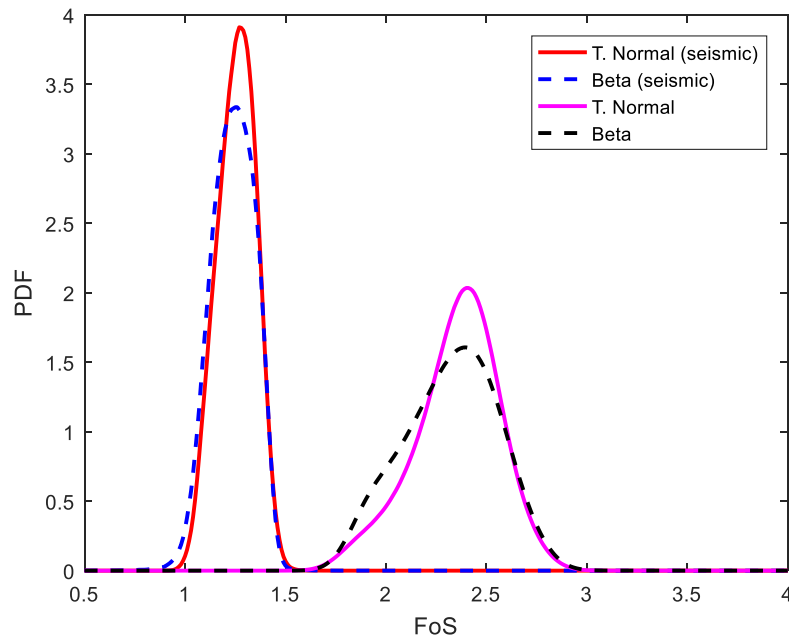


Figure 4.6 Comparison between the PDFs obtained by Beta and Truncated Normal distribution

According to Table 4.5, one can conclude that assuming Truncated normal distributions for the input variables lead to a smaller failure probability than Beta distributions. It should be noted that the failure probabilities presented in Table 4.5 for seismic loading conditions are the one considering a return period of 5000 years. Concerning the first two moments of FoS, a bigger mean value and a smaller standard deviation are obtained when Truncated normal distributions are used. This is in agreement with the observation of the PDF shapes in Figure 4.6. The differences are not significant.

Table 4.5 Reliability results obtained by two distribution types

Exploitation condition	Distribution	Pf_{sce}	$Mean_{FoS}$	Std_{FoS}	CoV_{FoS}
Seismic	Beta	2.8×10^{-6}	1.24	0.108	8.7%
	T. Normal	0.9×10^{-6}	1.25	0.096	7.6%
Normal	Beta	2.7×10^{-6}	2.32	0.242	10.5%
	T. Normal	1.0×10^{-6}	2.35	0.218	9.26%

As for the sensitivity index of each variable, Figure 4.7 gives a comparison between the two distribution types for the two exploitation conditions. Comparable results are

obtained from the two distributions types. The most two important variables are the same as the previous analyses. In addition, it is observed that the Sobol index of the variable c' in the Shell zone decreases while the one of ϕ' is increasing when the truncated normal distribution is used. The reason is that the variability of the variable c in the Shell zone is decreased when the fitted distribution type is changed from Beta to Truncated normal, as presented in Figure 3.9.

In summary, the two distribution types give comparable reliability results. Assuming Beta distribution for the input variables can lead to a higher Pf compared to a Truncated normal distribution. The assumption is thus conservative. However, this assumption is more realistic since it can represent better the soil variability of the considered dam than the Truncated normal distribution as shown in Figure 3.9.

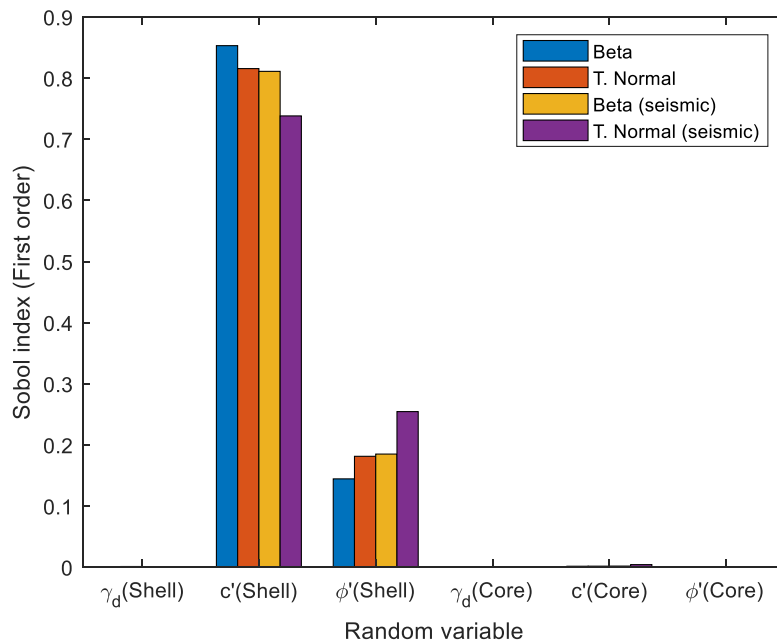


Figure 4.7 Sobol index of each variable for different distribution type of input variables

4.4 Conclusion

This chapter uses the RVs approach to probabilistically evaluate the dam stability condition. A global sensitivity analysis is performed at first for the purpose of understanding the contribution of each soil property on the dam FoS variation with a

focus on the effects of the soil hydraulic parameters. It is observed that the two most significant variables are c' and ϕ' of the Shell zone with a sum of the first-order Sobol index around 0.99 for both the two cases (normal and seismic operation). Another important remark is that the variabilities of the hydraulic conductivity (K_v and R_k) have almost no effect on the FoS variation. This finding can support the simplification made for the following studies in which the uncertainties related to K_v and R_k are ignored.

The dam reliability is assessed under two exploitation conditions (normal and seismic) by using the SPCE-MCS. The obtained failure probabilities related to the dam sliding stability are all in the order of 10^{-6} , indicating a good design of the studied dam for these two conditions. The effectiveness of the method SPCE is also checked by comparing it with a direct MCS and a direct GSA using the *LEM_GA* model under the seismic exploitation condition. The results show that using the SPCE can provide accurate estimates of the Pf , FoS statistics and sensitivity indices with a greatly reduced computational time compared to the direct analyses.

Additionally, two technical issues related to the dam probabilistic analysis are discussed in the chapter: one about the effects of using different distribution types for the input variables and another one about the comparison between the SRM and the LEM in probabilistic analyses. It is found that using Beta distributions can lead to a higher Pf compared to Truncated normal ones. Thus, the Beta is considered being conservative for the studied case. For the second issue, the results show that the two deterministic models can give basically similar results in terms of failure probability, distribution of the FoS and sensitivity index of each variable. However, a different performance between the two methods (SRM and LEM) within great FoS values for the present case is highlighted as shown in Figures 4.2 and 4.4. This is due to the fact that the variable ϕ' varies within a very narrow range compared to the c' while the SRM applies the same reduction factor to $\tan(\phi')$ and c' leading to the FoS with great values are

mainly influenced by ϕ' , thus showing a low variability at the region of these values. By using the *LEM_GA* model for the dam FoS evaluation, the computation time of a reliability analysis can be drastically reduced. It is thus recommended for a dam probabilistic analysis and could be applied at the preliminary dam design stage.

5 CHAPTER V: Probabilistic analysis using the random- fields approach

This chapter improves the dam probabilistic analysis of CHAPTER IV by introducing random fields (RF) of soils properties γ_d , ϕ' and c' . The γ_d RFs are based on the geo-localised measurements while the ϕ' RFs are obtained by transforming those of γ_d . Considering the lack of geo-localized c' data, the effect of c' RFs is also discussed in this chapter by adopting hypothetical values. The objective is to account for the soil spatial variability, which is unavoidable for earthen structures, in the dam reliability analysis. In accordance with the conclusions of the previous chapter, only the seismic scenario (considering a pseudo-static acceleration of $0.24g$) is considered in the following chapter, by the fact that the dam under normal exploitation conditions has a low failure probability (in the order of 10^{-6}). Two complementary studies, which could be beneficial for future applications, are conducted in the context of RFs-implemented probabilistic analysis. The first one compares five reliability methods for high dimensional stochastic problems and permits to provide relevant recommendations. The present dam problem is high dimensional since a large number of RVs are generated to represent the desired RFs for each simulation. The second study models the soil spatial variability by different kinds of RFs (e.g. conditional) and investigates their effects on the dam reliability.

This chapter starts with a performance survey of the *LEM_GA* model for nonhomogeneous soils. Then, the two complementary studies mentioned above are conducted in order to discuss the method selection for high dimensional cases and the modelling of different RFs.

5.1 Performance survey of the model *LEM_GA* within spatially varied soils

As presented before, three deterministic models are developed in this work. The *SRM_FDM* and *LEM_GA* can both be coupled with RFs easily, while the *SRM_FEM* presents difficulties for implementing RFs because a direct modification of the soil properties for each element is not permitted in the adopted platform (Plaxis). The

LEM_GA is preferred to the *SRM_FDM* because of its computational efficiency which enables a large number of deterministic calculations required for the subsequent studies (MCS, comparison of reliability methods and effects of different RFs). Indeed, according to the results of CHAPTER IV, the *LEM_GA* is able to provide similar reliability analysis results compared to the *SRM_FDM* in the context of RVs. This section aims to evaluate the *LEM_GA* performance for spatially varied soils modelled by RFs. To achieve this purpose, a comparison study is carried out. It involves generating a number of RFs for ϕ' and γ_d , and RVs for c' , and estimating the dam FoS for each set of input parameters by using both the two deterministic models (*LEM_GA* and *SRM_FDM*). In total 150 sets of input parameters are considered in the comparison study. Each set of input parameters is obtained randomly and is composed of three RFs of γ_d , three RFs of ϕ' and two RVs of c' which is the typical scenario considered for the following studies. Figure 5.1 presents a direct comparison of the FoS values computed by the two models for the 150 different input sets. It is shown that the results are close to the unit line and the relative errors are mainly smaller or around 5%. These observations indicate that the *LEM_GA* is able to provide reasonable estimates of the dam FoS considering RFs. Therefore, the *LEM_GA* effectiveness is validated for the cases of RFs and can be used for the following analyses.

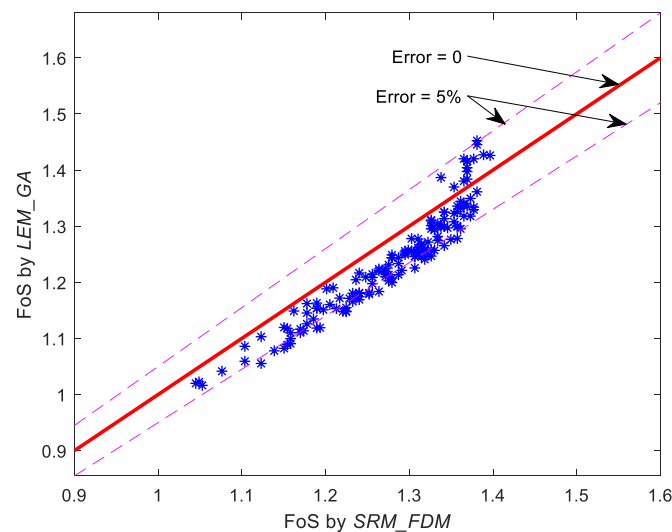


Figure 5.1 Comparison of the FoS estimates obtained by the two models for 150 random input sets

Additionally, a comparison concerning the failure surface location determined by the two models is conducted, and the results are presented in Figure 5.2. Two different cases are considered for the comparison: the first one (case 1) is randomly selected from the previous 150 sets of input parameters while the second one (case 2) is obtained by randomly generating RFs for all the three soil properties (γ_d , c' and ϕ'). The corresponding FoS estimates are also provided in Figure 5.2; a good agreement between the two models is observed. For the failure surface, it is found that the *LEM_GA* surface is not exactly the same as the one given by the *SRM_FDM*, but the two surfaces are similar and comparable with each other for both cases. For case 2, the failure surface is apparently non-circular according to *SRM_FDM*. This result is expected since the three soil properties are all modelled by RFs and the soil is more nonhomogeneous. This non-circular feature is also captured by the *LEM_GA* due to the non-circular trial slip surfaces generation method (Cheng et al., 2008), although it is not the same with the *SRM_FDM*. On the contrary, the failure surface of case 1 is close to a circular shape by the fact that the variabilities of γ_d and ϕ' , which are modelled by RFs, are not significant (their CoVs are lower than 5% according to Table 3.2). It is noted that the comparison of the critical slip surfaces shown in Figure 5.2 is less important than Figure 5.1 since the focus of using the deterministic model lies in providing the dam FoS estimates in this work. However, such a study helps to have an idea about the *LEM_GA* performance of locating the failure surface in nonhomogeneous soils, and could be useful for future studies which would consider the failure soil volume, for example, in a risk/damage assessment.

In order to obtain a sufficient accuracy in terms of the variance error for RFs, Li and Der Kiureghian (1993) recommended that the stochastic grid size can be set equal to 0.2 times the autocorrelation distance. This condition is well satisfied for all the RFs generation in this work with respect to the values of L_x and L_z given in Table 3.4.

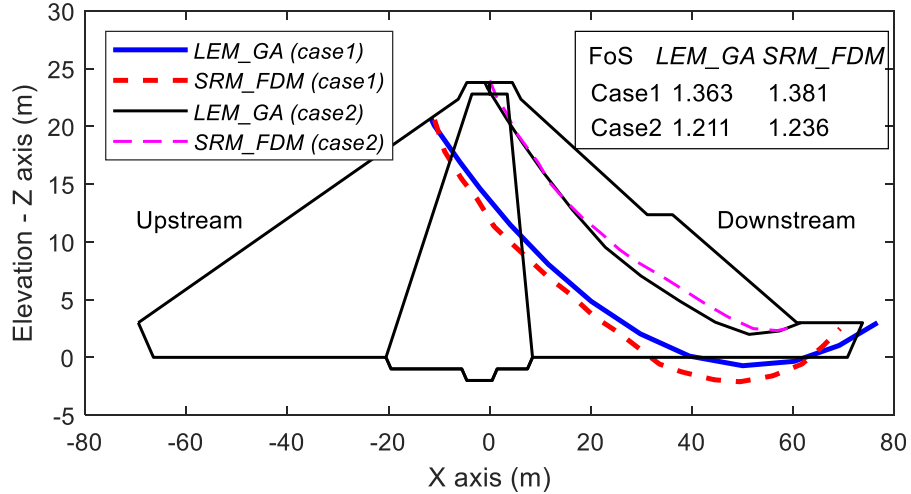


Figure 5.2 Comparison of the failure surfaces determined by the two models for two cases

5.2 Comparison of five reliability methods for high dimensional problems

As presented in section 2.2.3, a K-L expansion should be truncated to a limited number of series terms S_{KL} for practical applications of RFs simulations. The value of S_{KL} can be determined by evaluating the error defined by Eq. (2-38) with a prescribed accuracy. This error is dependent to the autocorrelation distances and the RF size. For an accuracy close to 10%, the S_{KL} is estimated to 30, 368 and 1710 for respectively the Shell-1, Core and Shell-2 zone (considering their site dimension and the relevant autocorrelation distances presented in Table 3.4). It means that, for example, at least 1710 RVs are needed to represent accurately a γ_d RF for the Shell-2 zone (downstream shell). Therefore, the present study involves a high dimensional stochastic problem due to the small autocorrelation distances determined with the measurements.

This section conducts a comparative study of several reliability methods with the purpose of evaluating their performance for high dimensional problems. In literature, few studies exist for the comparison of different reliability methods in real engineering problems, and no study has been done for the stochastic problems with more than 1000 RVs in the geotechnical field. The comparison results obtained in this section are

expected to help engineers/researchers in the method selection for such complex problems.

5.2.1 The considered reliability methods for the comparative study

For a reliability analysis, the MCS is always considered as a standard reference to test other methods (Rubinstein, 1981; Sudret and Der Kiureghian, 2000). However, it suffers from a very low computational efficiency. Based on the MCS, one advanced sampling method (SS (Au and Beck, 2001)) was proposed to reduce the variance of the MCS estimator with a limited number of deterministic model calls. It is applicable for the problems with spatially varying soils (Ahmed and Soubra, 2014) since the method is independent of the input dimension. Another reliability method is the Moment Method (MM) (Rosenblueth, 1975) which uses approximation by Taylor series to estimate the first moments of a system response and then to compute the reliability index with the estimated moments. Alternatively, the first moments can also be determined by performing an MCS until the convergence is reached. The MM, based on the MCS, is independent to the input dimension, so it is applicable for the present problem. Furthermore, the F/S-ORM are also commonly used in the field of reliability analysis (Babu and Srivastava, 2010; Mollon et al., 2009). The main task of these methods is to locate a so-called design point by solving a constrained problem. Unfortunately, these methods are not able to handle too many RVs (Pan and Dias, 2017b). During the last decades, meta-modelling techniques have received much attention in the reliability analysis due to their efficiency and accuracy (Sudret et al. 2017). In the context of high dimensional stochastic problems, some dimension reduction techniques were introduced and combined with the meta-modelling technique to improve its performance, such as the SPCE combined with the GSA (termed as SPCE/GSA) (Al-Bittar and Soubra, 2014) and the SPCE combined with the Sliced Inverse Regression (termed as SPCE/SIR) (Pan and Dias, 2017c) which were proposed in recent years. They use respectively the GSA and the SIR to reduce the number of the

involved RVs at first stage, and then to construct an accurate SPCE meta-model based on the reduced dimension.

In summary, the selected reliability methods for the comparative study are thus: a reference method (MCS), a variance reduced MCS (SS), an MCS-based moment method (MM), and two meta-modelling approaches (the SPCE/GSA and the SPCE/SIR). The first three methods are consistent with the presentations given in section 2.1.3. Specifically, the number of calls to the deterministic model in the MCS is determined by considering a CoV_{Pf} around or lower than 5%; the intermediate failure threshold P_{SS} is selected as 0.2 and the model evaluation number N_{SS} of each intermediate level is 1000 for the SS. Concerning the MM, the fourth moment approximation (Eq. 2-14) is used to estimate the reliability index and then the Pf by Eq. 2-3. The convergence of the four required moments is evaluated by adopting a dynamic criterion which can be satisfied only when a selected error is lower than a value ε_{MM} for N_{MM} continuous steps. In this work, the selected error is the relative difference of the target moment between two continuous iterations. The ε_{MM} and N_{MM} is set respectively as 0.1% and 100. Such a severe convergence criterion can guarantee that the values of the four moments, which are primary elements for the MM, are accurate enough.

The last two methods are based on the SPCE and share a similar analysis procedure in general. Figure 5.3 shows a flowchart for describing the procedure. It is followed by a brief presentation of the two dimension-reduction techniques (GSA and SIR) which are not reviewed in CHAPTER II. As mentioned above, the present dam problem is high dimensional due to the RF discretization. Directly using the metamodeling technique to create a surrogate is inefficient and reducing the input dimension is necessary under such a situation. It is noted that the SPCE surrogate model in the two methods are constructed with respect to the procedure of Table 2.2.

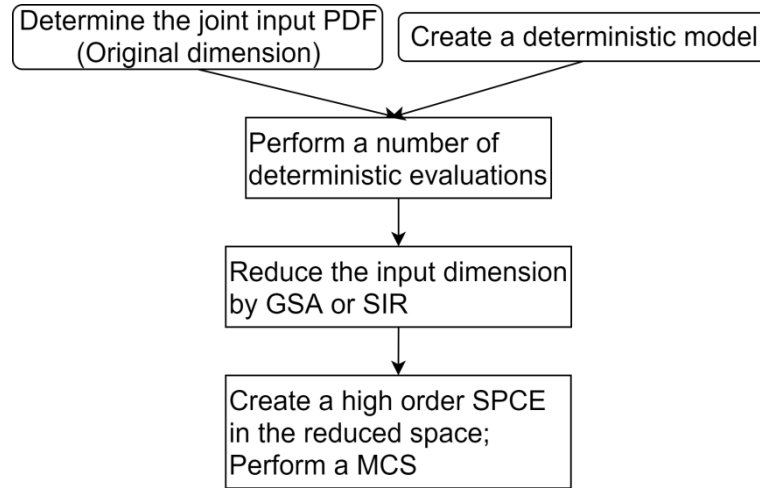


Figure 5.3 Flowchart for the methods SPCE/GSA and SPCE/SIR

For the SPCE/GSA, the dimension reduction is achieved by performing a SPCE-based GSA and regarding the negligible variables as deterministic according to the GSA results. At this stage, the SPCE is in 2nd order which needs a smaller *ED* than a high-order one. It is noted that the order of the SPCE has insignificant effects on the estimated Sobol indices (Al-Bittar and Soubra, 2014; Sudret, 2008). Particularly, this work proposes to select the variables by using a threshold for the sum of the obtained Sobol indices. Firstly, all the input variables are sorted with a descending order according to the GSA results. Then, the first N_{GSA} variables would be selected so that the sum of the selected Sobol indices is greater than a target value, saying 0.98 of the global sum in this work. This technique guarantees that the reduced dimension covers at least 98% of the total input variance. For the SPCE/SIR, it reduces the input dimension by using the SIR which is based on the principle that a few linear combinations of original input variables could capture essential information of a model response. It aims to find an effective dimension reduction space by considering an inverse regression relation which regresses input variables against model responses. For more details about these two dimension reduction techniques, readers are referred to (Guo et al., 2019a; Pan and Dias, 2017c).

5.2.2 Reliability analysis using the reference method MCS

This section aims to present the dam reliability analysis by using the MCS (reference for the comparative study) in combination with the computational model *LEM_GA*. This model has been proven to be effective for nonhomogeneous soils. The γ_d and ϕ' are represented by RFs while the c' is considered as RVs due to the lack of geo-localised data. Besides, the effects of the γ_d RFs autocorrelation distance on the dam reliability are examined by testing several values recommended in literature.

5.2.2.1 Numerical results

Similar to section 4.3.2, two distribution types are considered (Beta and Truncated normal) for the soil properties γ_d , c' and ϕ' . For each distribution type, 20 000 deterministic calculations are performed within the MCS framework. With regard to one deterministic simulation, three standard-normal γ_d RFs, for three different zones (Shell-1, Core and Shell-2), are firstly generated by using the K-L expansions with the parameters given in Table 3.4. They are then transform into physical-values space for the target distribution type by using the iso-probabilistic method (Cho and Park, 2010; Li et al., 2011) with the parameters shown in Table 3.2. Then the three ϕ' RFs are obtained with the Caquot's relation. The c' values for the zones Shell and Core are generated with the LHS. Figure 5.4 shows the PDF of the obtained 20 000 FoS values for the two distribution types, and Table 5.1 gives the reliability analysis results.

From Figure 5.4, it can be observed that the PDF curve obtained by the Truncated normal distribution (PDF_N) is taller and narrower than the one of Beta distribution (PDF_B). It means that the FoS values are less dispersive if a Truncated normal distribution is assumed for the random input variables. More precisely, the two PDF curves are almost superposed for relatively high FoS values (higher than 1.4), while the PDF_N is significantly lower than the PDF_B for relatively small FoS values (smaller than 1.2). This is because the probability of generating a small value of c' in the Shell zone drawn from the fitted Beta distribution is higher than the Truncated normal distribution,

as presented in Figure 3.9. In addition, the two curves are not symmetric. They are considered to be negatively skewed with a relatively bigger tail at the left. The reasons have been discussed in section 4.2.1.

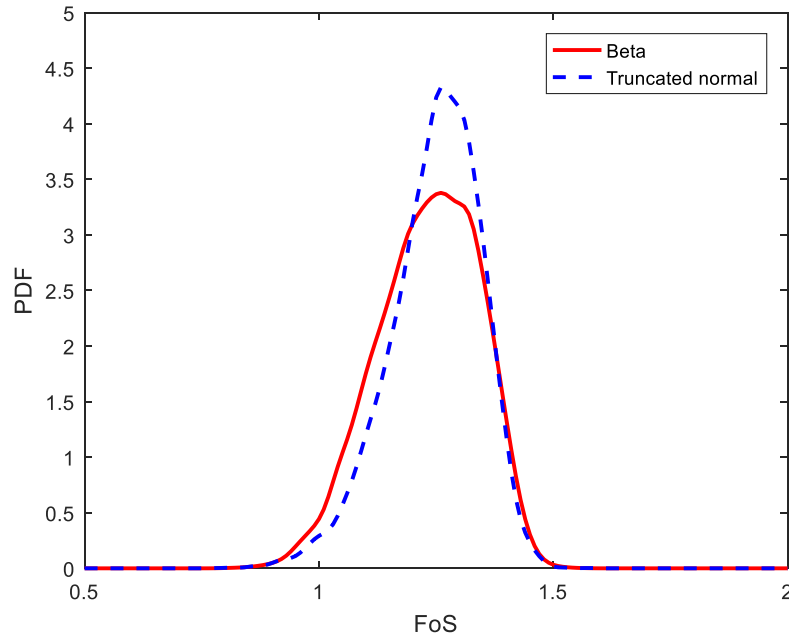


Figure 5.4 PDF of the FoS values obtained with RFs and MCS

Table 5.1 shows the failure probability and the statistical moments of FoS obtained by MCS. The direct failure probability Pf_{con} of the dam under a pseudo-static acceleration of 2.4 m.s^{-2} is estimated to be equal to 0.022 and 0.016 respectively by the Beta and Normal distributions. These values are then multiplied by the probability of the earthquake (simply assumed to be $1/5000$) and become equal to 4.4×10^{-6} and 3.2×10^{-6} respectively. As for the statistical moments of the FoS values, the Beta assumption gives a slightly lower value for the mean but a higher value for the standard deviation. A high value of standard deviation means a high level of data scatter. This is consistent with the observations in Figure 5.4. According to Table 4.4, the Pf_{con} of the Beta distribution is equal to 0.012. This is obtained by simulating γ_d , c' and ϕ' with RVs. It is close to the estimated result with RFs (0.022) in this section and both are relatively high. This is attributed to the variable c' which is dominant for the FoS variance (thus Pf_{con}) as presented in Figure 4.5 and is modelled identically by RVs in both cases. It is

also found that the Pf_{con} of this section is slightly higher than the one of Table 4.4. This finding is due to the different approaches for modelling the Shell-2 ϕ' in the two analyses, given that this variable is the second most important one as shown in Figure 4.5. In this section, the ϕ' is considered by RFs and is obtained by transforming γ_d RFs, while, in section 4.2.2, it is represented by RVs with the parameters of Table 3.2. By randomly generating 10 γ_d RFs for the zone Shell-2, 10 ϕ' RFs are obtained and the related mean and CoV are estimated as respectively equal to 34.8 and 7.5%. The mean value is approximately the same as the one used in section 4.2.2. However, the CoV is significantly increased with regard to the value of 3.7% presented in section 4.2.2. This observation explains why the Pf_{con} is slightly increased in this section.

In conclusion, the dam failure probability (Pf_{sce}) under a pseudo-static loading condition and using RFs is estimated to be around 4×10^{-6} . The two distribution assumptions lead to similar results with the same order of magnitude. The Beta distribution gives slightly more conservative results in terms of the failure probability. As the Beta distribution describes better the variability of the soil properties as shown in Figure 3.9 and is conservative in the design, this type of distribution is adopted for the following studies.

Table 5.1 Reliability analysis results obtained with RFs and MCS

Distribution	Failure probability			Statistical moments of FoS	
	Pf_{con}	Pf_{sce}	CoV_{Pf}	Mean	Standard deviation
Beta	0.022	4.4×10^{-6}	4.71%	1.232	0.108
Truncated normal	0.016	3.2×10^{-6}	5.61%	1.248	0.097

5.2.2.2 Influence of the autocorrelation distance

One of the factors which can influence the reliability results of RFs cases is the autocorrelation distance. It defines, by means of an autocorrelation function, the autocorrelation structure of an RF. According to a literature review given by El-Ramly

et al. 2003), the autocorrelation distance for natural soils is usually within a range of 10-40 m in the horizontal direction, while it varies between 1 and 3 m in the vertical direction. It is found that the L_x and L_z in the Shell-1 zone (Table 3.4) are bigger than the values indicated in El-Ramly et al. (2003) while the L_x in the Shell-2 zone is smaller than expected values. Therefore, careful attention must be done to these parameters and their induced influence on the reliability analysis.

Finally, the impact investigation is focused on the value of L_x in the Shell-2 zone while the estimated autocorrelation distances in the Shell-1 zone are accepted for the values in Table 3.4. The reasons are as follows: 1) the obtained large values of L_x and L_z are expected for the Shell-1 zone since the materials were carefully selected and more attention were given to its construction; 2) the upstream part of the backfill embankment is considered to have a very limited influence on the dam stability under steady-state flow conditions; 3) large values of autocorrelation distances may lead to higher failure probabilities so conservative designs, as pointed in (Cho, 2007; Guo et al., 2019b).

For the L_x value in the Shell-2 zone, a first improvement is made by fitting the experimental semi-variogram with other theoretical variogram models such as the Gaussian and the spherical models (Fenton and Griffiths, 2008). The L_x is estimated to be equal to 6.7m for the Gaussian model, and 4.7m for the spherical model. These values are both different to the one estimated with the exponential model (4.9m) as shown in Table 3.4, and these differences may induce an impact on the dam failure probability.

In order to quantify the influence induced by different values of L_x , a parametric study is conducted. Several values of L_x in the Shell-2 zone are tested using the MCS. The objective is to investigate the evolution of the dam failure probability with the L_x value. For the sake of simplicity and clarity, the other values of autocorrelation distance are

rounded to integer values (see details in Table 5.2). In addition, the L_x value in the Core zone is also varied. Totally, four cases are selected for the parametric study. The L_x value in the Core and Shell-2 zones are decreased from 80 to 10m. These four cases allow investigating the influence of the horizontal autocorrelation distance in the Core and Shell-2 zones on the dam failure probability. The reference case in Table 5.2 refers to the values estimated by the variogram analysis with the exponential model (see Table 3.4). As an illustration, one random realization of 3 γ_d RFs generated with the L_x - L_z values of Table 5.2 is presented in Figures 5.5 and 5.6 for respectively the case 1 and reference case. It can be seen that there exist some relatively uniform zones with high or small values in the Upstream RF for both two cases. This is due to the high values of L_x - L_z considered in the two cases for this zone. Significant difference between the two figures is observed for the Core and Downstream RFs. In case 1, the L_x is rather higher than the L_z for the two RFs; so, the vertical variation is more remarkable and relatively uniform layers are developed. In reference case, the L_x is reduced from 80m to less than 15m which leads to a more significant fluctuation in the horizontal direction. The modelled soil property is thus more heterogeneous. The generated RFs do not appear to be completely random. They have a streaky appearance which suggests a structure that could be related to the correlation distances and/or possible problems with the K-L method. Figures 5.5 and 5.6 show more pronounced streakiness in the horizontal direction which is consistent with the correlation distances used ($L_x > L_z$). This streakiness also appears (but less remarkable) in Figure 2.6 using $L_x = L_z$, which would appear to be associated with the K-L. The streakiness could have an effect in the numerical analysis of geotechnical stability, where a point area of weakness could trigger a slope failure. Careful investigations are required in future works in order to have better understanding on the induced effects and give relevant recommendations of using the K-L.

Table 5.2 Selected values of L_x and L_z for the parametric study

	Shell-1		Core		Shell-2	
	L_x (m)	L_z (m)	L_x (m)	L_z (m)	L_x (m)	L_z (m)
Case1	80	8	80	2	80	2
Case2	80	8	40	2	40	2
Case3	80	8	20	2	20	2
Case4	80	8	10	2	10	2
Reference case	78.1	7.8	13	1.5	4.9	1.9

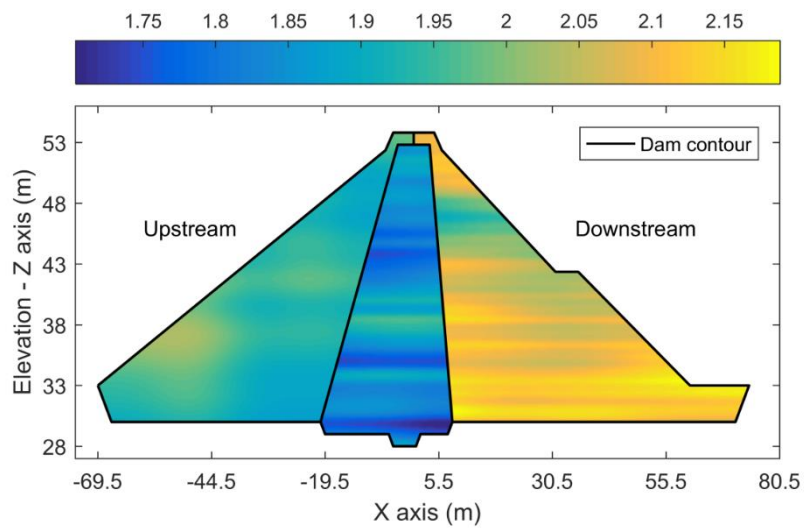


Figure 5.5 One random realization of $3 \gamma_d$ RFs generated for case 1 (unit: g/cm^3)

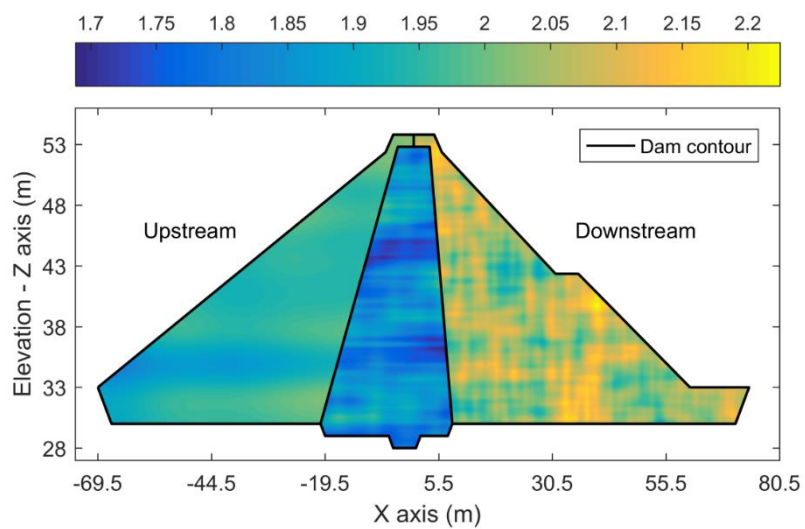


Figure 5.6 One random realization of $3 \gamma_d$ RFs generated for reference case (unit: g/cm^3)

By adopting different values of autocorrelation distance as shown in Table 5.2, four complementary MCSs are performed. Figure 5.7 plots the four obtained failure probabilities (Pf_{con}) together with the one of the reference case (section 5.2.2). The first two moments of the dam FoS for each case are also given in Figure 5.7. It can be observed that the L_x in the Core and Shell-2 zones have an influence on the dam failure probability. The Pf_{con} is decreased when decreasing L_x . For example, a reduction of L_x from 80 to 10 m results in a drop of about 10% for the Pf (from 0.0295 to 0.0259). This finding has already been confirmed by many researchers for different geotechnical works (Cho, 2007; Guo et al., 2019b; Pan and Dias, 2017b). A possible explanation is as follows. Taking a soil block of a length equal to 20m as an example (the thickness is fixed at 1m), a large L_x value (e.g. 40 or 80m) means that all the RF grid values within this soil body are strongly correlated and there is a great probability of forming a uniform weak area if the RF value at one side of the soil block is small. However, the probability of having a weak area covering the soil block is low if small L_x values (e.g. 10 or 4.9m) are considered since there are probably high values generated within the soil body by the nature of randomness and the weak correlation between two points over a distance larger than the L_x (see Figure 5.6). Therefore, the number of small FoS estimates is reduced in the case of low L_x values, and the Pf_{con} is decreased. Concerning the statistical moments, the mean value remains almost constant whereas the standard deviation is increased when increasing the L_x . This indicates that the L_x has no impact on the mean value of the dam FoSs, whereas it affects the FoSs dispersion of the dam. The reference case corresponds to the lowest failure probability and the smallest standard deviation.

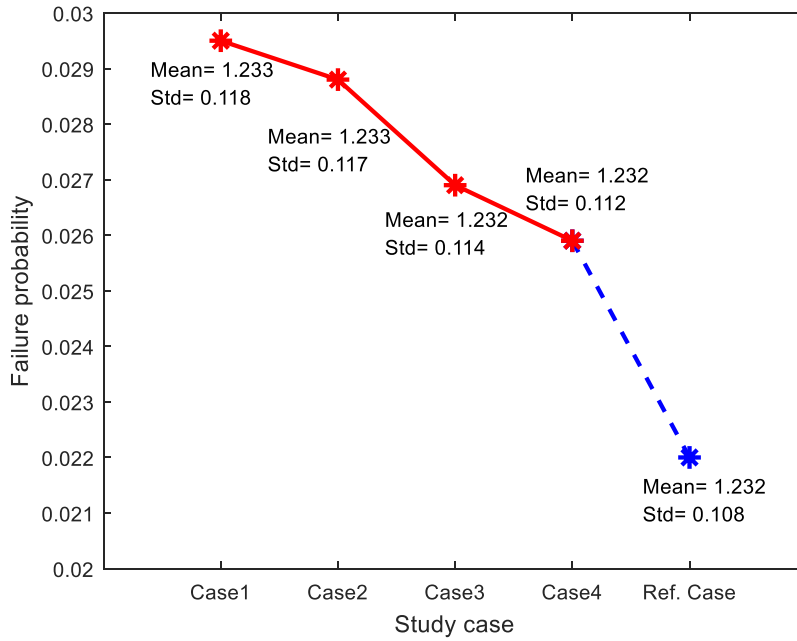


Figure 5.7 Influence of the L_x on the dam failure probability (Pf_{con})

5.2.3 Comparison results from five reliability methods

The parametric study on the autocorrelation distance conducted with MCS (the reference method presented in section 5.2.2) is re-performed by the four selected reliability methods (SS, MM, SPCE/GSA and SPCE/SIR). The obtained results from the five reliability methods in terms of the failure probability (Pf_{con}) for each case are plotted in Figure 5.8, and the numbers of calls to the deterministic model (N_{call}) for each case are summarized in Table 5.3. In this table, the number of the required RVs ($N_{RV} = N_{RV_{KL}} + 2$) for representing c' , ϕ' and γ_d by means of RFs or RVs is given as well. The $N_{RV_{KL}}$ is the RVs number needed for generating relatively accurate γ_d RFs by using the K-L method, and the number 2 represents the two RVs of c' in the Shell and the Core zone. The information in Table 5.3 helps to visualise the efficiency of each method by comparing the N_{RV} with the N_{call} .

A quick review of Figure 5.8 reveals that the four methods can all give relatively accurate Pf_{con} estimates compared to the MCS results. The values are varied within a

same order of magnitude for different methods. For example, the Pf_{con} is between 0.015 and 0.024 for the Reference case according to the five methods.

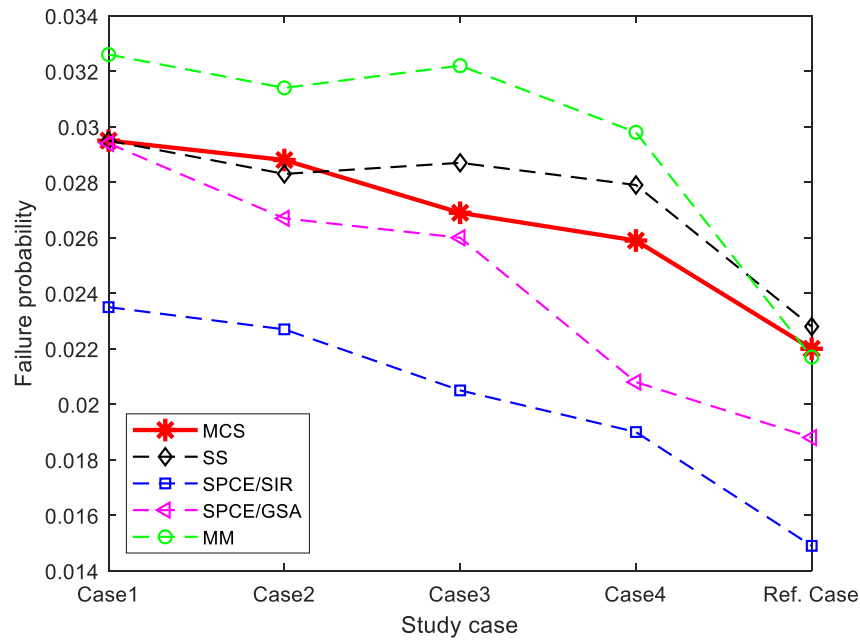


Figure 5.8 Comparison of the failure probability obtained by the five reliability methods

Concerning the efficiency comparison presented in Table 5.3, it is found that all the approximated methods need fewer calls of the deterministic model than the direct MCS. This is the reason why these methods are alternatives to the MCS for reliability analyses. Besides, the N_{RV} value is increased from Case 1 to Case 4, and the N_{RV} of the Reference Case is the biggest one. This is because the autocorrelation distance L_x value in the Core and Shell-2 zones are decreased from 80 to 10m. Smaller values of the autocorrelation distance mean that it needs more RVs to represent an RF with a specific error variance. By comparing the N_{RV} with the N_{call} of each method, it is observed that the N_{call} of the methods MCS, SS and MM is almost changeless to the N_{RV} . In other words, the efficiency of these three methods is not related to the number of input RVs, but depends on, in fact, the value of the target failure probability. However, the N_{call} of the two meta-modelling methods (SPCE/GSA and SPCE/SIR) is increased rapidly with increasing the N_{RV} . This indicates that the efficiency of the meta-modelling methods strongly depends on the number of input RVs. Indeed, more input variables

mean that more information is needed. Thus, a higher N_{call} will be required for constructing a meta-model which will be used to replace the original mechanical model.

Table 5.3 Approximated number of calls to the deterministic model for the five reliability methods

	Case 1	Case 2	Case 3	Case 4	Reference case
$N_{RV}^{(1)}$	225	370	647	1207	2110
MCS	20000	20000	20000	20000	20000
SS	3000	3000	3000	3000	3000
SPCE/SIR	1000	5000	8000	10000	15000
SPCE/GSA	3000	5000	8000	13000	18000
MM	1900	1800	2100	2000	2000

Note: ⁽¹⁾ Number of required RVs for representing c' , ϕ' and γ_d by means of RFs or RVs

The following section gives a detailed interpretation of the comparative study for the four alternative reliability methods. Some concluding remarks of the comparative study are also provided.

5.2.4 Discussions on the results

5.2.4.1 The SS

This method is efficient for high dimensional stochastic problems, according to Table 5.3, which requires only 3000 (an approximated value) calls to the deterministic model. The N_{call} of the SS is much less than the MCS one and is constant with the N_{RV} variation. This finding is not surprising since the target failure probability is relatively high (around 0.022) and changes slightly between the different cases in the present problem. If a conditional probability P_{SS} of 0.2 is adopted for each simulation level, only 3 simulation levels are needed to reach the final failure domain. In this study, the P_{SS} is set to 0.2 and the sample numbers in each simulation level (N_{SS}) is set to 1000. However, it is found that the SS cannot produce a consistent evolution of Pf with L_x . The obtained values of Pf are fluctuated from the Case 2 to 4, while they are expected

to be monotone decreasing as shown by the MCS. This limitation originates from the generation of the conditional samples in the SS. As a large number of RVs are considered, and more importantly those used for RF generation have no physical meanings, it is thus difficult to generate effective conditional samples. This results in a large number of repeated samples in the SS. Given that the number of these repeated samples is not constant (i.e. random) for each SS, the obtained results are thus not steady. The obtained results by considering a N_{SS} of 1000 are better than the ones of $N_{SS}=200$ presented in Guo et al. (2019a)g. However, the Pf inconstancy is still observed. Other algorithms (e.g. (Papaioannou et al., 2015)) can be tested in a next work in order to further investigate the SS performance for the stochastic problems with RFs (i.e. a large number of RVs with no physical meanings).

5.2.4.2 The SPCE/SIR

According to Figure 5.8, this method always gives slightly lower failure probability than the MCS. This can be explained by the fact that a dimension reduction technique is employed. As the dimension is reduced, the variability of the input parameters is reduced. The estimated Pf is thus smaller. Compared to the SS, this method has a better performance in the parametric study, i.e. the obtained values show a clear reduction trend of Pf with decreasing L_x . Concerning the efficiency, the N_{call} is found not constant for different cases but is increased from the Case 1 to the Reference case. The N_{call} for the Reference case is even very close to the MCS one. An explanation is given as follows. The required number of input RVs for the RF generation is increased since the L_x becomes smaller. Therefore, the construction of a meta-model needs more training samples, i.e. more deterministic simulations. As a result, it is not recommended to use this method if the N_{RV} is large (e.g. >2500) from a point of view of efficiency.

5.2.4.3 The SPCE/GSA

This method shows a good accuracy in estimating the Pf according to Figure 5.8. The obtained Pf values are close to the ones of the MCS. Except to this remark, similar

observations to the SPCE/SIR can also be noted: (1) the estimated Pf values are all lower than those of the MCS; (2) the parametric study can be correctly conducted; (3) the N_{call} is increased with decreasing the L_x and the N_{call} for the Reference case is even very close to the one of the MCS. The interpretation to these observations given above remains valid as well for this method. Besides, it is found that this method is always less efficient than the SPCE/SIR. This difference originates from the different dimension reduction techniques employed in the two methods. For the SPCE/GSA, it should always construct a 2-order meta-model with the full dimension. On the contrary, the dimension is reduced before constructing meta-models in the SPCE/SIR. For high dimensional stochastic problems, considerable deterministic simulations are required even for constructing a 2-order SPCE meta-model.

5.2.4.4 The MM

This method is also efficient and shows a good performance in estimating the value of Pf . Given its simplicity and easy implementation procedure, it is a good alternative to the MCS for such a very high dimensional stochastic problem. However, this work only evaluates the MM for the cases of relative high failure probability. Careful attention should be paid when applying this method to calculate low failure probabilities since it may lead to significant errors as pointed out in Napa-García et al. (2017). Besides, this method is not able to carry out a parametric study of L_x as expected since the obtained Pf results fluctuate. Theoretically, the collection of all the moments (of all orders, from 0 to ∞) uniquely describes a bounded distribution. Then, the Pf can be determined by estimating the tail area of the distribution. In the present study, only four moments are collected, and the tail area is estimated by an approximated way (Eqs. 2-14 and 2-3). The induced errors are not related to the N_{RV} or L_x of the problem but depend on the complexity of the FoS distribution and the target value of the dam Pf (tail area). It may lead to a large error for a lower Pf but a small error for a higher Pf . As a result, the obtained Pf values in the parametric study are not monotonously decreasing.

5.2.4.5 Concluding remarks

Here gives a summary of the remarks observed in Figure 5.8 and Table 5.3.

- a) All the four methods can provide reasonable Pf estimates compared to the reference method – MCS.
- b) The two sampling methods (SS and MM) show good efficiency for the considered cases which are high dimensional, while the efficiency of the two meta-modelling methods strongly depends on the number of input variables.
- c) The sampling methods cannot produce a consistent evolution of the dam Pf in the performed parametric study. The inconsistency observed in the SS is due to the difficulty of generating effective conditional samples, while the limited statistical moments and the assumed distribution type in the MM lead to biased Pf estimates. However, it seems that the considered meta-modelling methods perform well for providing a desired Pf evolution.
- d) The two meta-modelling methods give smaller estimates of Pf compared to the MCS. This is because that dimension reduction techniques are employed in these two methods.

It should be noted that the conducted comparative study is related to a case of a relatively high failure probability (order of 10^{-2}). The performance of the four methods for estimating low failure probabilities (e.g. $<10^{-4}$) in the context of very high dimensional stochastic problems is not investigated and thus unknown. This is a difficult issue in the field of reliability analysis to assess an approximated method for very low Pf , since the consuming time of running an MCS is very high even with a simplified deterministic model. The present study provides first insights into the performance of the four reliability methods in the context of very high dimensional stochastic problems, and some concluding remarks can be extended to the cases of low Pf .

5.3 Modelling and comparison of different random fields

5.3.1 Introduction

Having implemented the RFs of γ_d and ϕ' in the dam reliability analysis in section 5.2.2, this section aims to improve the modelling of the soil spatial variability by introducing two complex RFs: conditional and nonstationary (a varied mean). The induced effects on the reliability analysis results by using different RFs are also investigated. The previous sections are based on the generic RFs which refer to the unconditional and stationary type (noted as RF-a). Conditional RF means that the generated RF is conditioned on the available measurements of the site. The simulated values of the RF at the measurement locations are not stochastic but related to the collected data. Using this type of RFs can avoid wasting site investigations and reduce the variance of the underlying RF. As for nonstationary RFs, they account for the variation of the RF statistics (e.g. mean, coefficient of variation and covariance function) which are assumed to be constant over the whole domain in stationary RFs. It is well known that natural soil properties often exhibit nonstationary characteristics (Wu et al., 2019), such as linearly increasing mean value with depths for the undrained cohesion. In those cases, using nonstationary RFs is more appropriate for describing soil variability than stationary RFs. Examples of using the two mentioned complex RFs in probabilistic geotechnical analyses can be found in (Griffiths and Yu 2015; Jiang et al. 2017, 2018; Kim and Sitar 2013; Li et al. 2015; Li et al. 2014; Liu et al. 2017; Schöbi and Sudret 2017; Wu et al. 2019; Zhu et al. 2017). However, most of the previous studies are based on hypothetical engineering cases for RF modellings, without exploiting the construction or monitoring data in probabilistic analyses.

Compared to the studies in section 5.2, one assumption is proposed and adopted in this section in order to focus on the effects of different RFs. The assumption leads to ignoring the soil variability in the zones Core and Shell-1. In other words, this section takes into account only the soil variability in the downstream part (Shell-2) of the dam

and models the soil properties of other zones in a deterministic framework (with their mean values as given in Table 3.3). This assumption is based on the following two reasons: (1) under such a design scenario (steady-state flow conditions and a horizontal pseudo-static acceleration towards downstream), almost all slope failures will occur in the downstream part. Additionally, the results of section 4.2 indicate that the soil variability of the Core zone has a very limited influence on the dam reliability; (2) Neglecting the soil variability of the other zones than the Shell-2 can make the reliability analysis simpler and faster. More importantly, it allows focusing on the different RFs effects of only one zone.

Since the present study is based on the dam main cross-section, only the measurements located in this section (the profile Y6 in Figure 3.4) are adopted. Figure 5.9 presents the location of the considered measurements (with a quantity of 32) in the main cross-section. These 32 measurements are used to determine the Beta distribution parameters for γ_d and considered as observations in the generation of conditional RFs. The estimated γ_d distribution parameters are given in Table 5.4. It is noted that the autocorrelation distances (L_x and L_z) and the distribution parameters of the shear strength properties (c' and ϕ') used in this section are the same to the ones of Tables 3.2 and 3.4.

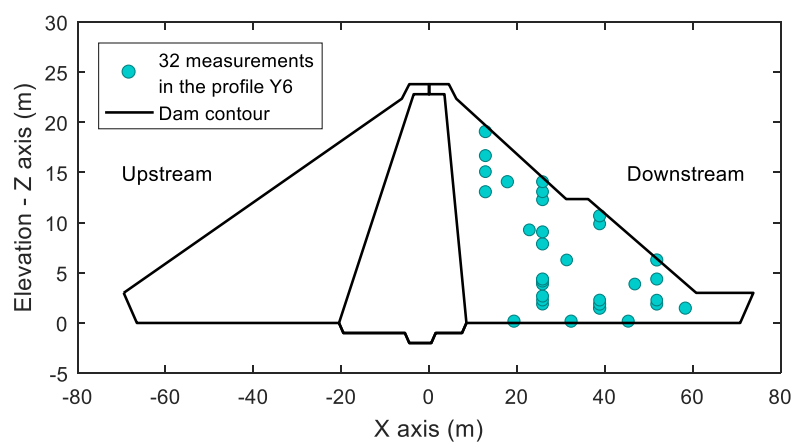


Figure 5.9 The 32 γ_d measurements located in the downstream shell of the main cross-section

Table 5.4 Probabilistic parameters of the soil properties for section 5.3

		γ_d (g/cm ³)	ϕ' (°)	c' (kPa)
Statistical moments	Mean	2.02	34.85	10.55
	CoV(%)	3.09	3.72	57.63

Parameters for Beta distributions	A ⁽¹⁾	18.71	28.71	1.48
	B ⁽¹⁾	18.03	29.61	2.78
	Min	1.63	25	0
	Max	2.40	45	30

Autocorrelation length (m)	Horizontal (L_x)	4.9	-	-
	Vertical (L_z)	1.9	-	-

Modelling approach		Random fields	Random fields ⁽²⁾	Random variables

Note: ⁽¹⁾Beta distribution parameters; ⁽²⁾Obtained by transforming the γ_d RFs with the Caquot's relation (Mouyeaux et al., 2018).

In total, three reliability analyses are performed in this section with respect to the three types of RFs defined in Table 5.5. All the analyses follow a same MCS procedure. The only difference lies in the way of representing the RFs. Comparison between the two first analyses allows investigating the effects of conditional RFs on the dam reliability, while the last one helps to understand the influences of the depth-dependent mean variation.

Table 5.5: The conducted three analyses with the three types of RFs

Analysis	RF Name	Description	Generation method
A	RF-a	Unconditional and stationary	KLE ⁽¹⁾
B	RF-b	Conditional	KLE + Kriging
C	RF-c	Nonstationary (a depth-dependent mean)	KLE + transformation ⁽²⁾

Notes: ⁽¹⁾ K-L expansions; ⁽²⁾ Iso-probabilistic or Nataf transformation

5.3.2 Modelling of different RFs for γ_d with the available data

This section presents in detail about how to generate the three types of γ_d RFs with the available data.

5.3.2.1 *The unconditional-stationary RFs (RF-a)*

Firstly, a standard-normal RF is generated by using K-L expansion. The exponential autocorrelation function is adopted in this study since it is recommended to be used in conjunction with K-L expansion according to Sudret and Der Kiureghian (2000). Then, the initial RF is transformed to the physical-values space via the iso-probabilistic transformation with the Beta-distribution parameters given in Table 5.4. In order to obtain a sufficient accuracy in terms of the variance error for RFs, Li and Der Kiureghian (1993) recommended that the stochastic grid size can be set equal to 0.2 times the autocorrelation distance. This condition is well satisfied for all the RFs generation in this study with respect to the L_x and L_z of Table 5.4. Figure 5.10 shows the location of the 32 measurements together with their values within the Shell-2 zone. The γ_d values vary between 1.9 and 2.15 g/cm³. It can be observed that the data is basically homogeneous in the sense that the variation is not significant (a small CoV of 3.09% as presented in Table 5.4) and there is no trend with depth or along the X axis. Figure 5.11 plots the γ_d values against the depth in order to explore the possible depth-dependent variation. This figure further confirms that the data has no depth-related trend, such as the linearly increasing relation which was reported in (Griffiths and Yu, 2015; Li et al., 2014; Zhu et al., 2017) for natural soils. Thus, the RFs modelling was performed without a de-trending process.

$RF_{k-un}(x, y)$ are generated with K-L expansions or the Kriging theory. A conditional RF in the standard normal space RF_{con_sn} can be obtained by combining the three RFs. At the end, the RF_{con_sn} is transformed back to the physical-values space and the final conditional RF is obtained. For the three components of the RF_{con_sn} , the $RF_{un}(x, y)$ is an unconditional RF generated by K-L expansions with zero mean and unit standard deviation. Both the $RF_k(x, y)$ and the $RF_{k-un}(x, y)$ are Kriging estimates over the RF domain but with respect to different sets of observations. The former is based on the 32 measurements shown in Figure 5.10 while the latter uses the simulated values of the $RF_{un}(x, y)$ at the 32-measurements locations as observations. It is noted that a simple Kriging is employed for generating the $RF_k(x, y)$ and the $RF_{k-un}(x, y)$ following the suggestion given in Johari and Gholampour (2018). This is because the mean and the standard deviation for the Kriging RF are already known (Table 5.4). It is then not necessary to estimate these statistics in the context of other Kriging types. Another reason of imposing the parameters of Table 5.4 into the conditional RFs is to be consistent with the previous RF type (RF-a). All the three components are based on a same covariance structure for the RF generation, saying the assumed exponential autocorrelation function and the autocorrelation distances of Table 5.4. By using the final obtained conditional RF, the 32 measurements can be perfectly respected, which means that the simulated values at such points are constant and equal to the collected measurements. Figure 5.12 shows an example of the obtained conditional RF mapped to the downstream shell. The position of the 32 data and the corresponding values of γ_d are presented as well.

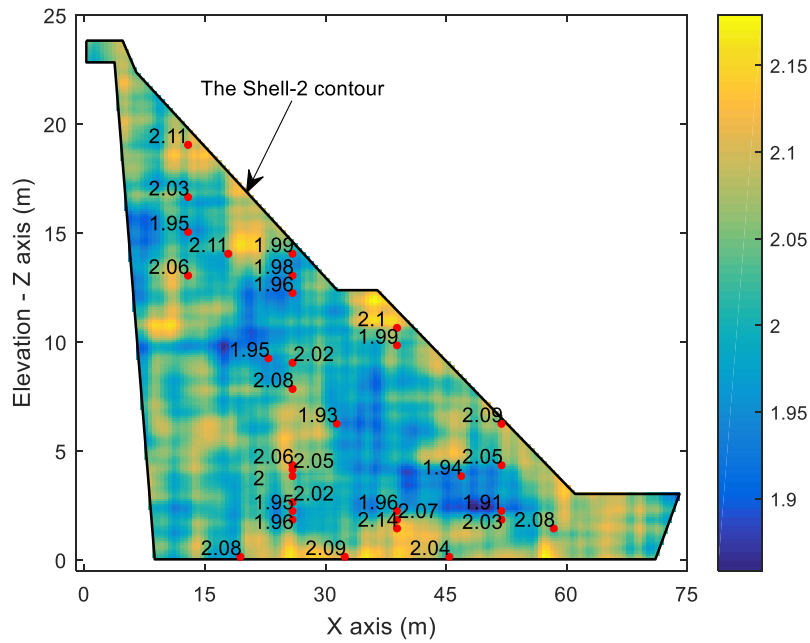


Figure 5.12 An example of the obtained conditional RF and the 32 γ_d measurements (g/cm^3)

5.3.2.3 The nonstationary RFs (RF-c)

Abundant site-specific data have confirmed that there are nonstationary characteristics within the soil profile (Jiang and Huang, 2018). One commonly encountered case is that the mean value of soil property changes with depth as pointed out in Lumb (1966). This case is considered in the present study for the modelling of the nonstationary RFs.

According to the procedure given in Table 2.5, there are three steps to be followed to obtain a RF with a varied mean value. A linear trend should be determined at first. However, the present data has no clear trend (monotone increase or decrease) with depth as shown in Figure 5.11. For this reason, a technique is proposed to describe the mean value variation. It is then implemented in the nonstationary RFs generation. The technique is presented as follows: For each depth Z_{RF} , the measurements located within the range $[Z_{RF} - L_z, Z_{RF} + L_z]$ (see Figure 5.13) are considered for computing the average at Z_{RF} . The obtained average is regarded as the mean value of γ_d at this depth. L_z , being 1.9m, represents the vertical autocorrelation distance of the γ_d for the Shell-2 zone. According to the definition of the L_z , the data within this zone are strongly

correlated. They are thus representative for determining the mean value of the zone. This solution guarantees that the obtained mean variation is conditioned on the measured data. Also, it is more flexible for describing the complex variation of mean value than the assumption of a linear trend as in the studies of (Griffiths and Yu, 2015; Jiang and Huang, 2018; Li et al., 2014). Figure 5.14 (left part) presents the obtained variation of the γ_d mean values. The global average value (see Table 5.4) determined by all the 32 measurements is presented as well. Due to the fact that only a small number of γ_d measurements are available near to the dam crest for the Shell-2 zone, it is impossible to estimate the γ_d statistics within the range $[Z_{RF} - L_y, Z_{RF} + L_y]$ at several depths. The solution adopted in the study is to use the global average of γ_d for the depths with no data. This leads to a vertical line (constant estimate) in Figure 5.14 at high Z-axis values, saying from 21-23.8m. It can be observed from Figure 5.14 that the variation is basically around the global average with small fluctuations for medium and low Z-axis values. An exception is found for the depths between 17m and 21m, for which the mean value is significantly higher than the global average.

The second step of Table 2.5 is to generate an initial stationary RF. In this study, it is achieved by simulating a standard normal stationary RF (RF_{SS}) with K-L expansions. Then, the nonstationary RF is obtained by adjusting the values of RF_{SS} at each depth. Table 2.5 uses a scaling factor for the adjustment in case of a Lognormal distribution while the iso-probabilistic transformation is employed in this study for the purpose. At each depth, the RF_{SS} is transformed to a physical-values space which is defined by the mean value at this depth (left part of Figure 5.14) and the standard deviation of Table 5.4. For illustration, an example of the generated non-stationary RFs (RF-c) is shown in Figure 5.14 (right part). The simulated values in the presented RF are basically between 1.85 and 2.15, and approximately follow the mean values shown at the left part of Figure 5.14.

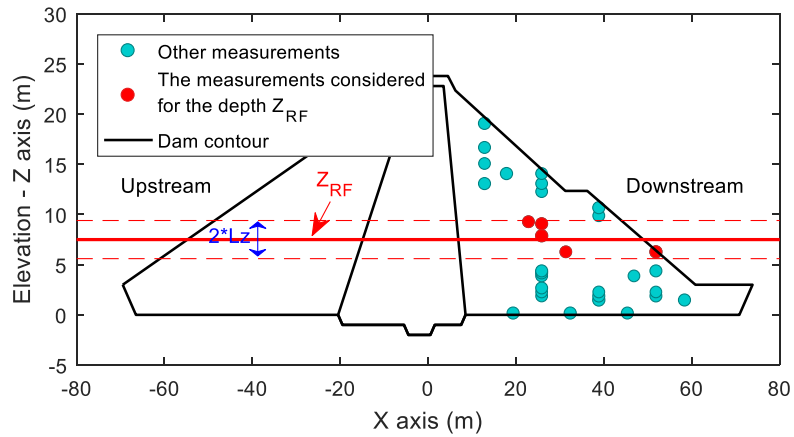


Figure 5.13 The measurements used for the estimation of γ_d mean value

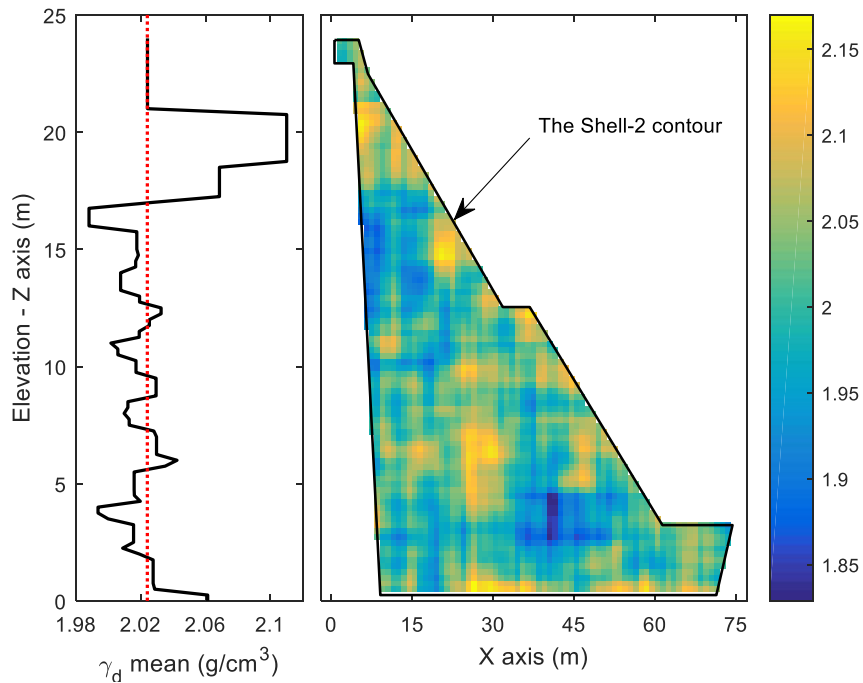


Figure 5.14 Left - variation of the γ_d mean value; Right - an example of the obtained nonstationary RFs

5.3.3 The obtained reliability analysis results

For each RF type defined in Table 5.5, an MCS-based reliability analysis is performed. The number of model evaluations (N_{MCS}) in the MCSs is equal to 15000 which guarantees that the estimated Pf is accurate enough (i.e. $CoV_{Pf_{dir}} < 5\%$).

Figure 5.15 plots the PDF of 15 000 FoS values obtained by the three analyses. The PDF curves are estimated with a normal kernel function on the FoS values. It is

observed that the PDF of Analysis C (PDF_c) is similar to the one of Analysis A (PDF_a) and the two curves are almost superposed. Analysis B leads to a PDF (PDF_b) slightly different than the other two analyses, with more dispersed FoS values. A detailed interpretation of the obtained results and discussion on the effect of different RFs are given later. Additionally, it is found that the three PDF curves are all negatively skewed with a bigger tail at the left. This is due to the fact that the input parameters are negatively skewed.

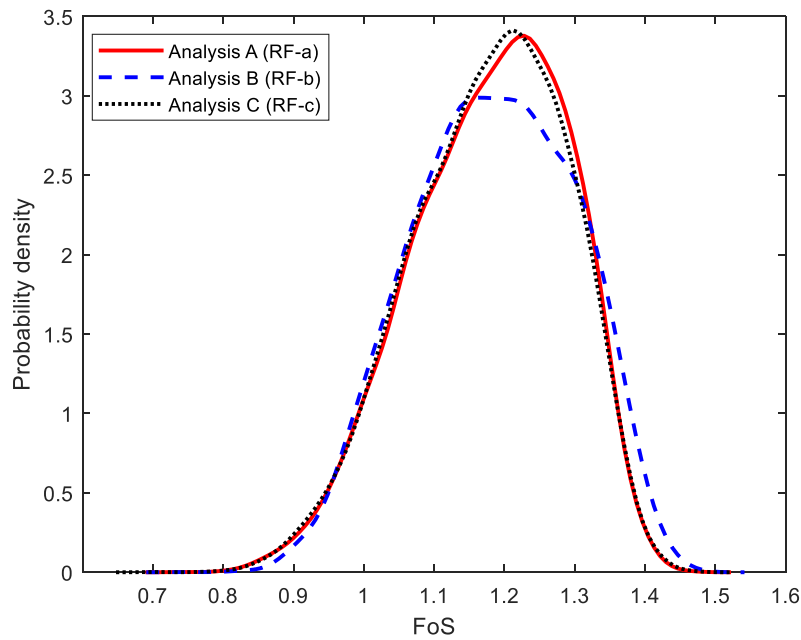


Figure 5.15 PDFs of the three analyses

Table 5.6 presents the post-processing results on the 15 000 FoS values for each analysis, including failure probability and statistical moments of the FoS. According to Table 5.6, the Pf_{sce} is lower than 1.3×10^{-5} for the three analyses. This proves that the dam was well designed. It is found that the Pf_{con} varies between 0.059 and 0.064. Analyses A and C lead to the same estimate of Pf_{con} , and are both bigger than the one of Analysis B. It is consistent with the observations made for Figure 5.15, in which the PDF_c and PDF_a are almost superposed and are higher than the PDF_b for the part $FoS \leq 1$. In conclusion, considering conditional RF leads to a slight underestimation of the Pf_{con} while the employed nonstationary RFs have practically no effect on the Pf_{con} .

Some statistics of the FoS values are presented as well in Table 5.6. The mean values are nearly the same for the three analyses. For the standard deviation, a slightly higher value is found for Analysis B. This is in accordance with Figure 5.15 where the FoS values of Analysis B are more dispersed than the other two PDF curves.

Table 5.6 Reliability results of the three analyses

Analysis	Failure probability			Statistical moments of FoS	
	Pf_{con} ($\times 10^{-2}$)	Pf_{sce} ($\times 10^{-5}$)	$CoV_{Pf_{con}}$ (%)	Mean	Standard deviation
A	6.35	1.27	3.13	1.180	0.110
B	5.89	1.18	3.26	1.183	0.114
C	6.35	1.27	3.13	1.177	0.110

5.3.4 Effects of using the two complex RFs

This section attempts to discuss and explain the effects of using a complex RF (conditional or nonstationary) on the dam probabilistic stability analysis by analyzing the results presented in Figure 5.15 and Table 5.6. In general, the differences in the obtained results (Pf and FoS statistics) induced by using a complex RF are not remarkable. The Pf_{con} values of the three analyses are varied within a narrow range [0.059, 0.064], and the differences among the FoS statistics (mean and standard deviation) can be found only after the second decimal number. This is due to the low variability of the considered measurements as shown in Figure 5.10. As each layer of the dam was constructed with a same material and was compacted identically, the collected γ_d data after the compaction are similar with each other: most of the γ_d values shown in Figure 5.10 are close to the global average (2.024 g/cm^3) with a difference lower than 3%. Therefore, the simulated complex RFs introduce only insignificant differences since they are all based on the 32 measurements which are relatively ‘homogeneous’. Consequently, the results obtained by the different RFs are only slightly changed. The following two subsections give a detailed interpretation on the effects of the two complex RFs.

5.3.4.1 *Effects of the conditional RFs (RF-b)*

As shown in Table 5.6, modelling the γ_d variability by conditional RFs leads to lower estimates of the Pf . The mean of the FoS values is nearly unchanged but the data dispersion slightly increases by using conditional RFs compared to RF-a. A possible interpretation about these observations is given as follows.

It is recalled that the variability of the three soil properties (γ_d , c' and ϕ') are considered in the three analyses (A, B and C). The γ_d and ϕ' are modelled by RFs while the c' is represented by RVs. The modelling technique, including the distribution and the relating parameters, is constant for the c' among the three analyses. The differences of the obtained reliability results shown in Table 5.6 are induced by the different ways of modelling the RFs of γ_d and ϕ' . Particularly, the RF of ϕ' is obtained by transforming the one of γ_d with an empirical relation. It can be understood that the variability of c' , which are modelled identically in the three analyses, define a reference PDF form (i.e. basic variation) for the estimated FoS values. The variabilities of γ_d and ϕ' , which are considered with different ways, will modify differently the reference form to obtain final PDF curves (i.e. the ones shown in Figure 5.15). The probability of getting a particular FoS value is different among the three analyses due to the presence of different RFs. As the probability of having high FoS values (>1.35) is bigger and there is less small FoS values by using conditional RFs, Analysis B leads to lower Pf and more scattered FoS values. Figure 5.16 and Figure 5.17 can explain why higher FoS values and less small FoS values can be found in Analysis B. In Figure 5.16, 50 possible critical slip surfaces are plotted with 50 random sets of soil properties (γ_d and ϕ' : RF; c' : RV) in Analysis B. It is observed that the majority of the critical slip surfaces pass through the main body of the downstream shell (from the crest to the toe). Although there will be some other forms of critical slip surfaces that are not covered by the 50 cases, Figure 5.16 shows a clear area which can comprise most of possible slip surfaces in the probabilistic analysis. The area is called as Principle Critical Slip Surface

Area (PCSSA) in this article and is illustrated in Figure 5.17. The ϕ' values at the measurement locations are presented as well in Figure 5.17. These values are obtained by transforming the γ_d values (shown in Figure 5.10) with the Caquot's relation. It is observed that around 16 measurements are located inside or around the area PCSSA. 11 of them are bigger than 33° which is the average of ϕ' for Analysis A. In conditional RFs, the ϕ' values of the zones that are close to the 11 values, are also probably bigger than 33° . As a result, most of the critical slip surfaces in conditional RFs pass more frequently through the zones with high ϕ' values than the case of RF-a. The probability of having high FoS values is thus bigger in Analysis B. This explains the larger tail at right for the PDF_b (Figure 5.15). In addition, as most of the critical slip surfaces are large enough with respect to the dam dimension, it is difficult to avoid all the zones with high ϕ' values in calculating the minimum FoS value of one realization. The probability of leading to very low FoS values is thus reduced. This explains why the PDF_b is lower than the PDF_a at left tail (see Figure 5.15). Note that the γ_d effects on the variation of the FoS values are negligible as pointed out in Guo et al. (2018).

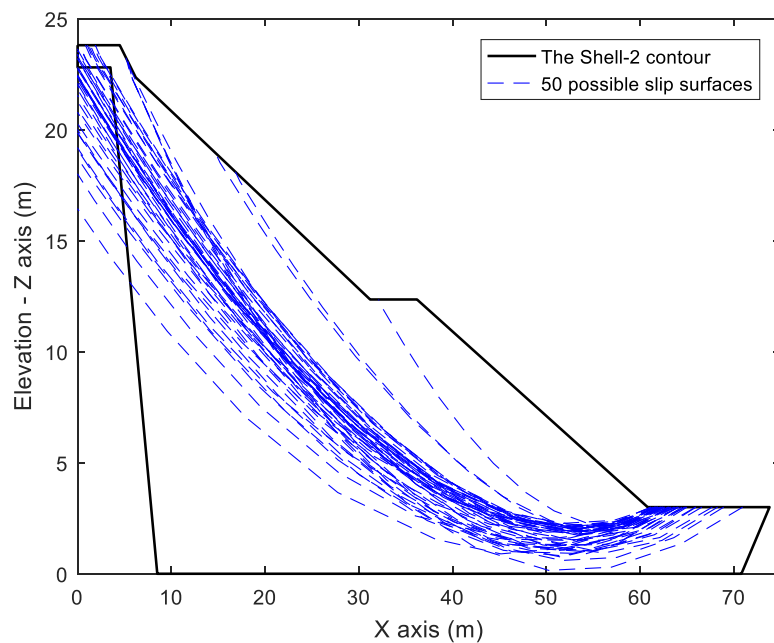


Figure 5.16 Slip surfaces with 50 random realizations of simulations (RF-b)

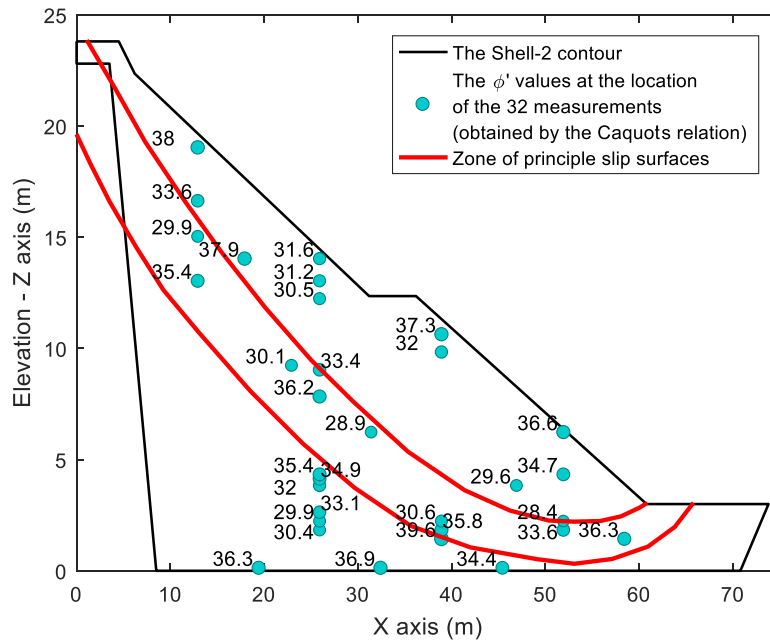


Figure 5.17 The principle area of slip surface and the 32 measurements with their values (ϕ' in degree)

5.3.4.2 Effects of the nonstationary RFs (RF-c)

According to Figure 5.15 and Table 5.6, using the nonstationary RFs, which consider the variation of the γ_d mean value, has no significant effects on the reliability results. The obtained failure probability and the statistics of the FoS values are almost the same to the ones of stationary RFs. This is due to the ‘homogeneity’ of the collected measurements. As shown in Figure 5.10, the γ_d values of the 32 measurements are not dispersed but varied with a small range ($1.95 \text{ g/cm}^3 - 2.1 \text{ g/cm}^3$). The variation of the mean values with depth is thus not significant as well. The estimated mean values fluctuate around the global average and they are mainly between 1.99 g/cm^3 and 2.04 g/cm^3 . The most scattered value is found near the crest and is around 2.117 g/cm^3 which corresponds to an error less than 5% compared to the global average. Non-stationarity is therefore only slightly marked in this case study. As shown in Figure 5.16, most of the critical slip surfaces start nearly from the crest and ends at the toe. Therefore, the FoS values are not significantly affected. Using the nonstationary RFs (RF-c) thus leads to very similar reliability results to stationary RFs for the case study.

The present study determines the variation of the mean value with depth by defining a zone related to the vertical autocorrelation distance. This is different to the traditional way (for natural soils) of modelling non-stationary characteristics for RFs which assumes a linearly increasing mean (Jiang and Huang, 2018). However, the parameters themselves (e.g. start value and slope) of the linear assumption are related to some uncertainties (Jiang and Huang, 2018). Also, not all the soil properties follow a simple linear increase with depth as the one shown in Figure 5.10, in particular for embankments with layers that have been compacted according to the same protocol. Therefore, the proposed technique is recommended to determine the nonstationary characteristics of a RF, since it is more flexible than a linear assumption.

5.3.5 Discussions of the obtained results

The previous section presents and compares the reliability results obtained by considering three types of RFs. A possible solution, which is based on the principle failure surface area, is provided to explain the effects of using a complex RF. Basically, the differences among the three analysis results are not remarkable since the considered data is relatively 'homogeneous'. Therefore, for the geo-structures realized under a high-quality construction control (e.g. careful selection of the construction materials and identical compaction), it is not necessary to employ a complex RF which requires extra computational efforts while using the generic one (unconditional and stationary) is sufficient to provide satisfactory results.

It is noted that the recommendation given above is only valid when a large number of geo-localized data are available since it permits to check if the construction was well controlled or not by regarding the homogeneity of the data. Then, for most cases, it is rare to have many measurements and know their location information. Considering this, it is better to use the conditional RFs in a probabilistic analysis. Such a suggestion is based on the following reasons:

- Adopting conditional RFs allows a full use of the available measurements and avoids waste of site investigation. It also permits to update the spatial modelling and the reliability results by adding new data that could be collected during a new project investigation or from monitoring phases.
- The input uncertainty can be reduced by conditioning RFs on the measurements. As mentioned in the next point, the variance at the measured points and their neighbors can be largely decreased. Theoretically, the uncertainty is reduced when considering more data and the obtained reliability results are thus more precise.
- Conditional RFs are also nonstationary. The non-stationarity of a soil property can be considered and determined by the data in a conditional RF. The variance is small for the points close to the measured locations and increases with the separate distance between known and unknown locations. Conditional RFs allows to directly consider non-stationarity by the geo-localized measurements (without making assumptions to describe the variation of mean and/or variance in space).
- Using conditional RFs usually leads to lower Pf estimates thus economic designs. This is supported by the results of Table 5.6 and other existing studies (Liu et al., 2017b; Lloret-Cabot et al., 2012).

In order to further check the last point within the framework of the studied dam which is a real engineering problem, two complementary reliability analyses are carried out here. Table 5.7 describes these two analyses. The idea is to implement the spatial modelling of c' into the dam probabilistic analysis and compare the obtained results between conditional and unconditional RFs. To this end, 32 c' values are randomly generated according to the Beta distribution defined in Table 5.4 and are randomly assigned to the 32 γ_d measurements' locations. These c' values are then regarded as observations for the RF generation. Figure 5.18 shows the generated c' values together with an example of the c' RFs conditioned on these data. It is noted that all the RFs in

this section are based on the exponential autocorrelation function with the L_x and L_z of Table 5.4.

Table 5.7 Definition of the two complementary analyses

Analysis	Soil variability modelling			Generation method
	γ_d	ϕ'	c'	
A'	RF-a	RF-a ⁽¹⁾	RF-a ⁽²⁾	KLE
B'	RF-b	RF-b ⁽¹⁾	RF-b ⁽²⁾	KLE + Kriging

Notes: ⁽¹⁾ obtained by transforming the γ_d RFs; ⁽²⁾ considering the values shown in Figure 5.18 as observations.

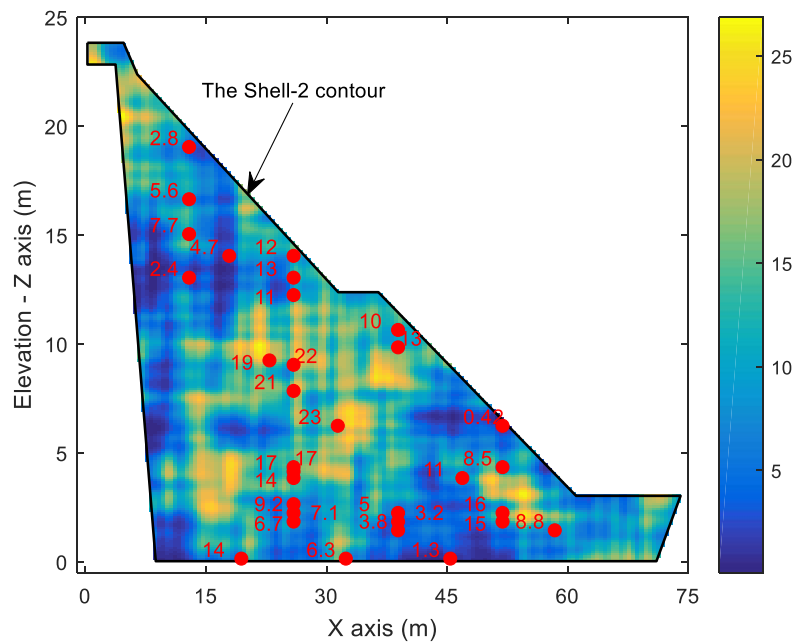


Figure 5.18 An example of the obtained c' conditional RF and the 32 c' data (kPa)

Figure 5.19 presents the obtained results of the two complementary analyses (A' and B') which are performed by using MCS. The number of model evaluations (N_{MCS}) is taken equal to 5000 for each MCS in order to have an efficient estimate on the dam Pf and a global picture of the FoS distribution. It is observed from this figure that the FoS varies within a narrower range in Analysis B' than in A' which corresponds to a smaller FoS standard deviation (σ_{FoS}). This finding shows the capacity of conditional RFs on the uncertainty reduction. Consequently, the dam Pf is lower in Analysis B', which

confirms the recommendation made above concerning the use of conditional RFs for an economic design. The mean of the FoS (μ_{FoS}) remains almost unchanged in the two analyses as also found in Table 5.6.

Then it is possible to compare the results of Figure 5.19 with the ones of Table 5.6. The only difference between the current analyses (A' and B') with the previous ones (A and B) lies in the way of modelling the c' uncertainty: RV is used in A and B, while RF is adopted in A' and B'. Based on this comparison, it is found that modelling c' by RFs instead of RVs can reduce the output variance (σ_{FoS}) and the dam Pf . This observation is consistent with many existing studies (Al-Bittar and Soubra, 2013; Guo et al., 2020; Pan and Dias, 2017b).

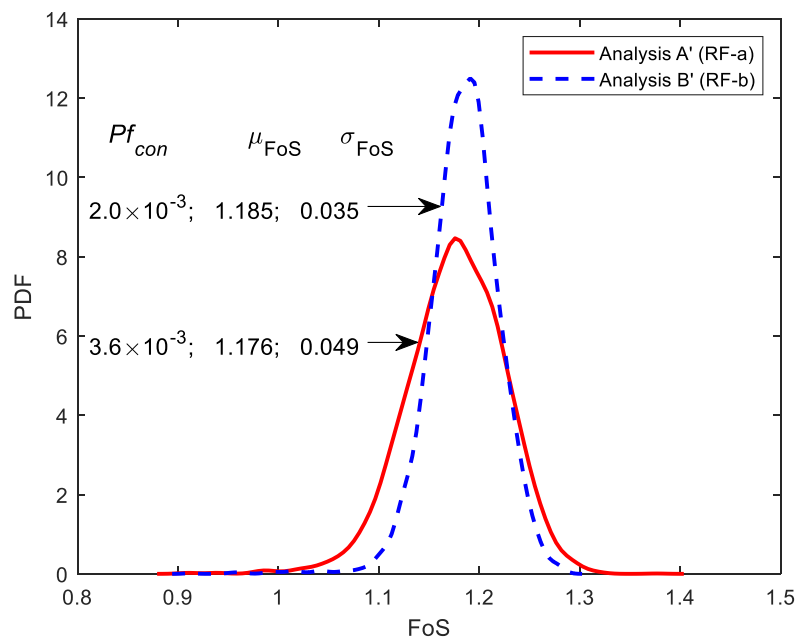


Figure 5.19 Reliability results of the two complementary analyses

5.4 Conclusion

This chapter presents the dam probabilistic analysis and discusses the obtained results in the context of RFs. Firstly, the performance of the *LEM_GA* model is assessed for spatially varied soils. By comparing with the *SRM_FDM* one, it is found that the *LEM_GA* is able to provide reasonable estimates of the dam FoS under the condition of

RF-simulated soil properties. Besides, the located critical slip surfaces by the *LEM_GA* are also comparable with the ones of *SRM_FDM* for heterogeneous soils. In consideration of the calculation efficiency, the *LEM_GA* is adopted in this chapter as the deterministic model.

Two studies related to the dam RFs are conducted. The first one compares the performance of different reliability methods for high dimensional stochastic problems. For this comparison, the reliability analysis of the dam is carried out beforehand with the MCS, which is considered as the reference method. The MCS is performed for two different input distribution types (Beta and Truncated normal). The obtained Pf is close to 0.02 under the considered seismic loading and is lower than 5×10^{-6} for the scenario. It is also found that the Beta assumption leads to a slightly higher Pf , which is in agreement with the observation of section 4.3.2 in the context of RVs. A parametric study about the autocorrelation distance is also performed. It investigates the effects of the Shell-2 L_x , which is smaller than the values recommended in literature. The obtained results indicate that the dam Pf is increased with increasing the L_x , and the Pf varies within a narrow range for the considered different L_x values. Then, the comparison study aims to evaluate the performance of four reliability methods (SS, MM, SPCE/GSA and SPCE /SIR) for high dimensional stochastic problems by comparing them with the MCS results. It is found that all the four methods can give relatively accurate estimates of the dam Pf with a lower number of deterministic calculations compared to the MCS. The efficiency of the two meta-modelling techniques (SPCE/GSA and SPCE/SIR) strongly depends on the number of input variables, and they give usually smaller Pf estimates due to the dimension reduction. The two sampling-based methods (SS and MM) are insensitive to the input dimension, but are not able to produce expected Pf evolution with the L_x change due to the complexity of generating effective conditional samples in SS and the approximated technique of estimating Pf in MM.

The second complementary study involves the modelling of different RFs with the available measurements and the investigation of their induced effects on the dam reliability. Two complex RFs (conditional and nonstationary) are introduced in this study and coupled with the same reliability analysis procedure performed for the generic RFs. Three different types of RFs are thus used to model the spatial variability of dam material properties γ_d and ϕ' . Basically, the differences between the results of the three kinds of RFs are not significant on the dam reliability. This is due to the low variability and the 'homogeneity' of the considered 32 measurements. Therefore, a simple RF can be used in practice without developing a complex one if the dam construction is well controlled. Additionally, two complementary analyses are carried out in which the c' spatial variability is also considered by regarding the artificial values as measurements. The results confirm that using conditional RFs can lead to lower Pf estimates (so economic designs).

6 CHAPTER VI: Three-dimensional probabilistic analysis

The conducted studies of previous chapters are based on 2D simulations. A cross-section, profile Y6 of Figure 3.4, was selected to evaluate the 2D dam stability condition. This chapter introduces the dam three-dimensional (3D) stability analysis and implements it into a probabilistic assessment procedure. The objective is to investigate the dam 3D geometry effects in a reliability analysis framework. The dam length in the third dimension is around 170 m for the crest and 50 m for the base, which are not long enough compared to the dam height (24 m) and width (140 m) to support the assumption of regarding the dam as an infinite one. Therefore, the obtained results (FoS and Pf) in a 2D context are biased and it is interesting to compare them with 3D ones in order to understand the dam geometry effects. For this purpose, a 3D computational model of the studied dam is constructed at first. Secondly, a probabilistic analysis is performed by using the 3D model and the target results (Pf and FoS statistics) are obtained. They are then compared with the 2D results. Additionally, the effects of two influential factors for the dam reliability are discussed for both 2D and 3D analyses. The first one is about the correlation between the c' and ϕ' , which is not accounted for in the previous chapters due to the lack of data. The second factor involves the discretization mesh used for the numerical model. As a number of deterministic calculations should be carried out in a probabilistic analysis, a possible way to alleviate the total computational burden is to use a relatively coarse mesh for the numerical model. This study aims to investigate the impacts of using a coarse deterministic mesh in a probabilistic analysis. It is noted that, in accordance with the previous chapters, a pseudo-static acceleration of $0.24g$ is considered for all the simulations in this chapter.

6.1 Construction of the 3D computational model

Figure 6.1 gives an aerial view of the studied dam. As stated in section 3.1, the dam closes a narrow valley which is covered with alluvial deposits. The first soil layer of the valley is composed of cracked schists and the depth varies between 3 and 8m. The second layer corresponds to a zone of the bedrock decompression and can be found

until a depth of 11 to 19m. The filter drain system of the dam is constituted by two parts: a continuous vertical filter wall and 19 separated horizontal drains. They are all composed of coarse gravels with diameters varying between 10 and 50mm. The filter wall is placed 8.5m to the central axis (X -axis=0 in Figure 3.1) in the downstream side, and its thickness is 1m. The 19 horizontal drains are separately distributed on the contact between the dam downstream part and the foundation with a centre distance of 5m. Each drain presents a width of 2.5m and a height of 0.5m.



Figure 6.1 Aerial view of the studied dam

The objective of this section is to construct a 3D computational model which can respect as much as possible the real 3D geometry (dam, valley and filter system), and enable the dam stability analysis considering a pseudo-static acceleration and a steady-state water flow. For the 3D slope stability analysis, some approximation methods (Wei et al., 2009), based on the extension and combination of various 2D techniques, exist to estimate the FoS. However, these methods present difficulties of considering complex 3D geometries which is the case for the studied dam, and are based on several assumptions which are difficult to justify for practical cases (e.g. failure direction and symmetry of the failure volume) (Huang et al., 2002). Besides, properly estimating the pore water pressure distribution inside the dam is an issue for these methods, given that

the filter wall and the horizontal drains should be considered. Therefore, it is necessary to create a numerical model which can address the above-mentioned problems. Between Plaxis and Flac, which are respectively the platforms for the *SRM_FEM* and *SRM_FDM* models, the former software is finally selected for the following two reasons: (1) Plaxis has a user-friendly interface which significantly facilitates the creation of the complex 3D model and the mesh discretization; (2) the flow calculations using Plaxis are faster than those of Flac.

Figure 6.2 shows the constructed 3D model in Plaxis. The model size is respectively 240m, 310m and 53.8m for the three directions (X, Y and Z -axis in Figure 6.2). The first soil layer (schist) of the valley is assumed to be 6 m for the thickness. Lower than the schist layer, a bedrock formation is modelled by considering high shear strength values. The model base is fully blocked and the four lateral faces are normally fixed. A reservoir water level of 50 m high is applied on the upstream slope. The mesh condition of the numerical model is also presented in Figure 6.2. There are in total 181149 10-noded tetrahedron elements for the mesh corresponding to 251870 nodes. As for the dam body (Shell-1 + Core + Shell-2), the elements number is equal to 68703. The adopted mesh is determined by a sensitivity analysis and a further discussion of using different mesh conditions for the dam reliability analysis will be provided later.

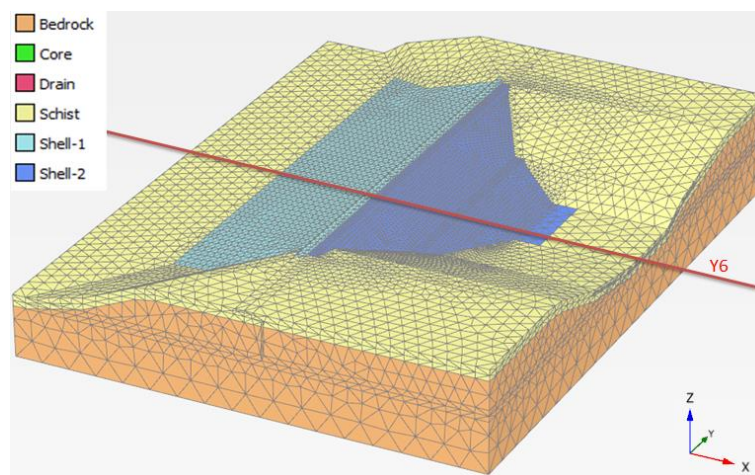


Figure 6.2 The 3D numerical model in Plaxis

Concerning the model creation procedure, a cubic soil volume with two layers should be defined at first. Then, the valley profile is represented by plotting several lines in the Y-Z plan and is extruded along the X-axis to form the valley. This procedure is repeated but by extruding the dam cross-section along the Y-axis to form the dam contour. The valley profile is determined by the field data which were collected during a geology survey before the dam construction, while the cross-section is consistent with the one shown in Figure 3.1 and considers the dam three zones (Shell-1, Core and Shell-2) together with the vertical filter wall. The next step is to split the original surfaces into smaller and independent ones by using the tool ‘*Intersect*’, and to delete the soil blocks which are unnecessary for the 3D model. Concerning the horizontal drains, they are added manually to the model according to their dimensions and the available installation map. Figure 6.3 shows an inner view of the model in order to illustrate the parts that are hidden in Figure 6.2, including the Core zone, the filter wall and the 19 horizontal drains.

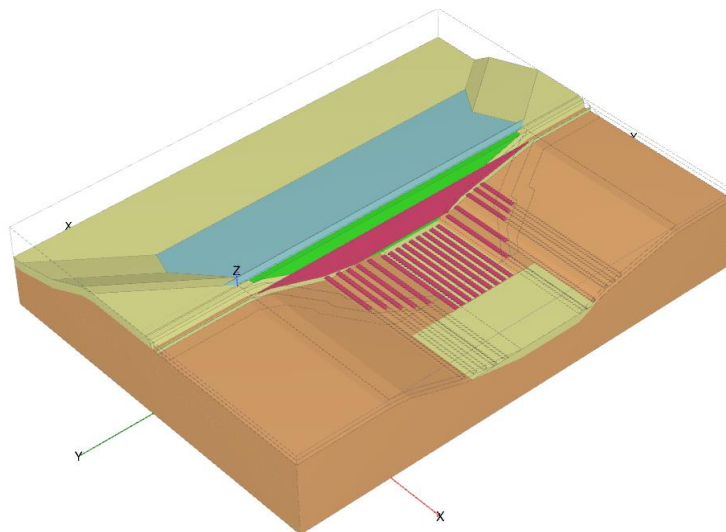


Figure 6.3 Illustration of the Core zone and of the drain system from an inner view

Figure 6.4 illustrates the failure surface determined by the 3D model with the mean values shown in Table 3.3. A view of the Shell-2 from the upstream part and a cut in the profile Y6 are provided as well. The incremental total displacements are used to visualize the failure surface. It is observed that the slip soil volume is principally located

in the Shell-2 zone and the deepest failure approximately takes place in the centre. The largest failure is found in the first stage of the downstream slope (lower than the crest) with a distance of about 60 m from the Y-axis.

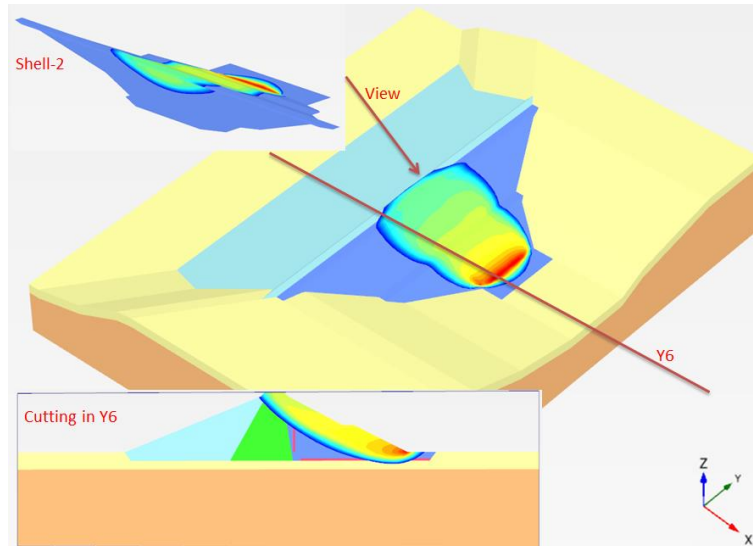


Figure 6.4 Failure surface of the dam in 3D with mean values of the soil properties

6.2 3D probabilistic analysis results

This section presents the dam probabilistic analysis results by using the created 3D numerical model. Firstly, a reference case is considered, which refers to the input configuration defined in Table 3.2 and assumes that the c' and ϕ' are uncorrelated. Then, the effects of the $c' - \phi'$ correlation on the dam 3D reliability are investigated by testing two values (-0.5 and 0.5) for the correlation coefficient $\beta_{c',\phi'}$. The soil variabilities are modelled by means of RVs and there are six RVs for three soil properties (γ_d , c' and ϕ') of two zones (Shell and Core). This is consistent with the analyses of section 4.2.2. All the six RVs follow a Beta distribution considering the parameters of Table 3.2. The reliability analyses in this chapter are performed by using the Adaptive bootstrap-based SPCE (termed as AbSPCE) method which is described in section 2.2.1. It consists in constructing a SPCE meta-model to replace the original deterministic model and then running an MCS to estimate the Pf and FoS statistics. Particularly, the meta-model is obtained by using an active learning algorithm which adds carefully-selected training samples to the Experimental Design (ED) and thus

gradually improves the model performance. This algorithm can lead to accurate estimates of the Pf with a limited number of calls to the deterministic model. Therefore, the total computational time of a reliability analysis can be significantly reduced. The procedure of Table 2.3 is followed to carry out the AbSPCE method. The necessary user-defined parameters are assumed as follows: the accepted tolerance error ε_{Pf} is equal to 0.15, the Bootstrap number $B_{PCE} = 20$, the q -quasi-norm is 0.75, the size for the initial ED is 30 and the maximal polynomial degree is tested between 2 and 10. The values of these parameters are in agreement with the recommendations given in Marelli and Sudret (2018).

6.2.1 Results for the reference case

The dam reliability is firstly assessed under a reference scenario as defined previously. By following the procedure of Table 2.3 for the AbSPCE method, 52 deterministic calculations are performed. It means that 22 training samples are gradually added to the initial ED whose size is 30. The finally obtained SPCE meta-model is 10-order with a Q^2 of 0.986. The accuracy of the adopted surrogate models for predicting the dam FoS in 3D will be discussed later. The number of the MCS population size N_{mc} is set large enough so that the CoV_{Pf} , evaluated by Eq. (2-9), is smaller than 5%.

Figure 6.5 plots the PDF and CDF of the FoS values obtained by an MCS which is based on the final SPCE meta-model. According to the two curves in Figure 6.5, almost all possible FoS values for the dam in 3D under the considered pseudo-static load are varied between 0.9 and 1.6. The PDF is not symmetric but with a bigger tail at its left (negatively skewed). This observation is consistent with the 2D one and the reasons discussed before remain valid for the 3D results. Plotting the CDF allows fast estimating the probability of being lower or higher than any a given threshold. For example, if the acceptable FoS for the dam stability condition is increased from unit to 1.2, the related Pf is around 0.18 based on the CDF.

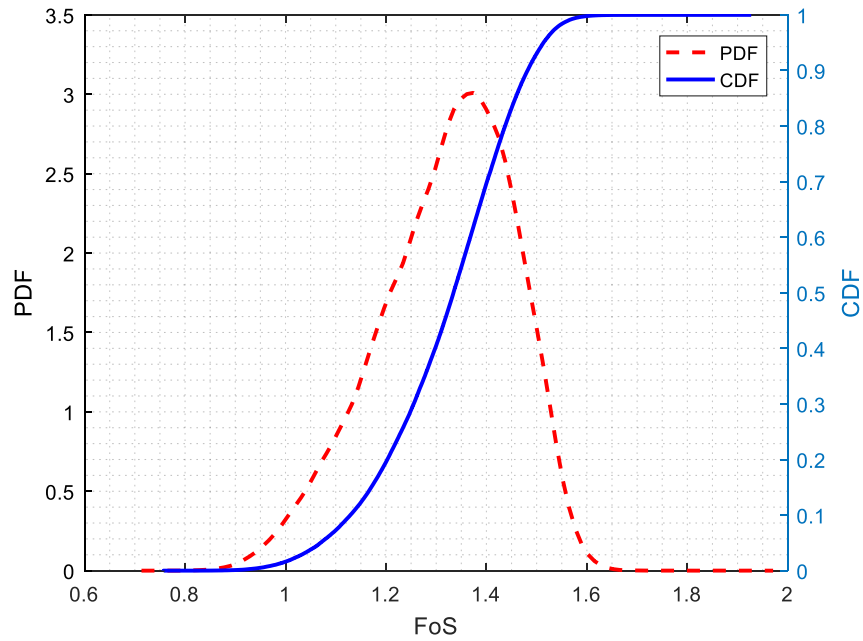


Figure 6.5 PDF and CDF of the dam possible FoS values obtained by the AbSPCE-MCS method

Table 6.1 presents other results of the reference case which are also available in the AbSPCE-MCS method including the failure probability (Pf_{con}), FoS statistics and the sensitivity index of each input variable. The dam Pf_{com} in 3D is estimated to be equal to 0.016 under a seismic loading of $0.24g$. This value is of the same order to the estimate obtained previously in 2D by using RVs or RFs. A detailed comparison between the 2D and 3D reliability analysis results will be given in the next section. The average of the possible FoS values is 1.318 which shows an increase compared with the 2D results, and the data scatter (CoV_{FoS}) is increased as well. Concerning the sensitivity indices, the 3D results are in agreement with the 2D ones. The two most important variables are c' and ϕ' of the Shell zone. The Core c' and the Shell γ_d are the following ones with slightly noticeable impacts while the other two have almost no effects.

Table 6.1 Probabilistic analysis results for the 3D reference case

Reliability analysis results			FoS statistics			Sobol index (total effect) (%)					
						Core			Shell		
Pf_{con}	Pf_{sce}	$CoV_{Pf_{con}}$	$Mean_{FoS}$	Std_{FoS}	CoV_{FoS}	γ_d	c'	ϕ'	γ_d	c'	ϕ'
0.016	3.2×10^{-6}	2.5%	1.318	0.135	10.2%	≈ 0	0.7	≈ 0	0.2	88.7	11.5

6.2.2 Influence of the correlation between c' and ϕ'

This section aims to investigate the $c' - \phi'$ correlation effects on the dam reliability in a 3D context. It is commonly recognized that there exists a correlation between the soil shear strength parameters. A negative correlation coefficient $\beta_{c',\phi'}$ is often encountered according to the laboratory tests (Javankhoshdel and Bathurst, 2016; Lumb, 1970; Wang and Akeju, 2016) and its value is usually in the range between -0.24 and -0.7 (Lumb, 1970; Yucemen et al., 1973). Besides, some studies also reported a positive correlation between the c' and ϕ' , such as $\beta_{c',\phi'}=0.25$ in Wolff (1985). Therefore, two $\beta_{c',\phi'}$ values (-0.5 and 0.5) are selected and two complementary reliability analyses are conducted with correlated $c' - \phi'$ in this section. It is noted that a same $\beta_{c',\phi'}$ is applied for both the two zones (Shell and Core). The objective is to quantify the effects of considering a nonzero $\beta_{c',\phi'}$ on the estimated Pf which remain unknown for the studied dam.

The AbSPCE-MCS method is also employed to perform the two complementary analyses with the user-defined parameters given before. Particularly, the already existing 52 deterministic calculations are used as the initial ED for the case of $\beta_{c',\phi'}=-0.5$. Considering a nonzero $\beta_{c',\phi'}$ will modify the joint distribution of the input variables and the MCS samples will be changed accordingly. Then, the active learning algorithm is carried out to select the best next samples from the new MCS candidate pool. This process will permit to improve the model performance for estimating the Pf . The algorithm is stopped when the stability of the Pf estimates is reached with respect to Eq. (2-27). Finally, 46 new samples are added to obtain the adopted SPCE meta-

model. As for the case of $\beta_{c',\phi'}=0.5$, the current available 98 deterministic results are used for the initial *ED*. The active learning algorithm is stopped with 32 new samples.

Figure 6.6 plots the PDF of the dam FoS values obtained in the two complementary analyses together with the one of the independent case. The three PDF curves are all negatively skewed with a bigger tail at left. This is due to the nature of the most important input variable (the c' of the Shell) which has more small values in its distribution according to Figure 3.9. For the parts with high or low FoS values (higher than 1.55 or lower than 1.1), Figure 6.6 clearly shows that the PDF of $\beta_{c',\phi'}=0.5$ ($PDF_{0.5}$) is the tallest while the one of $\beta_{c',\phi'}=-0.5$ ($PDF_{-0.5}$) is the smallest. This means that more high or small FoS values can be found if the $\beta_{c',\phi'}$ is equal to 0.5, while considering a $\beta_{c',\phi'}$ of -0.5 can reduce the number of these extreme values. A possible explanation is given as follows. When a negative correlation between the c' and ϕ' is considered, the probability of simultaneously generating two low or high values for the $c' - \phi'$ pairs is reduced compared to the case of independent $c' - \phi'$. As a result, less small or high FoS values will be obtained. In contrast, a positive $\beta_{c',\phi'}$ is favourable for having two low or high $c' - \phi'$ values in one simulation. The number of possible extreme FoS values is thus increased. This interpretation explains also why $PDF_{0.5}$ is wider than the other two cases.

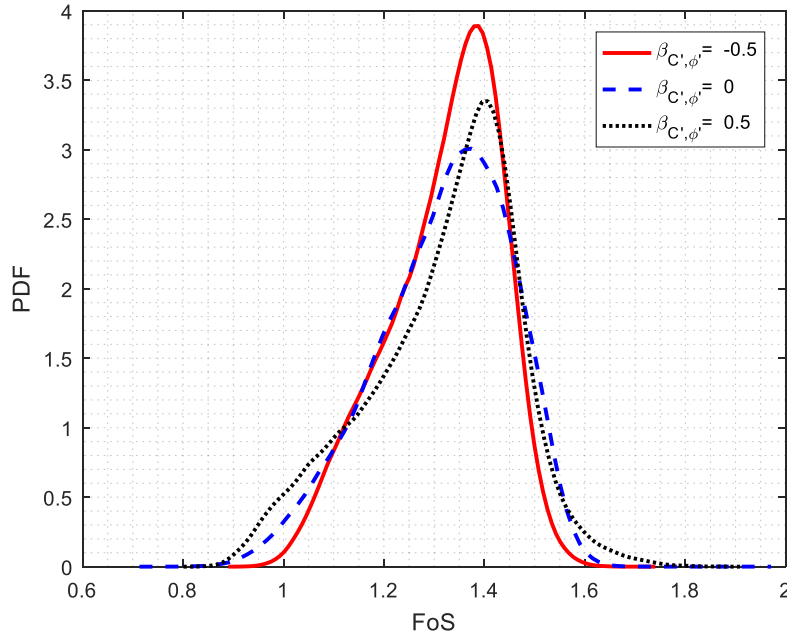


Figure 6.6 PDF of the dam possible FoS values in 3D considering different $\beta_{c', \phi'}$ values

Table 6.2 presents the reliability analysis results for the three analyses with three $\beta_{c', \phi'}$ values (-0.5, 0 and 0.5). It is observed that the Pf_{con} is reduced with decreasing the $c' - \phi'$ correlation coefficient. Considering a $\beta_{c', \phi'}$ of -0.5 can induce a change of one order of magnitude: from 1.6×10^{-2} to 2.1×10^{-3} for the Pf_{con} . This finding is consistent with the previous studies of (Babu and Srivastava, 2010; Guo et al., 2019b) and can be attributed to the fact that the cases of having a low value for both c' and ϕ' are partially avoided by accounting for a $\beta_{c', \phi'}$ of -0.5. The dam failure probabilities (Pf_{sce}) are all lower than 7×10^{-6} , indicating a low instability risk of the dam for the scenario. As for the FoS statistics, the mean value remains almost constant for the three analyses. Therefore, the $c' - \phi'$ correlation is considered to have negligible effects on the FoS mean. However, Table 6.2 shows a clear increase of the FoS standard deviation and CoV with increasing the $\beta_{c', \phi'}$. This observation is in good agreement with Figure 6.6 in which the $PDF_{0.5}$ is wider while the $PDF_{-0.5}$ is narrower compared to the PDF_0 .

Table 6.2 Reliability analysis results in 3D for different $\beta_{c',\phi'}$ values

$\beta_{c',\phi'}$	Reliability analysis results			FoS statistics		
	Pf_{con} ($\times 10^{-3}$)	Pf_{sce} ($\times 10^{-7}$)	$CoV_{Pf_{con}}$	$Mean_{FoS}$	Std_{FoS}	CoV_{FoS}
-0.5	2.1	4.2	3%	1.320	0.114	8.6%
0	16.2	32	2.5%	1.318	0.135	10.2%
0.5	31.5	63	1.8%	1.318	0.150	11.4%

6.3 Comparison with 2D results

As stated before, one objective of this chapter is to quantify the effects of the dam 3D geometry on the reliability analysis results. This can be achieved by comparing the 3D results, obtained previously, with the 2D ones. For this purpose, a 2D computational model is created in the same numerical platform as the 3D one using Plaxis. The geometry of the 2D model is an exact cut section of the 3D one considering the line Y6 shown in Figures 6.2 and 6.4 in order to be comparable with each other. Figure 6.7 shows the established 2D model together with the determined failure surface by considering the mean soil properties values shown in Table 3.3. It is observed that a global failure mechanism (from crest to slope toe) is formed and the shape is similar to the one of the cut section shown in Figure 6.4. The mesh used for the numerical 2D simulations is also illustrated in Figure 6.7. It includes 8294 15-noded triangular elements and 66877 nodes. The element number for the dam body is equal to 5335.

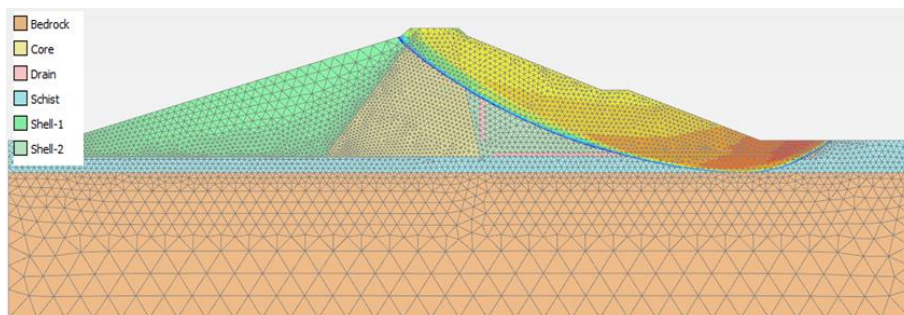


Figure 6.7 2D model and failure surface considering mean values of Table 3.3

The three reliability analyses of the previous section are performed again herein but with the 2D model. Other settings remain the same as before: the 6 Beta RVs of Table 3.2, the pseudo-static acceleration of $0.24g$ and the method AbSPCE-MCS. The technique proposed above for the AbSPCE is also employed here, which involves using the total deterministic results of the previous analysis as the initial ED for the next analysis. This can avoid wasting the deterministic results which are time expensive-to-evaluate, and accelerate the active learning process. Finally, 134 calls to the 2D computational models are required to obtain the target results for the three analyses by using the AbSPCE-MCS with the proposed technique.

Figure 6.8 compares the dam Pf_{con} estimates between the 2D and 3D models for the three considered cases. The corresponding Pf_{con} values are given in Table 6.3. First observation is that the Pf in 2D is also increased by increasing the $\beta_{c',\phi'}$, as found in 3D. Then, it can be seen that using a 3D model always leads to a lower Pf estimate than in 2D, with a reduction ratio of at least 43%. This means that the assumption of being infinite in the 3rd dimension, which is adopted in the 2D simulations, could give conservative results in terms of the Pf . This finding is expected for the studied dam since the 3D dam geometry is beneficial for the downstream slope stability, given that the dam closes a narrow valley and the length (3rd dimension size) is decreased from the central axis to the downstream slope toe (Figures 6.1 and 6.2). Table 6.3 also presents the FoS statistics in 2D and 3D for the three cases. It is observed that improving the dam simulation from 2D to 3D can increase the FoS mean from 1.19 to 1.32. The discussions made above about the favourable 3D geometry for the downstream slope stability remain valid to explain this observation. Additionally, the data scatter of the possible FoS values is increased as well by using a 3D model, because the Std_{FoS} and CoV_{FoS} values are higher in 3D than in 2D. This is due to the fact that the 3D model covers all the 2D failure possibilities, and presents additional failure mechanisms. On one hand, there are some high FoS values in 3D that cannot be provided in 2D. On the

other hand, the 3D model also gives similar small FoS estimates as by 2D if low strength parameters are considered, since local (small) failure surfaces will be formed and the 3D geometry effects are negligible for such cases. Therefore, the possible FoS values in 3D vary in a wider range than in 2D.

When comparing with the results of section 4.2.2, it is found that the 2D dam Pf_{con} of uncorrelated $c' - \phi'$ (0.038) is close to the previous one (0.024) shown in Table 4.4. The differences between the two estimates, although insignificant, can be explained by the following factors: (1) different numerical codes are used for the two analyses (Flac and Plaxis); (2) the previous analysis simplifies the dam geometry by linking the two drains and replacing the bedrocks with the schists; (3) the pore water pressures are slightly increased by default in the pseudo-static simulations of Plaxis as they consider the hydrodynamic overpressure effect, as discussed in section 4.2. Basically, the present Pf_{con} estimate is in relatively good agreement with the previous result of Table 4.4.

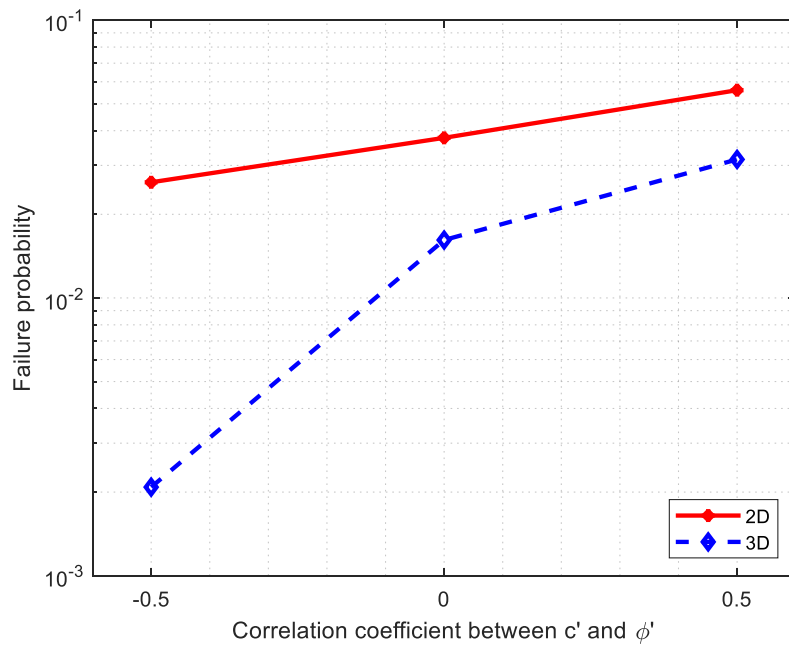


Figure 6.8 Comparison of the Pf_{con} values obtained by the 2D and 3D models

Table 6.3 Comparison of the reliability analysis results between the 2D and 3D cases

$\beta_{c',\phi'}$	2D or 3D	Pf_{con} ($\times 10^{-3}$)	$Mean_{FoS}$	Std_{FoS}	CoV_{FoS} (%)
-0.5	2D	26.1	1.191	0.081	6.8
	3D	2.1	1.320	0.114	8.6
0	2D	37.7	1.187	0.099	8.3
	3D	16.2	1.318	0.135	10.2
0.5	2D	56.0	1.195	0.100	8.4
	3D	31.5	1.318	0.150	11.4

An interesting finding from Figure 6.8 and Table 6.3 is that the 3D geometry effects on the dam Pf for the case of $\beta_{c',\phi'}=-0.5$ are much more significant than for the other two cases. The Pf_{con} is reduced from 2.6×10^{-2} to 2.1×10^{-3} when the $c' - \phi'$ correlation is set equal to -0.5, corresponding to a change of one order of magnitude and a reduction factor of 99.2%. On the contrary, the Pf_{con} remains in a same order of magnitude and the reduction factors are both smaller than 58% for the other two cases. This finding means that using a 2D model will lead to a highly overestimated Pf if the $\beta_{c',\phi'}$ is considered to be equal to -0.5, while the results of assuming 2D simulations are acceptable (close to 3D results) if the $\beta_{c',\phi'}$ is equal to 0 or 0.5. Figure 6.9 provides a possible explanation for the mentioned observation. As the FoS variation is mostly contributed by two variables (c' and ϕ' of the Shell) and the impact of other variables are negligible according to the sensitivity analysis results shown in Table 6.1, it is possible to only focus on these two RVs for understanding the findings about the Pf decrease, which in turn enables a visualization in plot. Figure 6.9 plots 10 000 random LHS samples ($c' - \phi'$ pairs) respectively for the independent case and a negative $\beta_{c',\phi'}$ (-0.5). It is observed that the c' values are mainly between 0 and 25 kPa, while the ϕ' RV varies within a narrower range ([32°, 38°]). In general, accounting for a negative $\beta_{c',\phi'}$ leads to a clockwise rotation of the samples. Figure 6.9 also presents the limit state surface (LSS) for the dam in 2D and 3D. The part left to the LSS represents the

failure domain, while the rest of the area represents the safe domain. The LSSs are estimated by directly searching the $c' - \phi'$ pairs which lead to unit FoS within physical ranges with the help of the SPCE surrogate models constructed previously. It can be seen that using a 3D model results in a more linear LSS and a movement towards the area where the joint probability densities are low which means low probabilities of generating samples in such area. Therefore, the Pf in 3D is smaller than the 2D one. In the case of a negative $\beta_{c',\phi'}$, there is an additional samples-rotation effect, which leads to a further Pf reduction compared to the uncorrelated case. A $\beta_{c',\phi'}$ of -0.5 can noticeably rotate the samples, as shown in Figure 6.9, so induces a significant Pf decrease. For the sake of clarity, the samples of $\beta_{c',\phi'}=0.5$ are not plotted in Figure 6.9 since the results can be predicted. Considering a positive $\beta_{c',\phi'}$ will also rotate the samples but in an anticlockwise way. Such a rotation is unfavourable for reducing the Pf estimate so the Pf decrease from the 2D to the 3D is less remarkable than for the other two cases, as shown in Figure 6.8 and Table 6.3.

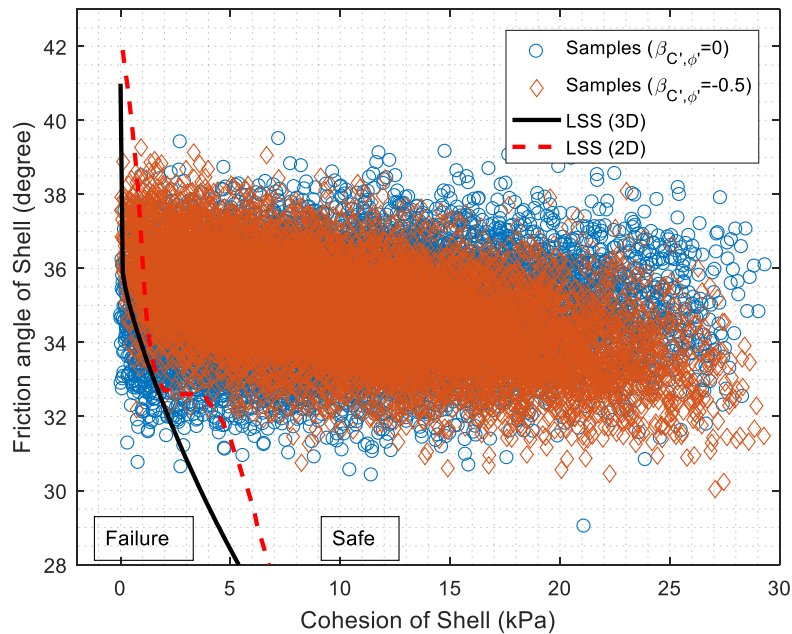


Figure 6.9 The LSS and 10 000 random samples for the 2D and 3D cases

6.4 Effects of using a coarse deterministic mesh

In a probabilistic analysis, a number of deterministic simulations should be performed. Having an unnecessary refined mesh for numerical models would aggravate the computational burden of one simulation, and thus significantly increase the total calculation time especially for complex situations (e.g. 3D simulation and large-scale models). Therefore, it is preferred to employ a relatively coarse mesh for these cases, as in Mollon et al. (2011). A coarse mesh can be determined by a mesh sensitivity study with deterministic input values (e.g. average of each input variable). This section aims to investigate the effects of using a simplified deterministic mesh on the dam reliability estimates in 2D and 3D. The objective is to check if a coarse-mesh model, which gives reasonable estimates in a deterministic framework with mean values, is able to provide acceptable reliability results or not?

At first, a mesh sensitivity analysis is performed for respectively the 2D and 3D model. The dam FoS for the 2D and 3D cases with deterministic input values (Table 3.3) are estimated by using 5 different mesh conditions. Figure 6.10 plots the obtained FoS estimates against different numbers of elements generated for the dam body (Shell-1, Core and Shell-2). It is observed that from the 4th mesh condition, a strict convergence is obtained for both the 2D and 3D since the difference between the two successive FoS estimates can be found only for the 3rd digit after the decimal point. The 4th mesh is thus adopted for the deterministic model and has been used for the previous analyses. However, other mesh conditions can also give satisfied FoS results. For example, the 2nd mesh leads to a FoS error lower than 2% for both the 2D and 3D cases. From a point of view of deterministic calculations, the 2nd mesh can also be accepted which is more favourable than the 4th one for a probabilistic analysis since it can reduce the CPU time of each simulation. Figure 6.11 illustrates the two 2D mesh conditions selected for the comparison study of this section: a coarse mesh (2nd one in Figure 6.10) and a refined mesh (noted as Adopted mesh in Figure 6.10). The former has 931 elements for the dam

body while there are 5335 elements in the latter. As for the 3D, Figure 6.12 shows the two selected mesh configurations with respectively 11275 and 68703 elements for the dam body. Using the coarse mesh instead of the adopted one can reduce the time of one deterministic calculation from 4.3 mins to 1 min in 2D, and from 73 mins to 17 mins in 3D.

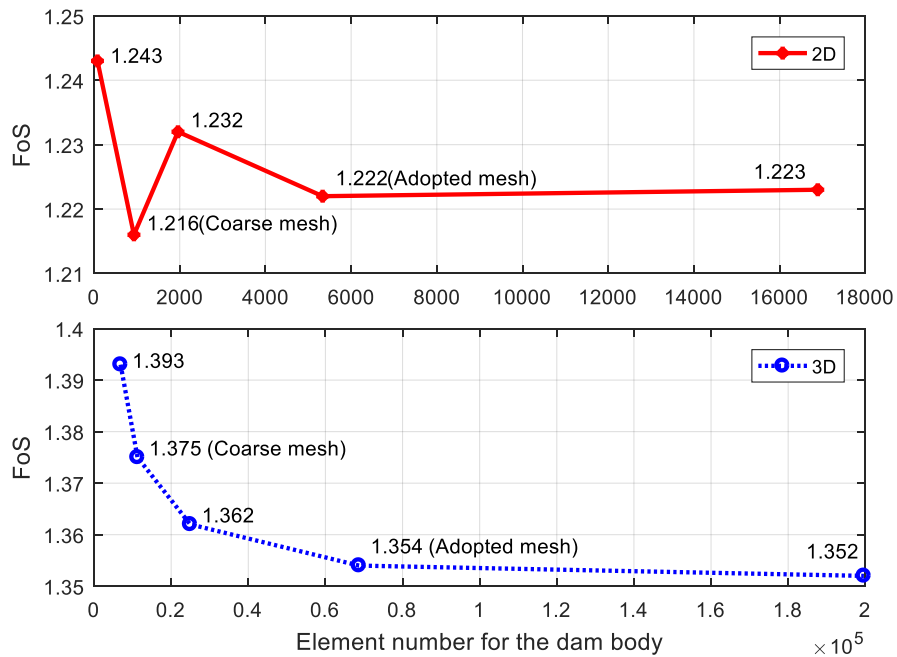


Figure 6.10 Dam FoS estimates for different mesh conditions

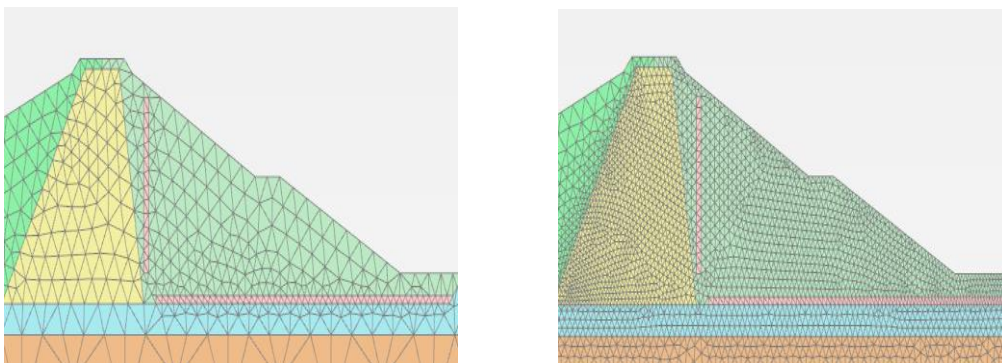


Figure 6.11 Illustration of the two mesh conditions in 2D (left: coarse mesh; right: adopted mesh)

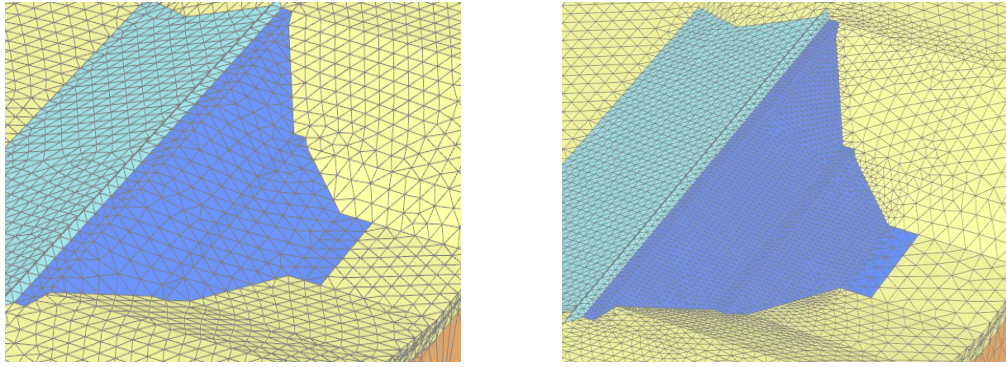


Figure 6.12 Illustration of the two mesh conditions in 3D (left: coarse mesh; right: adopted mesh)

For a purpose of comparison, the analyses shown in Figure 6.8 are conducted again but with the coarse-mesh model for both the 2D and 3D cases. Other settings, referring to the AbSPCE and the probabilistic input parameters, remain unchanged. Figure 6.13 presents the dam Pf_{con} estimates for different $\beta_{c',\phi'}$ values obtained with the coarse mesh. The existing results of the adopted mesh are plotted as well. The comparison of the FoS statistics between the two mesh conditions is presented in Table 6.4. It is observed from Figure 6.13 that using a coarse mesh will underestimate the dam Pf for any $\beta_{c',\phi'}$ values in 2D and 3D. The underestimation effect in 2D corresponds to a Pf decrease lower than 30% and the Pf remains in a same order of magnitude according to Table 6.4. This indicates that the results obtained by using the coarse-mesh model are roughly satisfied in 2D. However, using a 3D simplified mesh leads to unreasonable Pf estimates with a decrease over 60%. Especially, in the case of $\beta_{c',\phi'}=-0.5$, the Pf of the coarse mesh presents a difference of two orders of magnitude compared to the adopted one. Therefore, it is not recommended to use a coarse mesh in 3D, although the total computational time can be reduced, since the mesh-related error is propagated and amplified in a probabilistic analysis which leads to inaccurate Pf estimates.

From Table 6.4, it can be concluded that using a coarse mesh will slightly overestimate the $Mean_{FoS}$, but provide less scattered data (i.e. smaller Std_{FoS}). As a model with a rationally refined mesh enables more forms of failure mechanism, the possible FoS values by the adopted mesh are more dispersed than those of the coarse mesh.

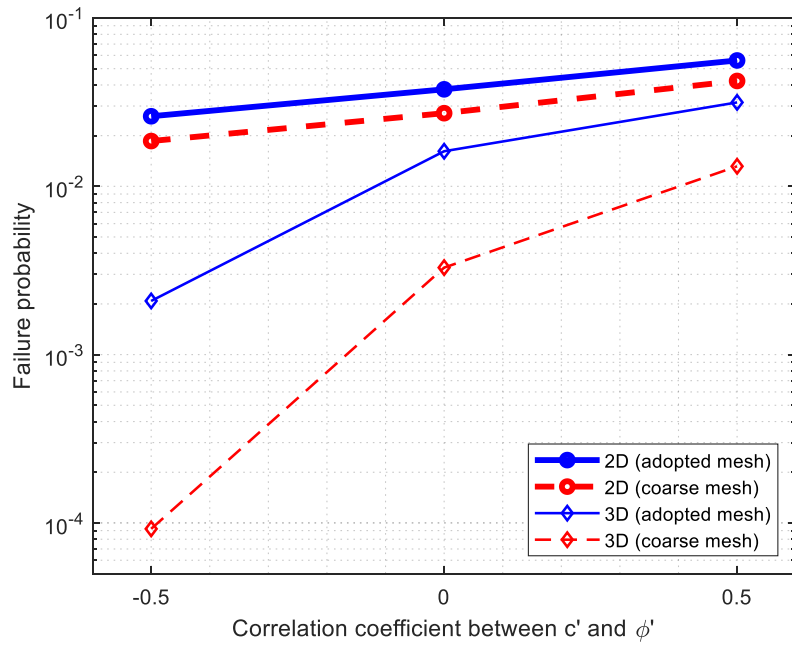


Figure 6.13 Comparison of the Pf estimates obtained by the two mesh conditions in 2D and 3D

Table 6.4 Comparison of the reliability analysis results obtained by the two mesh conditions in 2D and 3D

$\beta_{c',\phi'}$	2D or 3D	Mesh	$Pf_{con} (\times 10^{-3})$	$Mean_{FOS}$	Std_{FOS}	$CoV_{FOS} (\%)$
-0.5	2D	Coarse	18.6	1.200	0.079	6.6
		Adopted	26.1	1.191	0.081	6.8
	3D	Coarse	0.09	1.338	0.094	7.0
		Adopted	2.1	1.320	0.114	8.6
0	2D	Coarse	27.2	1.204	0.077	6.4
		Adopted	37.7	1.187	0.099	8.3
	3D	Coarse	3.3	1.335	0.113	8.5
		Adopted	16.2	1.318	0.135	10.2
0.5	2D	Coarse	42.3	1.204	0.086	7.1
		Adopted	56.0	1.195	0.100	8.4
	3D	Coarse	13.2	1.333	0.133	10.0
		Adopted	31.5	1.318	0.150	11.4

Concerning why the 2D-3D differences of $\beta_{c',\phi'}=-0.5$ are more noticeable than for other cases, Figure 6.14 can help for a better understanding. Similar to Figure 6.9, 10 000 random LHS $C' - \phi'$ samples are plotted in Figure 6.14 for respectively $\beta_{c',\phi'}$ equalling to 0 and -0.5. The LSSs determined by the two 3D mesh conditions are provided as well. It can be seen that the coarse mesh approximately translates the LSS towards the failure domain, which leads to a decrease of the failure area so a Pf reduction. When $\beta_{c',\phi'}$ is equal to -0.5, the samples are rotated such that most of the samples, which are originally located in the failure domain, are escaped from this zone. As a result, a very small Pf estimate (9×10^{-5}) is obtained in such case.

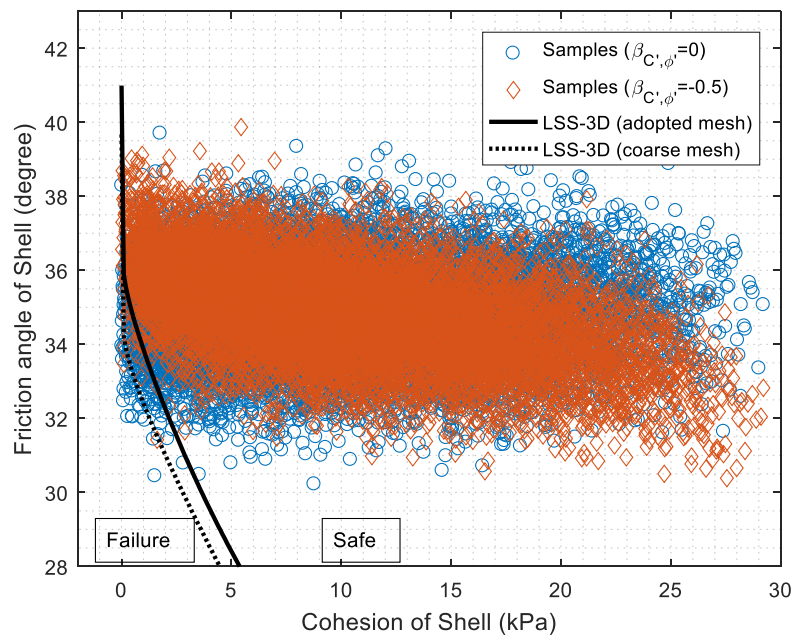


Figure 6.14 The LSS of 3D and 10 000 samples for the two cases with different $\beta_{c',\phi'}$ values

It should be noted that this comparison study is based on the Pf estimate which is obtained by simply counting the number of the failure samples (i.e. $FoS \leq 1$). The sliding mass and the induced damage (risk analysis) are not considered in the comparison. The increase in the Pf estimate by using a refined mesh is probably or at least partially due to the fact that some shallow slip surfaces can be captured by a refined mesh since the mesh sizes near to the surfaces are sufficiently small. Very shallow failures are of less interest for engineers since they are sometimes not realistic or

associated with limited damages. By giving a minimum sliding mass or considering the induced damages, the issue of very shallow failures could be addressed and the difference between a coarse and a refined mesh is expected to be decreased. A further study is necessary to make the discussions above clearer. The objective of the current comparison study (Figure 6.13) aims to provide first insights into the mesh effects on the dam reliability in 2D and 3D. Some findings could be useful for practitioners, for example it requires more attention when determining the mesh for a problem with a negatively correlated $c' - \phi'$.

6.5 Accuracy investigation of the constructed surrogate models

The reliability analyses in this chapter are performed by using a surrogate-based MCS. The surrogate model is obtained by the SPCE with an active learning algorithm. This section aims to evaluate the performance of the obtained SPCE models. As the calculation time of one deterministic simulation is not negligible, performing a direct MCS to assess the AbSPCE results is infeasible especially for the 3D case. Therefore, 100 input sets are considered for the accuracy investigation. The 100 samples are generated with the LHS technique which can guarantee that they could reasonably cover the whole input space. The original computational model created in Plaxis and the SPCE model obtained previously are both used to estimate the dam FoS for the 100 cases in 2D and 3D. All the FoS estimates are then collected and sorted by an ascending order according to the results of the 3D Plaxis model.

Figure 6.15 plots the FoS values of each case for 2D and 3D provided by the two models (Plaxis and SPCE). It reveals that the SPCE results fluctuate around the line of the Plaxis model. This indicates that the predictions made by the SPCE for the dam FoS are close to the reference values in 2D and 3D. For the parts where the FoS is near to the unit, the results given by the two models are extremely similar. This highlights the great accuracy of the SPCE surrogate model for the FoS values close to the limit state

surface, and can be explained by the employed active learning process. Additionally, this figure clearly shows that using a 3D model will give higher FoS estimates and the 2D-3D difference increases with increasing the FoS. Table 6.5 presents the errors of the SPCE predictions for the 100 samples by regarding the Plaxis results as a reference. It is seen that the maximum error is respectively equal to 12% and 5% for the 2D and 3D cases. The average errors are both smaller than 2.5%, indicating a good accuracy of the SPCE models. The term N_{F-S} in Table 6.5 means the number of misjudging failure samples, and is equal to 0 for both the two cases. Moreover, the FoS statistics estimated by the 100 FoS values of the Plaxis model are provided as well for a purpose of comparison. As the 100 samples are generated by assuming a $\beta_{c',\phi'}$ of 0, the results of the uncorrelated case given in Table 6.1 are considered for the comparison. It is shown that the SPCE models provide extremely close estimates for the $Mean_{FoS}$ and slightly higher Std_{FoS} values. In conclusion, the SPCE models, used to replace the original computational models, are accurate in predicting the dam FoS in 2D and 3D.

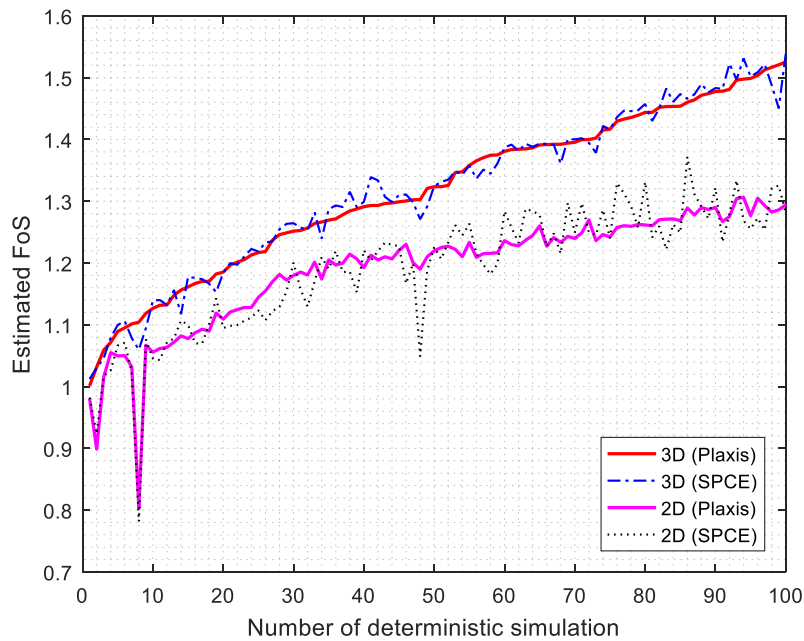


Figure 6.15 FoS estimates for the 100 samples by the original computational model and the SPCE model

Table 6.5 Accuracy survey of the SPCE models based on the 100 random samples

	Model	Surrogate model accuracy			FoS statistics	
		Max error	Average error	$N_{F-S}^{(1)}$	$Mean_{FoS}$	Std_{FoS}
2D	Plaxis	12%	2.2%	0	1.192	0.091
	SPCE				1.187	0.099
3D	Plaxis	5%	1%	0	1.317	0.130
	SPCE				1.318	0.135

Notes: ⁽¹⁾ number of misjudging failure samples

6.6 Conclusions

This chapter presents the dam reliability analyses by using a 3D computational model. One major objective is to account for the 3D dam geometry, which is ignored in previous chapters, and to quantify its effects on the probabilistic analysis results. Firstly, a 3D deterministic model, which describes the real geometry of the dam and valley, is created using the finite element software Plaxis. Such a model enables the dam stability calculation by considering a steady-state flow and a pseudo-static acceleration. Then, this model is coupled with the AbSPCE-MCS method to evaluate the dam reliability. The soil variabilities are modelled as in section 4.2.2 with means of RVs which follows the Beta distributions defined in Table 3.2. The $c' - \phi'$ correlation is also considered in the analyses by testing two $\beta_{c',\phi'}$ values (-0.5 and 0.5). The obtained results show that the dam Pf_{con} is equal to 0.016 in 3D. Assuming a $\beta_{c',\phi'}$ of 0.5 will increase the value to 0.032, while a significant reduction in the Pf (from 0.016 to 0.002) will be observed if the $\beta_{c',\phi'}$ is equal to -0.5. The results are then compared with the ones obtained in 2D which are based on the profile Y6 cross-section (Figure 6.2) of the 3D model. According to the comparison, it can be concluded that taking into account the 3D dam geometry leads to smaller estimates of the dam Pf . The reduction ratio of the Pf is about 50% for the cases of $\beta_{c',\phi'}=0$ or 0.5, but can reach 99% when the $c' - \phi'$ correlation coefficient is equal to -0.5 corresponding to a change of one order of

magnitude for the Pf . These findings can be explained by the movement of the LSS and the rotation of the MCS samples (Figures 6.9 and 6.14).

Additionally, the effects of using a coarse deterministic mesh on the dam reliability estimates are investigated. Two mesh conditions are selected for this study: a relatively coarse mesh and a refined mesh which is the one adopted for the previous analyses. Both of them can provide accurate FoS values in a deterministic framework considering the mean values of each soil property. However, the performance of the coarse mesh in a probabilistic analysis is not satisfactory, given that such a simplified mesh underestimates the dam Pf_{con} with an error of 30% for the 2D and 60% for the 3D case. For the case of $\beta_{c',\phi'}=-0.5$ in 3D, using the coarse mesh leads to a change of two orders of magnitude for the Pf estimates. Therefore, a careful attention should be paid when using a coarse deterministic mesh to reduce the total computational time of a probabilistic analysis. The sliding mass and the induced damages are not considered in the mesh effect investigation. These factors can be added in a further study in order to complete the observations concerning the effect of using a coarse mesh in a probabilistic analysis and a risk analysis. Besides, the effectiveness of the obtained SPCE models, used for replacing the original Plaxis models in the MCS, is assessed. It is achieved by comparing the FoS predictions made by the adopted SPCE models with the FoS estimates provided by the Plaxis models for 100 random LHS samples. The accuracy of the constructed SPCE models is validated since the average error of the FoS predictions for the 100 cases is equal to 2.2% for the 2D and 1% for the 3D case.

The present study is based on the RVs which assume that the soil properties are homogeneous for one simulation. A possible future research will be to incorporate the RFs into the 3D dam model in order to investigate the effects of the soil spatial variability in the 3rd dimension on the dam reliability.

7 CHAPTER VII: General conclusions, recommendations and perspectives

Due to the complexity of the construction materials (soils) and the non-uniform compaction of one layer or different layers, uncertainties exist in the material properties of earth dams. Recently, there is an increasing need of accounting for these uncertainties and quantifying their effects for a safe assessment of large dams, in particular, in the framework of risk analysis studies. Therefore, it is of great interest to implement probabilistic analyses into the safety assessment of these structures. Motivated by this fact, and by the limitations of the existing studies also the new requirement of national regulations, this work is established and is dedicated to presenting a comprehensive probabilistic stability analysis of an earth dam by using real measurements. It also permits to give insights for some issues that remain unknown or unclear in the field of dam probabilistic analyses.

In a first stage, the available data, that are relevant to the dam stability, are statistically analysed in order to model the soil variabilities by means of RVs or RFs. Then, three deterministic models (*LEM_GA*, *SRM_FEM*, *SRM_FDM*), used as the tool to estimate the dam FoS under steady state flow conditions, are developed. The second stage consists in performing the dam probabilistic analyses (reliability and sensitivity) within the framework of the RV approach which is simpler and faster than the RF one. Two deterministic models are employed and compared at this stage and the dam reliability is evaluated under two operation conditions. Then, the RF approach is utilized in the third stage, so that the soil spatial variability can be considered. Two complementary studies are carried out in the RF context: the first one compares five reliability methods including the classical MCS and advanced reliability methods (e.g. SPCE/GSA), while the second one generates different types of RFs for the dam including generic RFs and complex RFs (e.g. conditional and non-stationary). The previous analyses are all based on 2D computations. The fourth stage introduces a 3D model into the dam probabilistic analysis in order to investigate the 3D dam effect (e.g. narrow valley) on the reliability

results. Additionally, the influence of considering an input correlation and the mesh density of the deterministic model are examined as well.

7.1 Concluding remarks from the studied dam

This section gives a summary of the concluding remarks drawn from the obtained results based on the studied dam. They can be gathered by two groups: (1) remarks specific to the case study and (2) those which can be extended to more general cases.

The specific remarks can be listed as follows:

- The dam, regarding its stability of the downstream slope, has a very high safety probability under normal exploitation conditions since the estimated Pf with the RV approach is quite small (in the order of 10^{-6}).
- The dam Pf_{con} varies within the order of 10^{-2} if a pseudo-static acceleration of $0.24g$ is considered regardless of whether the γ_d and ϕ' are modelled by RVs or RFs. In the RV framework, the effects of the 3D geometry and the c' - ϕ' correlation are also investigated. It is shown that the dam Pf_{con} always falls into the same order of magnitude. An exception occurs in 3D when the c' - ϕ' correlation coefficient is considered equal to -0.5 which leads to a Pf_{con} of 2.1×10^{-3} . The above-mentioned Pf values represent the dam vulnerability under such a seismic loading. In order to consider the seismic occurrence probability, these values are multiplied by $1/5000$ in this work (a simple assumption from the return period) so that the dam Pf for the scenario (Pf_{sce}) can be obtained. The value of the dam Pf_{sce} is in the order of 10^{-6} .
- According to the sensitivity indices provided by the PCE-based Sobol solution, the most significant variable for the dam FoS variance is the c' of the Shell while the ϕ' of the Shell is the second important one under the current input configuration (Table 3.2). Other variables, including γ_d , c' - ϕ' of the Core and

the hydraulic parameters, are considered to have a lower impact on the dam FoS variance since their sensitivity indices are all smaller than 0.01.

- The Beta distribution describes better the soil variabilities and provides conservative Pf estimates.
- For the considered high dimensional stochastic problems, the SPCE/GSA shows good accuracy in estimating the dam Pf . The SS performs well in both the accuracy and efficiency, but cannot produce a consistent evolution of the dam Pf considering varied L_x .
- Modelling the γ_d and ϕ' by different types of RFs lead to insignificant differences on the Pf estimates. This is due to the ‘homogeneity’ of the γ_d measurements (at least for the main cross section) and the low variation of the two variables.

The following remarks can be extended, with caution, to general cases:

- The two slope stability analysis methods (SRM and LEM) are basically in good agreement for estimating the dam reliability results. However, it is also found that they have different performances within relatively great FoS values if the variation of one variable amongst the two strength parameters (c' and ϕ') is rather higher than the other one.
- The technique that combines the LEM, an optimization procedure (e.g. GA) and a non-circular slip surface generation method could be a good alternative to the SRM implemented in the FEM or FDM numerical models. It permits efficiently to provide reasonable results in both deterministic and probabilistic frameworks.
- In the context of the RF approach, the Pf estimate will be increased when increasing the horizontal autocorrelation distance (L_x). This finding of the present work can be complemented by the fact that increasing the vertical autocorrelation distance (L_z) also leads to an higher Pf estimate, which has been proven by other studies (Al-Bittar and Soubra, 2013; Cho and Park, 2010;

Guo et al., 2019b; Pan and Dias, 2017b) for different geo-structures. Recently, Zhu et al. (2018) pointed out that it exists a worst case for the autocorrelation distances which means that the relation between Pf and L_x (L_z) is not always monotonously increasing. Therefore, using the RV approach, which assumes the L_x and L_z being infinite, for conservative designs should be conducted with a great caution.

- For a numerical computational model, the mesh density, which is sufficient for a deterministic calculation (mean values for each input), could be questionable for giving accurate reliability estimates. This work shows that a relatively coarse mesh, although providing reasonable FoS for a deterministic analysis, can lead to non-negligible errors in the Pf estimate. As discussed in section 6.4, a next study is necessary to have more investigations on the mesh density effects in a risk analysis context in which the sliding mass and the induced damages can be accounted for.
- Considering a negative (respectively positive) correlation between c' - ϕ' , the Pf estimate will be decreased (respectively increased). This observation is consistent with previous studies (Babu and Srivastava, 2010; Guo et al., 2020; Pan and Dias, 2017b). It is also found in this work that the correlation effect is more significant in 3D than in 2D. This conclusion is effective if the dam or slope is built in a narrow valley.

7.2 Recommendations for relative studies

Based on the present work, some recommendations can be given to engineers and researchers, so they can better understand the functioning mode of such problems in geotechnical probabilistic analyses. The recommendations are listed as follows:

- It is important to collect and localise the measurements (e.g. density) for a great number after the compaction of each layer for earth dams. These data are useful

for the soil variability modelling and the determination of the autocorrelation structure.

- Having more than one deterministic model is a good idea for moderate or big projects since it permits a comparison/validation of the results and to select the appropriate model for a specific purpose. For example, the simplified model (e.g. LEM and limit analysis etc.) can be used at a preliminary design stage for fast estimates of Pf and FoS variance. The obtained results are also indicative for a further advanced analysis.
- The (sparse) PCE is a powerful tool for reliability and sensitivity analysis. It allows considerably reducing the computational time of a probabilistic analysis compared to the direct MCS, and providing a variety of interesting results (Pf , distribution of FoS and sensitivity indices). For a reliability analysis which focuses on estimating the Pf , the adaptive experimental design algorithm (e.g. the one of Table 2.3) is highly recommended.
- Concerning high dimensional problems, for cases where the number of RVs remains below 1000, the SPCE combined with a dimension reduction technique (GSA or SIR) is efficient and accurate. However, for the problems with more than 1000 RVs, these algorithms are less efficient and the SS, which is independent to the input dimension, could be used in such case.
- If the dam construction was well controlled (e.g. careful selection of the construction materials and controlled compaction), indicating a relatively homogenous field, it is then not necessary to describe the soil spatial variabilities by complex RFs (e.g. conditional or nonstationary) because using other RFs rather than the generic (unconditional and stationary) ones will add extra efforts but will only lead to insignificant differences in terms of reliability results. Alternatively, the conditional RFs are recommended since this type of RF allows a full use of the measurements, considers automatically the non-stationarity and normally leads to lower Pf estimate. Besides, one can also use

the spatial averaging method (Papaioannou and Straub, 2017) to consider nonstationary or conditional RFs.

- Performing a sensitivity analysis is suggested for the engineering problems which are related to uncertainties since it provides multiple benefits for designers/researchers: (1) better understand the role/contribution of each random input on the quantity of interest; (2) guide the future investigations/tests and variability modelling on the highly concerned variables. (3) reduce the computational time by treating certain random inputs as deterministic or modelling only the selected variables with RFs in a further sophisticated probabilistic analysis according to the sensitivity indices; (4) help in interpreting the obtained results. For example, the finding that the c' and ϕ' of the Shell are dominant for the FoS variance, makes it possible to regard the LSS in 2D (c' - ϕ' plan), while it cannot be plotted in the original space (6 dimensions).

7.3 Limitations and future works

This section attempts to discuss the limitations of the present work and some possible ideas for future developments which are of interest in the field of earth dam probabilistic analyses.

Firstly, the limitations of this work are discussed as follows:

- Due to the lack of relevant support information, the foundation is treated as deterministic in this work. This may be improved by adopting hypothetical data from literature so that some soil properties of foundation can be modelled in a probabilistic way.
- In the determination of the autocorrelation distance (L_x and L_z) using the variogram analysis, the exponential autocorrelation model is assumed to fit the experimental semi-variogram since it is commonly used in literature (Cho 2014; Li et al. 2017; Li et al. 2015; Wang et al. 2019). Although using different

autocorrelation models would lead to insignificant differences in L_x and L_z for the case study according to Mouyeaux et al. (2018) thus also similar Pf estimates as shown in Figure 5.7, such a subjective choice can be avoided by using the Bayesian theory as discussed in (Cao and Wang, 2014; Montoya-Noguera et al., 2019; Tian et al., 2016).

- Only the soil inherent variabilities are considered in the present work. The soil variations from other sources such as the measurement errors and transformation errors (e.g. the used Caquot's relation for predicting ϕ') are ignored. Additionally, the uncertainties related to external loadings (hydrostatic or seismic) need to be accounted for in a future work.
- Due to the difficulty of statistically quantifying the unsaturated soil parameters, the present work assumes that the soil is saturated. This assumption is conservative in terms of dam FoS and Pf estimates.

The limitations given above highlight the directions of ongoing works which are intended to further improve and extend the present work. Besides, the obtained results suggest some future works which could be interesting for dams engineering. The possible future works are listed as follows:

- The soil spatial modelling can be improved by using the Bayesian theory. The BUS method (Bayesian Updating with Structural reliability methods), proposed by Straub and Papaioannou (2015) and applied in Jiang et al. (2018, 2017), is a powerful tool for this purpose. It should be of interest to be applied in a dam context. An adaptation of the BUS to the RF modelling of hydraulic parameters can be done. In this case, the piezometric measurements of earth dams should be considered, so the distribution parameters can be updated/improved according to the monitoring data which are usually geo-localized and collected with time. In addition, the problem related to 'streaky appearance' of the K-L RFs, as discussed in section 5.2.2.2, needs further investigations.

- The sensitivity analysis performed in this work focuses on quantifying the contribution of each variable to the output variance. Other types of sensitivity indices, such as the one which measures the importance of each variable with respect to the failure (Bourinet, 2018; Ehre et al., 2020), could be used.
- A risk analysis regarding the dam slope instability could be carried out. The idea is to take into account the soil slip volume of each possible failure, which is related to the damage for the probabilistic analysis. Then a new reliability indicator in which the small local failures should have small weights could be proposed. Such an analysis can also improve the comparison study made for the coarse and refined mesh.
- As discussed in CHAPTER II, the probabilistic analysis of earth dams' failure due to piping remains an open issue since only few studies exist on this topic.
- In practice, soil properties vary in 3 dimensions. It will be of interest to incorporate 3D RFs for dams in order to investigate the effect of the 3rd-dimension spatial variability on the dam reliability.
- For a long-term design, a system reliability analysis could be performed in which other operation conditions for dams (e.g. rapid drawdown, strong rainfall and real seismic loadings) will be considered simultaneously.

8 Reference

- Ahmed, A., Soubra, A., 2014. Application of the subset simulation approach to spatially varying soils, in: Phoon, K.-K., Ching, J. (Eds.), *Risk and Reliability in Geotechnical Engineering*. CRC Press, pp. 561–577.
- Ahmed, A.A., 2009. Stochastic analysis of free surface flow through earth dams. *Comput. Geotech.* 36, 1186–1190. <https://doi.org/10.1016/j.compgeo.2009.05.005>
- Aigouy, S., Fry, J.-J., Couturier, B., 2015. Guidelines for the justification of embankment dams and levees. *Comité Français des Barrages et Réservoirs (CFBR)*.
- Al-Bittar, T., 2012. Probabilistic analysis of shallow foundations resting on spatially varying soils. *Université de Nantes*.
- Al-Bittar, T., Soubra, A.-H., 2014. Efficient sparse polynomial chaos expansion methodology for the probabilistic analysis of computationally-expensive deterministic models. *Int. J. Numer. Anal. Methods Geomech.* 38, 1211–1230. <https://doi.org/10.1002/nag.2251>
- Al-Bittar, T., Soubra, A.-H., 2013. Bearing capacity of strip footings on spatially random soils using sparse polynomial chaos expansion. *Int. J. Numer. Anal. Methods Geomech.* 37, 2039–2060. <https://doi.org/10.1002/nag.2120>
- Al-Homoud, A.S., Tanash, N., 2004. Modeling uncertainty in stability analysis for design of embankment dams on difficult foundations. *Eng. Geol.* 71, 323–342. [https://doi.org/10.1016/S0013-7952\(03\)00144-3](https://doi.org/10.1016/S0013-7952(03)00144-3)
- Andreini, M., Gardoni, P., Pagliara, S., Sassu, M., 2019. Probabilistic models for the erosion rate in embankments and reliability analysis of earth dams. *Reliab. Eng. Syst. Saf.* 181, 142–155. <https://doi.org/10.1016/j.ress.2018.09.023>
- Andreini, M., Gardoni, P., Pagliara, S., Sassu, M., 2016. Probabilistic Models for Erosion Parameters and Reliability Analysis of Earth Dams and Levees. *ASCE-ASME J. Risk Uncertain. Eng. Syst. Part A Civ. Eng.* 2. <https://doi.org/10.1061/AJRU6.0000878>
- Au, S.-K., Beck, J.L., 2001. Estimation of small failure probabilities in high dimensions by subset simulation. *Probabilistic Eng. Mech.* 16, 263–277. [https://doi.org/10.1016/S0266-8920\(01\)00019-4](https://doi.org/10.1016/S0266-8920(01)00019-4)
- Babu, G.S., Srivastava, A., 2010. Reliability Analysis of Earth Dams. *J. Geotech. Geoenvironmental Eng.* 136, 995–998. [https://doi.org/10.1061/\(ASCE\)GT.1943-5606.0000313](https://doi.org/10.1061/(ASCE)GT.1943-5606.0000313)
- Babu, G.S., Srivastava, A., Sahana, V., 2007. Analysis of stability of earthen dams in kachchh region, Gujarat, India. *Eng. Geol.* 94, 123–136. <https://doi.org/10.1016/J.ENGCEO.2007.05.007>
- Baecher, G.B., Christian, J.T., 2005. *Reliability and Statistics in Geotechnical Engineering, Reliability and Statistics in Geotechnical Engineering*. John Wiley & Sons. <https://doi.org/10.1198/tech.2005.s838>
- Blatman, G., 2009. Adaptive sparse polynomial chaos expansions for uncertainty propagation and sensitivity analysis. *Université Blaise Pascal, Clermont-Ferrand, France*.
- Blatman, G., Sudret, B., 2011. Adaptive sparse polynomial chaos expansion based on least angle regression. *J. Comput. Phys.* 230, 2345–2367. <https://doi.org/10.1016/j.jcp.2010.12.021>

- Blatman, G., Sudret, B., 2010. An adaptive algorithm to build up sparse polynomial chaos expansions for stochastic finite element analysis. *Probabilistic Eng. Mech.* 25, 183–197.
<https://doi.org/10.1016/j.probengmech.2009.10.003>
- Blatman, G., Sudret, B., 2008. Sparse polynomial chaos expansions and adaptive stochastic finite elements using a regression approach. *Comptes Rendus Mécanique* 336, 518–523.
<https://doi.org/10.1016/j.crme.2008.02.013>
- Bourinet, J.-M., 2018. Reliability analysis and optimal design under uncertainty - Focus on adaptive surrogate-based approaches. Université Clermont Auvergne.
- Breitung, K., 1989. Asymptotic approximations for probability integrals. *Probabilistic Eng. Mech.* 4, 187–190. [https://doi.org/10.1016/0266-8920\(89\)90024-6](https://doi.org/10.1016/0266-8920(89)90024-6)
- Brinkgreve, R.B.J., Kumarswamy, S., Swolfs, W.M., 2015. *Plaxis, Reference Manual*. Delft.
- Burgess, J., Fenton, G.A., Griffiths, D.V., 2019. Probabilistic Seismic Slope Stability Analysis and Design. *Can. Geotech. J.* <https://doi.org/10.1139/cgj-2017-0544>
- Calamak, M., Kentel, E., Yanmaz, A.M., 2013. Spatial Variability in Seepage Flow through Earth-fill Dams, in: *Canadian Dam Association 2013 Annual Conference*. Montréal, p. 37.
<https://doi.org/10.13140/2.1.1245.3769>
- Calamak, M., Kentel, E., Yanmaz, A.M., 2012. Seepage Analysis through Earth-Fill Dams having Random Fields, in: *10th International Congress on Advances in Civil Engineering*. Ankara, pp. 97–105. <https://doi.org/10.13140/2.1.3866.8169>
- Calamak, M., Yanmaz, A.M., 2014. Probabilistic assessment of slope stability for earth-fill dams having random soil parameters, in: *5th International Symposium on Hydraulic Structures*. Brisbane.
<https://doi.org/10.14264/uql.2014.16>
- Cao, Z., Wang, Y., 2014. Bayesian model comparison and selection of spatial correlation functions for soil parameters. *Struct. Saf.* 49, 10–17. <https://doi.org/10.1016/j.strusafe.2013.06.003>
- Carvajal, C., Peyras, L., Arnaud, P., Boissier, D., Royet, P., 2009. Probabilistic modeling of floodwater level for dam reservoirs. *J. Hydrol. Eng.* 14, 223–232. [https://doi.org/10.1061/\(ASCE\)1084-0699\(2009\)14:3\(223\)](https://doi.org/10.1061/(ASCE)1084-0699(2009)14:3(223))
- Chang, K.-H., 2015. Multiobjective Optimization and Advanced Topics, in: *Design Theory and Methods Using CAD/CAE*. Elsevier, pp. 325–406. <https://doi.org/10.1016/b978-0-12-398512-5.00005-0>
- Chapuis, R.P., Aubertin, M., 2003. On the use of the Kozeny–Carman equation to predict the hydraulic conductivity of soils. *Can. Geotech. J.* 40, 616–628. <https://doi.org/10.1139/t03-013>
- Chen, Q., Chang, L.-Y., 2011. Probabilistic Slope Stability Analysis of a 300 m High Embankment Dam. *GeoRisk* 403–410. [https://doi.org/10.1061/41183\(418\)42](https://doi.org/10.1061/41183(418)42)
- Cheng, Y.M., Lansivaara, T., Wei, W.B., 2007. Two-dimensional slope stability analysis by limit equilibrium and strength reduction methods. *Comput. Geotech.* 34, 137–150.
<https://doi.org/10.1016/j.compgeo.2006.10.011>
- Cheng, Y.M., Liang, L., Chi, S.C., Wei, W.B., 2008. Determination of the Critical Slip Surface Using Artificial Fish Swarms Algorithm. *J. Geotech. Geoenvironmental Eng.* 134, 244–251.
[https://doi.org/10.1061/\(ASCE\)1090-0241\(2008\)134:2\(244\)](https://doi.org/10.1061/(ASCE)1090-0241(2008)134:2(244))
- Cho, S., 2009. Probabilistic Assessment of Slope Stability That Considers the Spatial Variability of Soil Properties. *J. Geotech. Geoenvironmental Eng.* 136, 975–984.
[https://doi.org/10.1061/\(ASCE\)GT.1943-5606.0000309](https://doi.org/10.1061/(ASCE)GT.1943-5606.0000309)

- Cho, S.E., 2014. Probabilistic stability analysis of rainfall-induced landslides considering spatial variability of permeability. *Eng. Geol.* 171, 11–20. <https://doi.org/10.1016/j.enggeo.2013.12.015>
- Cho, S.E., 2012. Probabilistic analysis of seepage that considers the spatial variability of permeability for an embankment on soil foundation. *Eng. Geol.* 133–134, 30–39. <https://doi.org/10.1016/j.enggeo.2012.02.013>
- Cho, S.E., 2009. Probabilistic stability analyses of slopes using the ANN-based response surface. *Comput. Geotech.* 36, 787–797. <https://doi.org/10.1016/j.compgeo.2009.01.003>
- Cho, S.E., 2007. Effects of spatial variability of soil properties on slope stability. *Eng. Geol.* 92, 97–109. <https://doi.org/10.1016/j.enggeo.2007.03.006>
- Cho, S.E., Park, H.C., 2010. Effect of spatial variability of cross-correlated soil properties on bearing capacity of strip footing. *Int. J. Numer. Anal. Methods Geomech.* 34, 1–26. <https://doi.org/10.1002/nag.791>
- Dawson, E.M., Roth, W.H., Drescher, A., 1999. Slope stability analysis by strength reduction. *Géotechnique* 49, 835–840. <https://doi.org/10.1680/geot.1999.49.6.835>
- Der Kiureghian, A., Ke, J.-B., 1988. The stochastic finite element method in structural reliability. *Probabilistic Eng. Mech.* 3, 83–91. [https://doi.org/10.1016/0266-8920\(88\)90019-7](https://doi.org/10.1016/0266-8920(88)90019-7)
- Dolinski, K., 1982. First-order second-moment approximation in reliability of structural systems: Critical review and alternative approach. *Struct. Saf.* 1, 211–231. [https://doi.org/10.1016/0167-4730\(82\)90027-3](https://doi.org/10.1016/0167-4730(82)90027-3)
- Echard, B., Gayton, N., Lemaire, M., 2011. AK-MCS: an active learning reliability method combining Kriging and Monte Carlo simulation. *Struct. Saf.* 33, 145–54. <https://doi.org/10.1016/j.strusafe.2011.01.002>
- Ehre, M., Papaioannou, I., Straub, D., 2020. A framework for global reliability sensitivity analysis in the presence of multi-uncertainty. *Reliab. Eng. Syst. Saf.* 195, 106726. <https://doi.org/10.1016/j.ress.2019.106726>
- Eiben, A.E., Smith, J.E., 2003. *Introduction to Evolutionary Computing*, Natural Computing Series. Springer Berlin Heidelberg, Berlin, Heidelberg. <https://doi.org/10.1007/978-3-662-05094-1>
- El-Ramly, H., Morgenstern, N.R., Cruden, D.M., 2003. Probabilistic stability analysis of a tailings dyke on presheared clay-shale. *Can. Geotech. J.* 40, 192–208. <https://doi.org/10.1139/t02-095>
- Fenton, G.A., Griffiths, D.V., 1997. Extreme hydraulic gradient statistics in stochastic earth dam. *J. of Geotechnical Geoenvironmental Eng.* 123, 14775. [https://doi.org/10.1061/\(ASCE\)1090-0241\(1997\)123:11\(995\)](https://doi.org/10.1061/(ASCE)1090-0241(1997)123:11(995))
- Fenton, G.A., Griffiths, D. V., 2008. *Risk Assessment in Geotechnical Engineering*, Risk Assessment in Geotechnical Engineering. <https://doi.org/10.1002/9780470284704>
- Fenton, G.A., Griffiths, D. V., 1996. Statistics of free surface flow through stochastic earth dam. *J. Geotech. Eng.* 122, 427–436. [https://doi.org/10.1061/\(asce\)0733-9410\(1996\)122:6\(427\)](https://doi.org/10.1061/(asce)0733-9410(1996)122:6(427))
- Fenton, G.A., Griffiths, D. V., 1993. Statistics of block conductivity through a simple bounded stochastic medium. *Water Resour. Res.* 29, 1825–1830. <https://doi.org/10.1029/93WR00412>
- Foster, M., Fell, R., Spannagle, M., 2000a. The statistics of embankment dam failures and accidents. *Can. Geotech. J.* 37, 1000–1024. <https://doi.org/10.1139/t00-030>
- Foster, M., Fell, R., Spannagle, M., 2000b. A method for assessing the relative likelihood of failure of embankment dams by piping. *Can. Geotech. J.* 37, 1025–1061. <https://doi.org/10.1139/t00-029>

- Geyer, S., Papaioannou, I., Straub, D., 2019. Cross entropy-based importance sampling using Gaussian densities revisited. *Struct. Saf.* 76, 15–27. <https://doi.org/10.1016/j.strusafe.2018.07.001>
- Ghanem, R., Saad, G., Doostan, A., 2007. Efficient solution of stochastic systems: Application to the embankment dam problem. *Struct. Saf.* 29, 238–251. <https://doi.org/10.1016/j.strusafe.2006.07.015>
- Griffiths, D., Fenton, G., 2007. *Probabilistic methods in geotechnical engineering*. Springer Vienna, Vienna.
- Griffiths, D.V., Fenton, G.A., 1993. Seepage beneath water retaining structures founded on spatially random soil. *Géotechnique* 43, 577–587. <https://doi.org/https://doi.org/10.1680/geot.1993.43.4.577>
- Griffiths, D. V., Huang, J., Fenton, G. a., 2009. Influence of Spatial Variability on Slope Reliability Using 2-D Random Fields. *J. Geotech. Geoenvironmental Eng.* 135, 1367–1378. [https://doi.org/10.1061/\(ASCE\)GT.1943-5606.0000099](https://doi.org/10.1061/(ASCE)GT.1943-5606.0000099)
- Griffiths, D. V., Lane, P.A., 1999. Slope stability analysis by finite elements. *Géotechnique* 49, 387–403. <https://doi.org/10.1680/geot.1999.49.3.387>
- Griffiths, D. V., Yu, X., 2015. Another look at the stability of slopes with linearly increasing undrained strength. *Géotechnique* 65, 824–830. <https://doi.org/10.1680/jgeot.14.T.030>
- Griffiths, D. V, Zhu, D., Huang, J., Fenton, G.A., 2016. Observations on probabilistic slope stability analysis, in: *6th Asian-Pacific Symposium on Structural Reliability and Its Applications (APSSRA 2016)*.
- Gui, S., Zhang, R., Turner, J.P., Xue, X., 2000. Probabilistic Slope Stability Analysis with Stochastic Soil Hydraulic Conductivity. *J. Geotech. Geoenvironmental Eng.* 126, 17178. [https://doi.org/10.1061/\(ASCE\)1090-0241\(2000\)126:1\(1\)](https://doi.org/10.1061/(ASCE)1090-0241(2000)126:1(1))
- Guo, X., Dias, D., 2020. Kriging based reliability and sensitivity analysis – Application to the stability of an earth dam. *Comput. Geotech.* 120, 103411. <https://doi.org/10.1016/j.compgeo.2019.103411>
- Guo, X., Dias, D., Carvajal, C., Peyras, L., Breul, P., 2019a. A comparative study of different reliability methods for high dimensional stochastic problems related to earth dam stability analyses. *Eng. Struct.* 188, 591–602. <https://doi.org/10.1016/j.engstruct.2019.03.056>
- Guo, X., Dias, D., Carvajal, C., Peyras, L., Breul, P., 2018. Reliability analysis of embankment dam sliding stability using the sparse polynomial chaos expansion. *Eng. Struct.* 174, 295–307. <https://doi.org/10.1016/j.engstruct.2018.07.053>
- Guo, X., Dias, D., Pan, Q., 2019b. Probabilistic stability analysis of an embankment dam considering soil spatial variability. *Comput. Geotech.* 113, 103093. <https://doi.org/10.1016/j.compgeo.2019.103093>
- Guo, X., Sun, Q., Dias, D., Antoinet, E., 2020. Probabilistic assessment of an earth dam stability design using the adaptive polynomial chaos expansion. *Bull. Eng. Geol. Environ.* 79. <https://doi.org/10.1007/s10064-020-01847-2>
- Hariri-Ardebili, M.A., 2018. Risk, Reliability, Resilience (R3) and beyond in dam engineering: A state-of-the-art review. *Int. J. Disaster Risk Reduct.* 31, 806–831. <https://doi.org/10.1016/j.ijdrr.2018.07.024>

- Hariri-Ardebili, M.A., Sudret, B., 2019. Polynomial chaos expansion for uncertainty quantification of dam engineering problems. *Eng. Struct.* 109631. <https://doi.org/10.1016/j.engstruct.2019.109631>
- Hasofer, A.-M., Lind, N.-C., 1974. Exact and invariant second moment code format. *J. Eng. Mech.* 100, 111–121.
- Helton, J.C., Davis, F.J., 2003. Latin hypercube sampling and the propagation of uncertainty in analyses of complex systems. *Reliab. Eng. Syst. Saf.* 81, 23–69. [https://doi.org/10.1016/S0951-8320\(03\)00058-9](https://doi.org/10.1016/S0951-8320(03)00058-9)
- Hohenbichler, M., Gollwitzer, S., Kruse, W., Rackwitz, R., 1987. New light on first- and second-order reliability methods. *Struct. Saf.* 4, 267–284. [https://doi.org/10.1016/0167-4730\(87\)90002-6](https://doi.org/10.1016/0167-4730(87)90002-6)
- Hu, Z., Mahadevan, S., 2016. Global sensitivity analysis-enhanced surrogate (GSAS) modeling for reliability analysis. *Struct. Multidiscip. Optim.* 53, 501–521. <https://doi.org/10.1007/s00158-015-1347-4>
- Huang, C.-C., Tsai, C.-C., Chen, Y.-H., 2002. Generalized Method for Three-Dimensional Slope Stability Analysis. *J. Geotech. Geoenvironmental Eng.* 128, 836–848. [https://doi.org/10.1061/\(ASCE\)1090-0241\(2002\)128:10\(836\)](https://doi.org/10.1061/(ASCE)1090-0241(2002)128:10(836))
- Huang, X., Chen, J., Zhu, H., 2016. Assessing small failure probabilities by AK–SS: An active learning method combining Kriging and Subset Simulation. *Struct. Saf.* 59, 86–95. <https://doi.org/10.1016/J.STRUSAFE.2015.12.003>
- ICOLD, 2019. World Register of Dams - General Synthesis [WWW Document]. URL https://www.icold-cigb.org/GB/world_register/general_synthesis.asp (accessed 12.11.19).
- Iman, R.L., Conover, W.J., 1982. A Distribution-Free Approach to Inducing Rank Correlation Among Input Variables. *Commun. Stat. - Simul. Comput.* 11, 311–334. <https://doi.org/10.1080/03610918208812265>
- Iooss, B., Lemaître, P., 2015. A review on global sensitivity analysis methods, in: Meloni, C., Dellino, G. (Eds.), *Uncertainty Management in Simulation-Optimization of Complex Systems: Algorithms and Applications*. Springer. https://doi.org/10.1007/978-1-4899-7547-8_5
- Itasca, 2011. *FLAC 7.0 reference manual*. Minneapolis.
- Janbu, N., 1973. *Slope Stability Computations*. Wiley (John) and Sons.
- Javankhoshdel, S., Bathurst, R.J., 2016. Influence of cross correlation between soil parameters on probability of failure of simple cohesive and c- ϕ slopes. *Can. Geotech. J.* 53, 839–853. <https://doi.org/10.1139/cgj-2015-0109>
- Jiang, S.H., Huang, J., 2018. Modeling of non-stationary random field of undrained shear strength of soil for slope reliability analysis. *Soils Found.* 58, 185–198. <https://doi.org/10.1016/j.sandf.2017.11.006>
- Jiang, S.H., Papaioannou, I., Straub, D., 2018. Bayesian updating of slope reliability in spatially variable soils with in-situ measurements. *Eng. Geol.* 239, 310–320. <https://doi.org/10.1016/j.enggeo.2018.03.021>
- Jiang, S.H., Papaioannou, I., Straub, D., 2017. Optimizing Borehole Locations for Slope Reliability Assessment. *Geotech. Spec. Publ.* 0, 420–430. <https://doi.org/10.1061/9780784480717.040>
- Johari, A., Gholampour, A., 2018. Discussion on “Conditional random field reliability analysis of a cohesion-frictional Slope” by Lei-Lei Liu, Yung-Ming Cheng and Shao-He Zhang [Comput.

- Geotech. 82 (2017) 173–186]. Comput. Geotech. 94, 247–248.
<https://doi.org/10.1016/j.compgeo.2017.05.017>
- Kartal, M.E., Başağa, H.B., Bayraktar, A., 2011. Probabilistic nonlinear analysis of CFR dams by MCS using Response Surface Method. Appl. Math. Model. 35, 2752–2770.
<https://doi.org/10.1016/j.apm.2010.12.003>
- Kim, J.M., Sitar, N., 2013. Reliability approach to slope stability analysis with spatially correlated soil properties. Soils Found. 53, 1–10. <https://doi.org/10.1016/J.SANDF.2012.12.001>
- Kiureghian, A. Der, Dakessianb, T., 1998. Multiple design points in first and second-order reliability. Struct. Saf. 20, 37–49. [https://doi.org/10.1016/S0167-4730\(97\)00026-X](https://doi.org/10.1016/S0167-4730(97)00026-X)
- Kroese, D.P., Taimre, T., Botev, Z.I., 2011. Handbook of Monte Carlo Methods, Handbook of Monte Carlo Methods. Wiley Blackwell. <https://doi.org/10.1002/9781118014967>
- Kucherenko, S., Tarantola, S., Annoni, P., 2012. Estimation of global sensitivity indices for models with dependent variables. Comput. Phys. Commun. 183, 937–946.
<https://doi.org/10.1016/J.CPC.2011.12.020>
- Lataniotis, C., Marelli, S., Sudret, B., 2019. UQLAB user manual – The Input module, Report UQLab-V1.2-102. Zurich.
- Lataniotis, C., Marelli, S., Sudret, B., 2018. UQLab user manual – Kriging (Gaussian process modelling), Report UQLab-V1.1-105. ETH Zurich.
- Le, T.M.H., Gallipoli, D., Sanchez, M., Wheeler, S.J., 2012. Stochastic analysis of unsaturated seepage through randomly heterogeneous earth embankments. Int. J. Numer. Anal. Methods Geomech. 36, 1056–1076. <https://doi.org/10.1002/nag.1047>
- Lebrun, R., Dutfoy, A., 2009a. A generalization of the Nataf transformation to distributions with elliptical copula. Probabilistic Eng. Mech. 24, 172–178.
<https://doi.org/10.1016/J.PROBENGMECH.2008.05.001>
- Lebrun, R., Dutfoy, A., 2009b. Do Rosenblatt and Nataf isoprobabilistic transformations really differ? Probabilistic Eng. Mech. 24, 577–584. <https://doi.org/10.1016/j.probengmech.2009.04.006>
- Lemaire, M., Chateauneuf, A., Mitteau, J.C., 2010. Structural Reliability, Structural Reliability. Wiley-ISTE. <https://doi.org/10.1002/9780470611708>
- Li, C.-C., Der Kiureghian, A., 1993. Optimal discretization of random fields. J. Eng. Mech. 119, 1136–1154. [https://doi.org/10.1061/\(ASCE\)0733-9399\(1993\)119:6\(1136\)](https://doi.org/10.1061/(ASCE)0733-9399(1993)119:6(1136))
- Li, D.-Q., Qi, X.-H., Cao, Z.-J., Tang, X.-S., Zhou, W., Phoon, K.-K., Zhou, C.-B., 2015. Reliability analysis of strip footing considering spatially variable undrained shear strength that linearly increases with depth. Soils Found. 55, 866–880. <https://doi.org/10.1016/J.SANDF.2015.06.017>
- Li, D., Chen, Y., Lu, W., Zhou, C., 2011. Stochastic response surface method for reliability analysis of rock slopes involving correlated non-normal variables. Comput. Geotech. 38, 58–68.
<https://doi.org/10.1016/j.compgeo.2010.10.006>
- Li, D.Q., Qi, X.H., Phoon, K.K., Zhang, L.M., Zhou, C.B., 2014. Effect of spatially variable shear strength parameters with linearly increasing mean trend on reliability of infinite slopes. Struct. Saf. 49, 45–55. <https://doi.org/10.1016/j.strusafe.2013.08.005>
- Li, H.S., Cao, Z.J., 2016. Matlab codes of Subset Simulation for reliability analysis and structural optimization. Struct. Multidiscip. Optim. 54, 391–410. <https://doi.org/10.1007/s00158-016-1414-5>

- Li, J.H., Zhou, Y., Zhang, L.L., Tian, Y., Cassidy, M.J., Zhang, L.M., 2016. Random finite element method for spudcan foundations in spatially variable soils. *Eng. Geol.* 205, 146–155. <https://doi.org/10.1016/j.enggeo.2015.12.019>
- Li, X.Y., Zhang, L.M., Gao, L., Zhu, H., 2017. Simplified slope reliability analysis considering spatial soil variability. *Eng. Geol.* 216, 90–97. <https://doi.org/10.1016/j.enggeo.2016.11.013>
- Li, X.Y., Zhang, L.M., Li, J.H., 2015. Using Conditioned Random Field to Characterize the Variability of Geologic Profiles. *J. Geotech. Geoenvironmental Eng.* 142, 04015096. [https://doi.org/10.1061/\(ASCE\)GT.1943-5606.0001428](https://doi.org/10.1061/(ASCE)GT.1943-5606.0001428)
- Li, Y.-C., Chen, Y.-M., Zhan, T.L.T., Ling, D.-S., Cleall, P.J., 2010. An efficient approach for locating the critical slip surface in slope stability analyses using a real-coded genetic algorithm. *Can. Geotech. J.* 47, 806–820. <https://doi.org/10.1139/T09-124>
- Liang, R.Y., Nusier, O.K., Malkawi, A.H., 1999. A reliability based approach for evaluating the slope stability of embankment dams. *Eng. Geol.* 54, 271–285. [https://doi.org/10.1016/S0013-7952\(99\)00017-4](https://doi.org/10.1016/S0013-7952(99)00017-4)
- Liang, Y., Yeh, T.-C.J., Wang, Y.-L., Liu, M., Wang, J., Hao, Y., 2017. Numerical simulation of backward erosion piping in heterogeneous fields. *Water Resour. Res.* 53, 3246–3261. <https://doi.org/10.1002/2017WR020425>. Received
- Liu, L.L., Cheng, Y.M., Jiang, S.H., Zhang, S.H., Wang, X.M., Wu, Z.H., 2017a. Effects of spatial autocorrelation structure of permeability on seepage through an embankment on a soil foundation. *Comput. Geotech.* 87, 62–75. <https://doi.org/10.1016/j.compgeo.2017.02.007>
- Liu, L.L., Cheng, Y.M., Zhang, S.H., 2017b. Conditional random field reliability analysis of a cohesion-frictional slope. *Comput. Geotech.* 82, 173–186. <https://doi.org/10.1016/j.compgeo.2016.10.014>
- Lloret-Cabot, M., Hicks, M.A., van den Eijnden, A.P., 2012. Investigation of the reduction in uncertainty due to soil variability when conditioning a random field using Kriging. *Géotechnique Lett.* 2, 123–127. <https://doi.org/10.1680/geolett.12.00022>
- Loudière, D., Hoonakker, M., Le Delliou, P., 2014. Risque sismique et sécurité des ouvrages hydrauliques.
- Low, B.K., Tang, W.H., 2007. Efficient Spreadsheet Algorithm for First-Order Reliability Method. *J. Eng. Mech.* 133, 1378–1387. [https://doi.org/10.1061/\(ASCE\)0733-9399\(2007\)133:12\(1378\)](https://doi.org/10.1061/(ASCE)0733-9399(2007)133:12(1378))
- Lumb, P., 1970. Safety factors and the probability distribution of soil strength. *Can. Geotech. J.* 7, 225–242. <https://doi.org/10.1139/t70-032>
- Lumb, P., 1966. The Variability of Natural Soils. *Can. Geotech. J.* 3, 74–97. <https://doi.org/10.1139/t66-009>
- Marelli, S., Schobi, R., Sudret, B., 2019. UQLAB user manual – Structural reliability (Rare event estimation), Report, UQLab-V1.2-107. Zurich.
- Marelli, S., Sudret, B., 2019. UQLab user manual – Polynomial chaos expansions, Report # UQLab-V1.3-104. Zurich.
- Marelli, S., Sudret, B., 2018. An active-learning algorithm that combines sparse polynomial chaos expansions and bootstrap for structural reliability analysis. *Struct. Saf.* 75, 67–74. <https://doi.org/10.1016/J.STRUSAFE.2018.06.003>
- Mathworks, I., 2015. MATLAB - the language of technical Computing.

- McKay, M.D., Beckman, R.J., Conover, W.J., 1979. Comparison of three methods for selecting values of input variables in the analysis of output from a computer code. *Technometrics* 21, 239–245. <https://doi.org/10.1080/00401706.1979.10489755>
- Mínguez, R., Delgado, F., Escuder, I., de Membrillera, M.G., 2006. Reliability assessment of granular filters in embankment dams. *Int. J. Numer. Anal. Methods Geomech.* 30, 1019–1037. <https://doi.org/10.1002/nag.511>
- Mollon, G., Dias, D., Soubra, A.-H., 2011. Probabilistic Analysis of Pressurized Tunnels against Face Stability Using Collocation-Based Stochastic Response Surface Method. *J. Geotech. Geoenvironmental Eng.* 137, 385–397. [https://doi.org/10.1061/\(ASCE\)GT.1943-5606.0000443](https://doi.org/10.1061/(ASCE)GT.1943-5606.0000443)
- Mollon, G., Dias, D., Soubra, A.-H., 2009. Probabilistic Analysis of Circular Tunnels in Homogeneous Soil Using Response Surface Methodology. *J. Geotech. Geoenvironmental Eng.* 135, 1314–1325. [https://doi.org/10.1061/\(ASCE\)GT.1943-5606.0000060](https://doi.org/10.1061/(ASCE)GT.1943-5606.0000060)
- Mollon, M.G., Phoon, K.-K., Dias, D., Soubra, A.-H., 2011. Influence of the scale of fluctuation of the friction angle on the face stability of a pressurized tunnel in sands. *Geotech. Spec. Publ.* 225–232. [https://doi.org/10.1061/41183\(418\)14](https://doi.org/10.1061/41183(418)14)
- Montoya-Noguera, S., Zhao, T., Hu, Y., Wang, Y., Phoon, K.-K., 2019. Simulation of non-stationary non-Gaussian random fields from sparse measurements using Bayesian compressive sampling and Karhunen-Loève expansion. *Struct. Saf.* 79, 66–79. <https://doi.org/10.1016/j.strusafe.2019.03.006>
- Morgenstern, N.R., Price, V.E., 1965. The Analysis of the Stability of general slip surfaces. *Geotechnique* 15, 725–726. <https://doi.org/10.1680/geot.1965.15.1.79>
- Morio, J., 2012. Extreme quantile estimation with nonparametric adaptive importance sampling. *Simul. Model. Pract. Theory* 27, 76–89. <https://doi.org/10.1016/j.simpat.2012.05.008>
- Moustapha, M., Lataniotis, C., Marelli, S., Sudret, B., 2018. UQLab user manual – Support vector machines for classification. ETH Zurich.
- Mouyeaux, A., 2017. Analyse par éléments finis stochastiques de la fiabilité des barrages en remblai vis-à-vis du risque de glissement. Université Clermont Auvergne.
- Mouyeaux, A., Carvajal, C., Bressolette, P., Peyras, L., Breul, P., Bacconnet, C., 2019. Probabilistic analysis of pore water pressures of an earth dam using a random finite element approach based on field data. *Eng. Geol.* 259, 105190. <https://doi.org/10.1016/j.compgeo.2018.04.017>
- Mouyeaux, A., Carvajal, C., Bressolette, P., Peyras, L., Breul, P., Bacconnet, C., 2018. Probabilistic stability analysis of an earth dam by Stochastic Finite Element Method based on field data. *Comput. Geotech.* 101, 34–47. <https://doi.org/10.1016/j.compgeo.2018.04.017>
- Napa-García, G.F., Beck, A.T., Celestino, T.B., 2017. Reliability analyses of underground openings with the point estimate method. *Tunn. Undergr. Sp. Technol.* 64, 154–163. <https://doi.org/10.1016/j.tust.2016.12.010>
- Nishimura, S. ichi, Murakami, A., Matsuura, K., 2010. Reliability-based design of earth-fill dams based on the spatial distribution of strength parameters. *Georisk* 4, 140–147. <https://doi.org/10.1080/17499511003676655>
- Olsson, A.M.J., Sandberg, G.E., 2002. Latin hypercube sampling for stochastic finite element analysis. *J. Eng. Mech.* 128, 121–125. [https://doi.org/10.1061/\(ASCE\)0733-9399\(2002\)128:1\(121\)](https://doi.org/10.1061/(ASCE)0733-9399(2002)128:1(121))

- Pan, Q., Dias, D., 2017a. An efficient reliability method combining adaptive Support Vector Machine and Monte Carlo Simulation. *Struct. Saf.* 67, 85–95.
<https://doi.org/10.1016/j.strusafe.2017.04.006>
- Pan, Q., Dias, D., 2017b. Probabilistic evaluation of tunnel face stability in spatially random soils using sparse polynomial chaos expansion with global sensitivity analysis. *Acta Geotech.* 12, 1415–1429. <https://doi.org/10.1007/s11440-017-0541-5>
- Pan, Q., Dias, D., 2017c. Sliced inverse regression-based sparse polynomial chaos expansions for reliability analysis in high dimensions. *Reliab. Eng. Syst. Saf.* 167, 484–493.
<https://doi.org/10.1016/j.ress.2017.06.026>
- Pan, Q., Jiang, Y., Dias, D., 2017. Probabilistic stability analysis of a three dimensional rock slope characterized by the Hoek-Brown failure criterion. *J. Comput. Civ. Eng.* 31, 04017046.
[https://doi.org/10.1061/\(ASCE\)CP.1943-5487.0000692](https://doi.org/10.1061/(ASCE)CP.1943-5487.0000692)
- Pang, R., Xu, B., Zou, D., Kong, X., 2018. Stochastic seismic performance assessment of high CFRDs based on generalized probability density evolution method. *Comput. Geotech.* 97, 233–245.
<https://doi.org/10.1016/j.compgeo.2018.01.016>
- Papaioannou, I., Betz, W., Zwirgmaier, K., Straub, D., 2015. MCMC algorithms for Subset Simulation. *Probabilistic Eng. Mech.* 41, 89–103. <https://doi.org/10.1016/j.probengmech.2015.06.006>
- Papaioannou, I., Ehre, M., Straub, D., 2019. PLS-based adaptation for efficient PCE representation in high dimensions. *J. Comput. Phys.* 387, 186–204. <https://doi.org/10.1016/j.jcp.2019.02.046>
- Papaioannou, I., Straub, D., 2017. Learning soil parameters and updating geotechnical reliability estimates under spatial variability—theory and application to shallow foundations. *Georisk* 11, 116–128. <https://doi.org/10.1080/17499518.2016.1250280>
- Phoon, K.-K., Kulhawy, F.H., 1999a. Characterization of geotechnical variability. *Can. Geotech. J.* 36, 612–624. <https://doi.org/10.1139/t99-038>
- Phoon, K.-K., Kulhawy, F.H., 1999b. Evaluation of geotechnical property variability. *Can. Geotech. J.* 36, 625–639. <https://doi.org/10.1139/t99-039>
- Phoon, K.K., 2008. Numerical recipes for reliability analysis – a primer, in: Phoon, K.-K., Ching, J. (Eds.), *Reliability-Based Design in Geotechnical Engineering*. CRC Press, p. 545.
- Preziosi, M.-C., 2008. Probabilistic assessment of small earthfill dams. *Dams Reserv.* 18, 27–30.
<https://doi.org/10.1680/dare.2008.18.1.27>
- Rathje, E.M., Saygili, G., 2008. Probabilistic Seismic Hazard Analysis for the Sliding Displacement of Slopes: Scalar and Vector Approaches. *J. Geotech. Geoenvironmental Eng.* 134, 804–814.
[https://doi.org/10.1061/\(ASCE\)1090-0241\(2008\)134:6\(804\)](https://doi.org/10.1061/(ASCE)1090-0241(2008)134:6(804))
- Rosenblueth, E., 1975. Point estimates for probability moments. *Proc. Natl. Acad. Sci.* 72, 3812–3814.
<https://doi.org/10.1073/pnas.72.10.3812>
- Rubinstein, R.Y., 1981. *Simulation and the Monte Carlo Method*. John Wiley & Sons Ltd, New York.
- Saltelli, A., Annoni, P., Azzini, I., Campolongo, F., Ratto, M., Tarantola, S., 2010. Variance based sensitivity analysis of model output. Design and estimator for the total sensitivity index. *Comput. Phys. Commun.* 181, 259–270. <https://doi.org/10.1016/j.cpc.2009.09.018>
- Sandberg, G., Olsson, A., 1999. Failure sensitivity analysis of engineering structures. *Comput. Struct.* 72, 525–534. [https://doi.org/10.1016/S0045-7949\(98\)00334-4](https://doi.org/10.1016/S0045-7949(98)00334-4)

- Schöbi, R., Sudret, B., 2017. Application of conditional random fields and sparse polynomial chaos expansions in structural reliability analysis, in: 12th Int. Conf. Struct. Safety and Reliability. Vienna.
- Schweckendiek, T., Vrouwenvelder, A.C.W.M., Calle, E.O.F., 2014. Updating piping reliability with field performance observations. *Struct. Saf.* 47, 13–23.
<https://doi.org/10.1016/j.strusafe.2013.10.002>
- Sheikholeslami, R., Razavi, S., 2017. Progressive Latin Hypercube Sampling: An efficient approach for robust sampling-based analysis of environmental models. *Environ. Model. Softw.* 93, 109–126.
<https://doi.org/10.1016/J.ENVSOFT.2017.03.010>
- Shields, M.D., Zhang, J., 2016. The generalization of Latin hypercube sampling. *Reliab. Eng. Syst. Saf.* 148, 96–108. <https://doi.org/10.1016/j.res.2015.12.002>
- Smith, I.M., Griffiths, D. V., Margetts, L., 2015. *Programming the Finite Element Method*, Fifth Edition. John Wiley & Sons, Ltd. <https://doi.org/10.1002/9781119189237>
- Smith, M., Konrad, J.-M., 2011. Assessing hydraulic conductivities of a compacted dam core using geostatistical analysis of construction control data. *Can. Geotech. J.* 48, 1314–1327.
<https://doi.org/10.1139/t11-038>
- Straub, D., Papaioannou, I., 2015. Bayesian updating with structural reliability methods. *J. Eng. Mech.* 141, 1–13. [https://doi.org/10.1061/\(ASCE\)EM.1943-7889.0000839](https://doi.org/10.1061/(ASCE)EM.1943-7889.0000839)
- StructX, 2015. Density Ranges for Different Soil Types [WWW Document]. URL http://structx.com/Soil_Properties_002.html (accessed 10.24.17).
- Sudret, B., 2014. Polynomial Chaos Expansions and Stochastic Finite Element Methods, in: Phoon, K.-K., Ching, J. (Eds.), *Risk and Reliability in Geotechnical Engineering*. CRC Press, pp. 265–300.
- Sudret, B., 2008. Global sensitivity analysis using polynomial chaos expansions. *Reliab. Eng. Syst. Saf.* 93, 964–979. <https://doi.org/10.1016/j.res.2007.04.002>
- Sudret, B., 2007. Uncertainty propagation and sensitivity analysis in mechanical models - Contributions to structural reliability and stochastic spectral methods. Université Blaise Pascal - Clermont 2.
- Sudret, B., Der Kiureghian, A., 2000. *Stochastic finite element methods and reliability. A state-of-the-art-report*. University of California.
- Sudret, B., Marelli, S., Wiart, J., 2017. Surrogate models for uncertainty quantification: An overview, in: 2017 11th European Conference on Antennas and Propagation (EuCAP). IEEE, pp. 793–797.
<https://doi.org/10.23919/EuCAP.2017.7928679>
- Tang, X.S., Li, D.Q., Chen, Y.F., Zhou, C.B., Zhang, L.M., 2012. Improved knowledge-based clustered partitioning approach and its application to slope reliability analysis. *Comput. Geotech.* 45, 34–43. <https://doi.org/10.1016/j.compgeo.2012.05.001>
- Tian, M., Li, D.Q., Cao, Z.J., Phoon, K.K., Wang, Y., 2016. Bayesian identification of random field model using indirect test data. *Eng. Geol.* 210, 197–211. <https://doi.org/10.1016/j.enggeo.2016.05.013>
- Tipireddy, R., Ghanem, R., 2014. Basis adaptation in homogeneous chaos spaces. *J. Comput. Phys.* 259, 304–317. <https://doi.org/10.1016/j.jcp.2013.12.009>
- Tsilifis, P., Papaioannou, I., Straub, D., Nobile, F., 2020. Sparse Polynomial Chaos expansions using variational relevance vector machines. *J. Comput. Phys.* 416, 109498.
<https://doi.org/10.1016/j.jcp.2020.109498>

- U.S. Army Corps of Engineers, 2006. Reliability Analysis and Risk Assessment for Seepage and Slope Stability Failure Modes for Embankment Dams. Washington, D.C.
- Vapnik, V., Golowich, S.E., Smola, A.J., 1997. Support Vector Method for Function Approximation, Regression Estimation, and Signal Processing, in: Mozer, M.C., Jordan, M.I., Petsche, T. (Eds.), *Advances in Neural Information Processing Systems 9 (NIPS 1996)*. MIT Press, pp. 281–287.
- Wang, Y., Akeju, O.V., 2016. Quantifying the cross-correlation between effective cohesion and friction angle of soil from limited site-specific data. *Soils Found.* 56, 1055–1070.
<https://doi.org/10.1016/j.sandf.2016.11.009>
- Wang, Y., Asce, F., Zhao, T., Hu, Y., Asce, S.M., Phoon, K., Asce, F., 2019. Simulation of Random Fields with Trend from Sparse Measurements without Detrending. *J. Eng. Mech.* 145, 04018130.
[https://doi.org/10.1061/\(ASCE\)EM.1943-7889.0001560](https://doi.org/10.1061/(ASCE)EM.1943-7889.0001560).
- Wei, W.B., Cheng, Y.M., Li, L., 2009. Three-dimensional slope failure analysis by the strength reduction and limit equilibrium methods. *Comput. Geotech.* 36, 70–80.
<https://doi.org/10.1016/j.compgeo.2008.03.003>
- Wolff, T.H., 1985. Analysis and design of embankment dam slopes: A probabilistic approach. Purdue University.
- Wu, X.Z., 2013. Trivariate analysis of soil ranking-correlated characteristics and its application to probabilistic stability assessments in geotechnical engineering problems. *Soils Found.* 53, 540–556. <https://doi.org/10.1016/j.sandf.2013.06.006>
- Wu, Y., Zhou, X., Gao, Y., Zhang, L., Yang, J., 2019. Effect of soil variability on bearing capacity accounting for non-stationary characteristics of undrained shear strength. *Comput. Geotech.* 110, 199–210. <https://doi.org/10.1016/j.compgeo.2019.02.003>
- Xu, C., Gertner, G.Z., 2008. Uncertainty and sensitivity analysis for models with correlated parameters. *Reliab. Eng. Syst. Saf.* 93, 1563–1573. <https://doi.org/10.1016/j.res.2007.06.003>
- Yuan, J., Papaioannou, I., Straub, D., 2019. Probabilistic failure analysis of infinite slopes under random rainfall processes and spatially variable soil. *Georisk* 13, 20–33.
<https://doi.org/10.1080/17499518.2018.1489059>
- Yucemen, M.S., Tang, W.H., Ang, A.-S., 1973. A probabilistic study of safety and design of earth slopes. University of Illinois at Urbana-Champaign.
- Zhang, L., Peng, M., Chang, D., Xu, Y., 2016. Internal Erosion in Dams and Their Foundations, in: *Dam Failure Mechanisms and Risk Assessment*. John Wiley & Sons Singapore Pte. Ltd, Singapore, pp. 67–126. <https://doi.org/10.1002/9781118558522.ch6>
- Zhao, Y.G., Ono, T., 2001. Moment methods for structural reliability. *Struct. Saf.* 23, 47–75.
[https://doi.org/10.1016/S0167-4730\(00\)00027-8](https://doi.org/10.1016/S0167-4730(00)00027-8)
- Zhu, D., Griffiths, D. V., Fenton, G.A., 2018. Worst-case spatial correlation length in probabilistic slope stability analysis. *Géotechnique* 69, 85–88. <https://doi.org/10.1680/jgeot.17.t.050>
- Zhu, D., Griffiths, D. V., Huang, J., Fenton, G.A., 2017. Probabilistic stability analyses of undrained slopes with linearly increasing mean strength. *Géotechnique* 67, 733–746.
<https://doi.org/10.1680/jgeot.16.p.223>
- Zhu, D.Y., Lee, C.F., Qian, Q.H., Chen, G.R., 2005. A concise algorithm for computing the factor of safety using the Morgenstern-Price method. *Can. Geotech. J.* 42, 272–278.
<https://doi.org/10.1139/t04-072>

- Zienkiewicz, O.C., Humpheson, C., Lewis, R.W., 1975. Associated and non-associated visco-plasticity and plasticity in soil mechanics. *Géotechnique* 25, 671–689.
<https://doi.org/10.1680/geot.1975.25.4.671>
- Zolfaghari, A.R., Heath, A.C., McCombie, P.F., 2005. Simple genetic algorithm search for critical non-circular failure surface in slope stability analysis. *Comput. Geotech.* 32, 139–152.
<https://doi.org/10.1016/j.compgeo.2005.02.001>
- Zuev, K.M., Beck, J.L., Au, S.K., Katafygiotis, L.S., 2012. Bayesian post-processor and other enhancements of Subset Simulation for estimating failure probabilities in high dimensions. *Comput. Struct.* 92–93, 283–296. <https://doi.org/10.1016/j.compstruc.2011.10.017>